ENVIRONMENTAL DEGRADATION OF ELASTOMERIC ADHESIVES AND RUBBERS IN HYGROTHERMAL AND HYDROLYTIC AGING CONDITIONS

By

Mamoon Shaafaey

A DISSERTATION

Submitted to
Michigan State University
in partial fulfillment of the requirements
for the degree of

Civil Engineering – Doctor of Philosophy

2023

ABSTRACT

The corrosion of elastomeric adhesives and rubbers within electrical and structural components poses significant challenges across industries, notably in the automotive sector. Cross-linked polymeric adhesives play pivotal roles, serving as joints for dissimilar material interfaces, protective matrices against environmental factors, and thermal interfaces for electronics. The degradation of such adhesives due to environmental factors can drastically impact vehicle performance and reliability.

This dissertation delves into the intricate effects of environmental aging on elastomeric adhesives, specifically hygrothermal, hydrolytic, and thermo-oxidative aging. Experiments were meticulously designed, encompassing various temperatures and durations, utilizing diverse viscoelastic materials like rubbers and structural adhesives. The primary goal was to cultivate a nuanced understanding of aging mechanisms and their impact on polymeric materials, providing insights for predictive models and ensuring component reliability.

The research initially focused on analyzing thermo-oxidation and hydrolytic aging, individually and combined. This analysis extended to silicone-based adhesives, investigating their behavior in distilled water and seawater. For PDMS-based silicone adhesive, saltwater showed higher initial corrosion rates, yet distilled water proved more damaging due to water absorption initiating chain scission and leaching. Saltwater conditions formed a protective barrier, safeguarding against water absorption. Thermo-oxidation and hydrolytic aging involved simultaneous cross-link formation/reduction and chain scission. Characterization methods highlighted the cumulative damage caused by environmental conditions.

The study proceeded to examine damage kinetics in polyurethane adhesives, deepening understanding of each condition. Curiosity led to exploring interactions between environmental agents, in isolation or combination. Hygrothermal aging fostered competition between thermal-oxidation and hydrolytic environments, yielding diverse material responses and degradation pathways. Specific factors could accelerate or decelerate degradation, influencing elastomeric adhesive performance.

A critical insight emerged: mechanical damage and environmental degradation are independent mechanisms. This finding prompted separate consideration of mechanical stress and environmental factors when assessing material performance. This enhanced understanding facilitated targeted predictions of material behavior.

The investigation expanded to explore dual environmental exposure effects on polyurethane adhesive. This two-phase study evaluated synergistic and antagonistic interplay between conditions and exposure sequence's role in degradation. Exposure sequence significantly shaped material response, potentially accelerating degradation or revealing novel pathways. Combined environmental factors yielded non-linear material behavior, emphasizing complex interactions' significance in assessing elastomeric adhesives.

This holistic approach illuminated complex relationships between multiple environmental factors and elastomeric adhesive performance. Findings informed predictive models and material selection strategies in the automotive sector and beyond.

The research concluded by examining FEPM degradation under extreme HPHT downhole conditions. Analytical techniques revealed chemical structure shifts due to degradation, enhancing understanding of elastomeric adhesives' behavior. Insights guide fluoroelastomer development, ensuring component reliability in diverse industries.

This comprehensive study deepened comprehension of elastomeric materials under diverse environmental aging, essential for predictive models ensuring component reliability across industries, especially automotive. Insights into environmental degradation resistance offer sustainable solutions for elastomer-reliant applications.

Dedicated to my family.

To the loving memory of my late father, who always believed in me.
To my beloved mother for her unconditional love and prayers.
To my dear wife, who has been my rock in every challenge life has thrown at us.
And to my beautiful daughters, whose smiles add meaning and purpose to my life.

ACKNOWLEDGMENTS

Praise be to The Lord Allah, The Most Beneficent, The Most Merciful. I extend my deepest gratitude to my advisor, Dr. Roozbeh Dargazany, for his mentorship and guidance throughout my PhD journey. I am thankful for his trust in my abilities and his support within the High-Performance Materials (HPM) research group.

I appreciate the time and valuable feedback provided by my PhD committee members, Dr. Mahmood ul Haq, Dr. Weiyi Lu, and Dr. Shiwang Cheng, which greatly influenced my research.

My fellow scholars in HPM – Sharif Al Azhary, Abdul Korayem, Amir BahroloIoumi, Mindy, and Lili – have been instrumental in my progress. I am grateful for their contributions in various aspects of this research.

I dedicate this thesis to my late father, Colonel Musleh ud din Saadi for his love and support, and am grateful for the prayers and strength of my mother, Shahina, and the support of my wife, Maryam Abbasi, and daughters, Neea, Aena, and Naba.

I am indebted to Dr. Soroushian, who initially guided me towards Dr. Dargazany and taught me the essentials and basics of research methods.

My heartfelt appreciation goes to Omid Nabinejad and Mike Rich for their assistance in understanding material testing procedures.

I acknowledge Dr. Katy Luchini Colbry and Brooke H.M. Stokdyk for their exceptional support at the College of Engineering and the Office for International Students and Scholars.

Virginia Martz from the Resource Center for Persons with Disabilities provided crucial academic accommodations that supported my success.

This research was made possible with the support of the US Department of Energy Office of Energy Efficiency and Renewable Energy (EERE, Award Number DE-EE0008455), CNPC USA, and the Department of Civil Engineering at Michigan State University. Financial aid from the Higher Education Commission (HEC) Pakistan, the Graduate School at Michigan State University, and the US-Pakistan Knowledge Corridor program is appreciated.

I extend my gratitude to the Pakistan Army and the Corps of Engineers for their continued trust and unwavering support.

In conclusion, I am deeply grateful to all who supported me on this academic journey. Your encouragement and belief in my abilities were the driving force behind my achievements, and I will cherish the lessons learned and memories shared with each of you.

TABLE OF CONTENTS

Chapter 1:

Environmental Aging

1.1 Introduction

In today's modern industries, such as automotive, transportation, power distribution, medical and aerospace industries, cross-linked polymers have unarguably become omnipresent globally due to their outstanding properties such as sustainability, flexibility in the range of applications, durability, abrasion, and chemical resistance, and toughness [94, 69]. Given their critical and challenging applications, rubber-like components have to be designed keeping their reliability and sustainability in focus. During service life, these materials are subjected to a high number of cyclic loadings in a variety of harsh environments. Resultantly, these materials degrade considerably over time due to the process termed aging. The aging process instigates significant temporary and/or permanent changes in the mechanical behavior and oftentimes alters the chemical makeup of these cross-linked polymers over their service life [37]. Considering the wide range of applications and exposures to harsh environments, accurate lifetime estimation of products made by cross-linked elastomers can be highly challenging, especially for exposures involving multiple degradation factors.

The aging mechanism takes effect due to individual or synergized effects of different environmental agents such as temperature, water, relative humidity, and radiation [127, 133]. These environmental agents act in combinations, facilitating degradation mechanisms such as hygro-thermal, hydrolysis [13, 20], thermo-oxidation [140, 130, 134], photo-oxidation [132], and those with the less severe impact such as chemical corrosion [163], and ozone cracking [105]. These mechanisms can significantly damage the materials and reduce the service life of elastomeric components. Although predicting the individual contribution of different mechanisms has been reported in the literature, there is limited information on the synergized effects and contributions of multi-factor aging mechanisms.

New materials need to be designed keeping in view their service life exposure and its impacts; it would immensely add to their sustainability and durability performance. Harsh environments change the constitutive behaviors of the cross-linked polymers over time. Predicting these changes per service conditions can prevent catastrophic disasters due to aging that can cause the unexpected failure of elastomers. Therefore, understanding the environmental impact on the mechanical

properties of cross-linked polymers during aging is of high value. Albeit their popularity, there exists a minimal account of theoretical efforts for hygrothermal and hydrolytic aging of cross-linked elastomer adhesives.

We assert that the involved environmental agents should not be considered mere theoretical parameters, as they possess tangible significance, as reported by Dargazany [49]. The experimental data obtained from studying these factors can greatly contribute to the creation of predictive models that can potentially capture the constitutive behavior of elastomers. This realization largely sparked our interest in this specific area of study. The primary goal of this research is to gain a comprehensive understanding of both elastic and inelastic responses of elastomers when subjected to various aging environments. Our study mainly concentrates on hygrothermal and hydrolytic induced aging in order to examine the impact of different parameters on the material's behavior.

1.2 Environmental Aging

This dissertation focuses on both individual and combined-environment aging, incorporating a diverse range of conditions involving hygrothermal, hydrolytic, and thermo-oxidative aging. These experiments were conducted at varying temperatures and for different lengths of time, involving different viscoelastic materials like rubbers and structural adhesives. It presents a general review of aging, its impacts on polymeric materials, the types of aging environments, and aging regimes for designed experimental methods.

Environmental aging encompasses the unavoidable modifications that materials experience over time when subjected to various environmental factors [177]. This process can be divided into chemical aging, physical aging, or a combination of both [82].

i. **Chemical Aging:** Chemical aging relates to the effects of chemicals on materials, often characterized by a decrease in molecular weight due to chemical reactions such as chain scission. This type of aging can be caused by factors like exposure to UV radiation, interaction with aggressive chemicals, moisture absorption, and exposure to high temperatures. These factors can cause material degradation, leading to a decrease in performance and a shorter service life.

ii. **Physical Aging:** Physical aging, on the other hand, involves changes in the mechanical properties of materials, which can result in a reduction in strength and toughness. Factors contributing to physical aging include mechanical stress and strain, creep and stress relaxation, fatigue loading, and thermal cycling. Physical aging can lead to material deformation, embrittlement, or even failure, depending on the severity of the applied stresses and environmental conditions.

iii. Combined Effects of Chemical and Physical Aging: In many cases, materials undergo a combination of chemical and physical aging, leading to complex interactions and synergistic effects. The combined effects of both types of aging can result in a faster degradation rate, ultimately compromising the material's performance and reliability. Understanding these interactions and predicting material behavior under various environmental conditions is crucial for the design and selection of materials for specific applications.

iv. Environmental Aging of Elastomeric Polymers Elastomeric polymers, which include adhesives, are particularly vulnerable to environmental aging, especially in outdoor applications. Factors such as humidity, heat, and aggressive chemicals can lead to physical and chemical alterations in the polymer structure, resulting in diminished performance and a shortened lifespan. To counteract the effects of environmental aging on these materials, various strategies can be implemented, including selecting materials with improved resistance to environmental factors, applying protective coatings or barriers, incorporating additives that enhance the material's resistance to weathering, and designing products capable of enduring exposure to harsh environments.

v. Water-Induced Aging in Polymers Water represents a unique case of aging, as it can induce physical or chemical changes, and even both effects can be present simultaneously, depending on the conditions. Some polymers, such as nylons, polyesters, and epoxies, can easily absorb water, leading to plasticization which can cause reduction in their glass transition temperature.

In the case of physical aging, water can act as a plasticizer, causing the material to swell or soften. This occurs when water molecules penetrate the polymer matrix, leading to a decrease in the glass transition temperature and changes in mechanical properties such as strength and stiffness. This type of aging is typically reversible once the material dries out, and the water molecules are removed. On the other hand, chemical aging involves water participating in hydrolysis reactions with the material. This process can lead to the degradation of the polymer structure, resulting in chain scission, crosslinking, or other chemical modifications. Chemical aging due to water exposure is generally irreversible and can cause permanent damage to the material.

vi. Importance of Understanding Environmental Aging in Material Design Comprehending the effects of environ- mental aging on polymers, plastics, and components made from similar substances is vital when designing materials that can withstand harsh environments. The impact of environmental factors on these materials can manifest as chemical, physical, or a combination of both types of aging. Consequently, it is crucial to consider potential aging regimes

when designing materials for specific service applications to ensure their long-term performance and durability.

1.2.1 Hydrolytic Environment

i. Mechanism of Hydrolysis The hydrolytic environment generally refers to the aging condition where materials degrade through exposure to water or moisture. In this dissertation we shall refer to submerged conditions as hydrolytic environment and the humid conditions as hygrothermal aging condition. In this environment, the hydrolysis of polymer chains occurs due to the cleavage of covalent bonds, leading to the breakdown of the material's structure and a subsequent decline in mechanical properties.

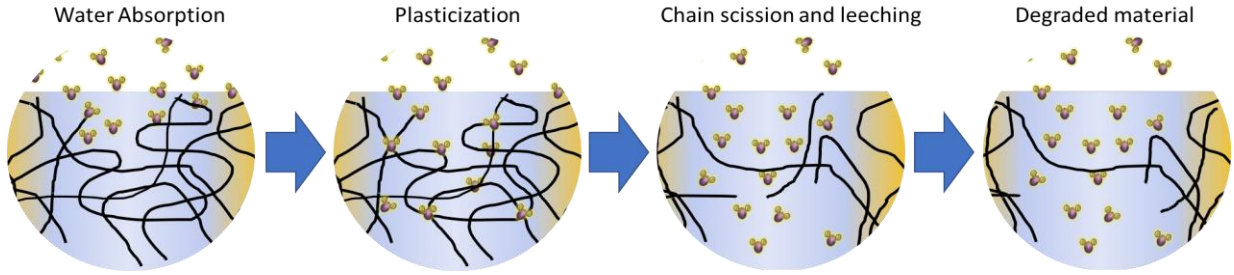

Figure 1.1: Schematic showing the degradation of polymer matrix exposed to hydrolytic conditions.

ii. Impact on Polymer Materials Our investigation revealed that hydrolytic environment significantly affects the PDMS- based flexible silicone and polyurethane adhesives. Hydrolytic degradation involves the cleavage of polymer chains, forming smaller molecular weight species and thus reducing the materials' mechanical strength and elasticity. The general mechanism of hydrolysis can be represented as follows:

$$\text{Polymer} - \text{X} - \text{Polymer} + \text{H}_2\text{O} \rightarrow \text{Polymer} - \text{OH} + \text{Polymer} - \text{XH} \qquad (1.1)$$

In this equation, X represents a functional group, such as esters, siloxanes, urethanes, or amide linkages. The hydrolysis reaction can lead to chain scission and the formation of smaller molecular weight species, reducing the mechanical strength and elasticity of the materials. For instance, an illustration of plausible degradation mechanisms of liquid silicone rubber (LSR) in hydrolytic environment has been similarly reported by Ghanbari [70] (see Fig. 1.2). Furthermore, it is possible that this reaction can also generate acidic or basic species, which can further catalyze the degradation process.

iii. Hydrolysis of Specific Materials PDMS-based flexible silicone adhesives can undergo hydrolytic cleavage of siloxane linkages, while polyurethane-based elastomeric adhesives are susceptible to hydrolytic attack on urethane linkages. In contrast, fluoroelastomers are generally more

resistant to hydrolytic degradation, but specific formulations may still be vulnerable to hydrolytic conditions. Therefore, fluoroelastomers were investigated in fluid environments which were harsher and sourer in nature.

1.2.2 Hygrothermal Environment

Combined Effects of Moisture and Temperature The hygrothermal environment encompasses the combined effects of moisture and temperature on material degradation. This environment is particularly important for polymer materials, since it provides an opportunity to study the synergistic effect of sub-aging conditions, i.e., thermal-oxidation and hydrolytic aging. Interaction of environmental agents can be either competing, collaborative, or multiplicative in nature. For instance, the synergistic effect of both factors can accelerate the aging process. This aspect has been investigated and discussed in more detail in Chapter-3.

Degradation Mechanisms in Hygrothermal Environment In the hygrothermal environment, water molecules penetrate the polymer matrix, interact with polymer chains, and facilitate molecular motion. Elevated temperatures are expected to further increase reaction rates, such as hydrolysis and oxidation, as well as promote thermal degradation mechanisms like chain scission and crosslinking. Certain phases during the aging process complicate it further when the environment facilitates a simultaneous crosslink development process, thus slowing down the deterioration mechanisms.
Hygrothermal Aging of Specific Materials Hygrothermal aging of flexible silicone adhesive, polyurethane-based adhesive leads to a combination of hydrolytic and thermal degradation, ultimately reducing the materials' mechanical properties. In addition to the hydrolytic reactions mentioned earlier, increased temperature can promote the formation of oxidative species, which attack the polymer chains, resulting in chain scission, crosslinking, and oxidation.

Implications of Hygrothermal Aging Understanding the effects of hydrolytic and hygrothermal environments on the aging of polymer materials is crucial for improving material performance. By studying the degradation mechanisms in these environments, researchers can gain insight into the factors influencing materials' aging behavior, potentially leading to the development of more resistant and durable materials for a variety of applications.

1.3 Aging Regimes

Understanding and predicting the environmental aging response for elastomeric adhesives is complicated due to their complex chemical composition. In addition, most manufacturers treat this information as confidential, which adds to the challenge.

To address this issue, our experimental data has been instrumental in developing reliable models that can successfully capture and predict the elastomeric adhesive behavior under various mechanical and environmental damages. Aging regimes involving several experimental conditions were designed to produce accurate data sets for this purpose. Broadly, the experiments can be divided into three categories, namely:

i. Single aging environment.
ii. Sequential Dual aging environment.
iii. Multi factor High Temperature High Pressure (HTHP) aging.

1.3.1 Single environment aging

In this aging regime, the selected materials were exposed to one environmental condition throughout the designed aging span. Examples of these conditions include thermal oxidation with 0% relative humidity (RH), hydrolysis (submerged state), and hygrothermal aging (80%RH). The results from post-aging characterization tests, such as mechanical testing, morphological and structural analysis, and thermal analysis, helped us understand the kinetics of material degradation and the specific impact of each aging environment on the understudy polymer materials.

1.3.2 Sequential Dual aging environment

In this aging regime, we exposed the materials to two different aging environments in a sequential manner. The objective was to investigate the impact of one environmental factor followed by another, such as thermal oxidation followed by hydrolysis, hydrolysis followed by hygrothermal aging, or thermal oxidation followed by hygrothermal aging. This approach allowed us to study the potential synergistic or antagonistic effects that may arise from the combination of different environmental factors on the elastomeric adhesives.

In this regard, we designed a 2-phase environmental-jump experiment where the temperature was kept constant while the specimens were rotated between two aging environments during the aging period. This study was planned for two adhesives, i.e., silicone (DOWSIL-7091) and polyurethane (3M-590 black). The aging was done considering the following environmental regimes:

i. Hygrothermal dual aging (0%RH to 80%RH).
ii. Hydrolytic dual aging (0%RH to hydrolysis).
iii. Thermo-hygro dual aging (80%RH to 0%RH).
iv. Thermo-hydro dual aging (hydrolysis to 0%RH).

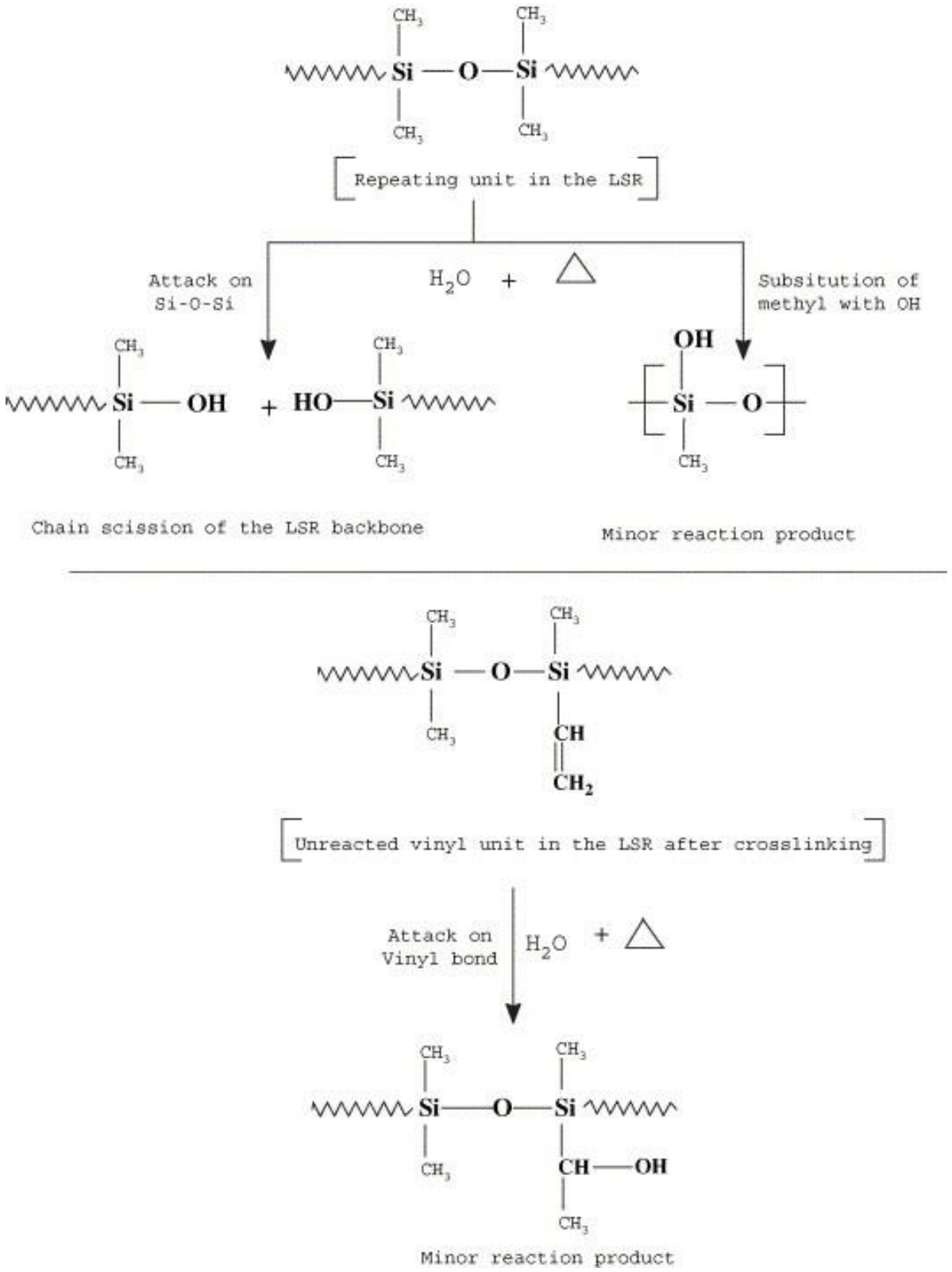

Figure 1.2: Suggested hydrolytic degradation reaction mechanism for silicone rubber [70].

The dual environment aging allowed us to study the combined effects of different aging environments on the material properties and degradation mechanisms. By comparing the results obtained from single and dual environment aging, we could identify synergistic or antagonistic effects between the different aging factors. A detailed discussion of the results, including the changes in material properties and degradation mechanisms to assist the development of predictive models for material behavior under above mentioned aging conditions, is covered in Chapter-5 of this dissertation.

1.3.3 Multi factor High Temperature High Pressure (HTHP) aging

In this aging regime, considering the intense and harsh conditions, we selected fluoroelastomer rubbers to a combination of high temperature, high pressure, and multiple environmental factors simultaneously. This approach aimed to simulate real-world downhole conditions especially in oil and gas industries where materials experience various environmental factors concurrently, such as temperature, humidity, and mechanical stress in sour and corrosive environmental exposure. By studying the material behavior under HTHP aging, we aimed to understand the combined effects of multiple factors on the material degradation kinetics and the overall performance of the material.

The comprehensive understanding of the effects of single environment, sequential dual environment, and multi factor HTHP aging on elastomeric polymers enables the researchers to develop more accurate predictive models for their behavior under various environmental conditions. As a result, we can better evaluate their long-term performance and durability, which is crucial for their successful application in various industries.

1.4 Investigating Degradation Mechanisms

1.4.1 Characterization Techniques

Morphological and Structural Analysis To understand the degradation mechanisms in hydrolytic and hygrothermal environments, various characterization techniques were employed. Techniques such as scanning electron microscopy (SEM), can reveal morphological changes in the polymer materials. Additionally, structural analysis techniques, such as Fourier-transform infrared spectroscopy (FTIR) can help identify the chemical changes and functional groups formed during the degradation process.

Mechanical Property Evaluation Mechanical properties of aged polymer materials were evaluated using tensile testing, and dynamic mechanical analysis (DMA), among other techniques.

These tests provide valuable information about the materials' strength, elasticity, and viscoelastic behavior, allowing to correlate the observed changes in properties with the degradation mechanisms. Thermal Analysis Differential scanning calorimetry (DSC) along with already mentioned dynamic mechanical analysis (DMA) were employed to investigate the thermal properties and stability of aged polymer materials. These techniques provided insight into the materials' glass transition temperature (T_g), and thermal degradation behavior, which can be correlated with the extent of degradation in hydrolytic and hygrothermal environments.

1.4.2 Developing Improved Materials

Material Modifications A comprehensive understanding of the degradation mechanisms in hydrolytic and hygrothermal environments is vital for developing more robust and durable polymer materials. By employing various characterization techniques, the performance and reliability of these materials can be improved in their intended ap- plications. The understanding gained and reported through this investigation about the degradation mechanisms in hydrolytic and hygrothermal environments, will help improve materials modification in terms of their chemical com- position, molecular architecture, or processing techniques. These modifications can enhance the materials' resistance to aging, improve their mechanical properties, and extend their service life in various applications.

In summary, we believe the study of hydrolytic and hygrothermal aging of understudy elastomers, has far-reaching implications for material selection, design, maintenance, and sustainability. Through a combination of case studies, practical applications, and industry impact, researchers can continue to advance the development of more robust and durable materials for various applications, improving their performance, reliability, and environmental footprint.

1.5 Outline of the Present Work

This dissertation presents a detailed experimental work including environmental regimes that can provide great value and insight into developing an understanding of the nonlinear behavior of elastomeric materials during the different types of environmental aging. Reviewing the resulting data, we hope to develop a keen understanding of the material behavior and responses. This will provide important insight into the nature of each environment and how different environments interact with each other in order to translate the resultant effect on the materials being exposed. We believe this work shall be of much value for developing models that can predict the nonlinear behavior of elastomeric materials during different types of chemical aging. The current study is divided into six

chapters, each of which is briefly summarized as follows. After covering the general framework of experiments and the design of aging regimes in Chapter-1, Chapter-2, we investigated the behavior of silicone-based adhesive in two hydrolytic environments, i.e., distilled water and seawater. Chapter-3 highlights the thermo-oxidation and hydrolytic aging environments in isolation and how they interact to assume the role of a sub-aging phenomenon in case of hygrothermal aging. Chapter-4 further probes the kinetics of damage evolution in polyurethane adhesives by showing that mechanical damage and environmental degradation are independent mechanisms. Chapter-5 reviews the effect of sequential dual environmental exposure of polyurethane adhesive. In Chapter-6, we investigated the degradation of tetrafluoroethylene propylene (FEPM) rubber exposed to multi factor high-pressure, high-temperature (HPHT) and sour downhole conditions. Finally, in Chapter-7, we conclude by briefly mentioning the way forward for future research work.

Chapter 2:

Effects of hydrolytic aging on constitutive behavior of silicone adhesives in seawater and distilled water

2.1 Introduction

Adhesives, specifically silicone-based adhesives, are outstanding for their characterization of sealing joints [2] between various materials and accordingly have a wide variety of applications such as aerospace [16], electronic field [91], medical treatment [129, 193] and construction industries [95]. It is acknowledged that silicone-based adhesive is outlined as high permeability, low glass transition temperature, and high surface tension material [51]. Single component silicone adhesive, PDMS (polydimethylsiloxane), which is a semi-crystalline polymer [172], has been widely applied in marine environments due to its hydrophobic property [39]. PDMS displays high flexibility, elasticity and heat resistance attributed to its Si−O bond [109]. Yet when exposed to harsh environments such as ultraviolet light, high temperature, moisture, oxygen, or their combinations for long periods, adhesives might undergo a degradation process often referred to as aging [131]. Since elastomeric parts may often be out of reach, visual inspection is not always an option, accurate understanding of their service life reduction due to aging is of utmost significance in preventing disasters. Therefore, it necessitates further investigations in this direction to better understand the influences of this phenomenon on material behavior.

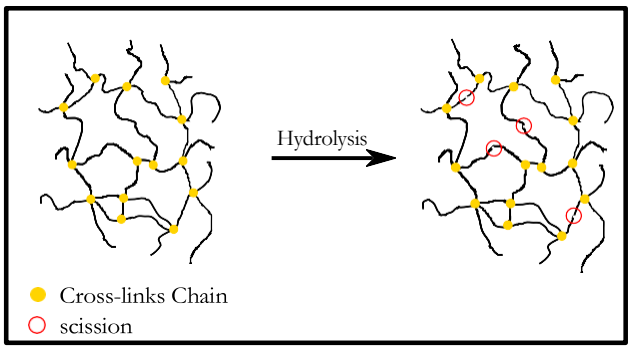

Figure 2.1: The changes of polymer network during hydrolytic aging.

Accelerated weathering, commonly categorized into thermal-oxidation aging [131, 12], photo-oxidation aging [132], hygro-thermal aging [14, 166], and hydrolytic aging [13, 11], is the process of physical (mostly reversible) and chemical (irreversible) deterioration of material resulting from

exposure to above mentioned environmental agents over time. Physical alterations embody the variation of mechanical properties [175, 137] with weight and mass variations as a reversible process. While chemical changes, an irreversible mechanism, emanate from altering material chain structure at a molecular level due to environmental exposure [34]. Aging mechanisms play an active and imperative role in inducing the alteration of molecular configurations. Those changes are reflected in physical properties, contributing to the evolution of thermodynamic equilibrium. Material properties, including toughness, viscoelasticity, and permeability, could change from physical aging [145, 88]. Given chemical aging, oxidation [77, 96], and hydrolysis [135, 164] are regarded as aging procedures that cause prominent cross-linking and chain-scission reactions, simultaneously. Hydrolysis is a chemical reaction where water molecules attack the vulnerable bonds of polymer matrix and alter the macro-molecular structure, which over a prolonged duration can be termed hydrolytic aging. Plasticization, loss of cross-links, and main chain-scission resulting in smaller chains are typical phenomena observed in materials due to hydrolytic aging. In most weathering circumstances, physical and chemical aging simultaneously engender the degradation of materials.

Hydrolytic aging can be interpreted as a degradation mechanism where materials are immersed in various liquid solutions for the long term. It induces a series of changes without involving oxidative influences. These governing phenomena in hydrolytic aging have impeded the comprehension and understanding of the mechanisms that cause swelling [117], cracking [4], post-curing [125] and plasticization [160] taking place simultaneously or subsequently. Conversion of mechanical properties is another aspect of assessing the degree of deterioration of hydrolytic aging. Such alterations provoke deep levels of research to trace their structural changes. In prolonged hydrolytic aging, water acting as a plasticizer penetrates materials and causes plasticization, which is characterized by a declining Tg (glass transition temperature) [32]. Plasticization is identified as physical transformations acting on the amorphous regions of materials such that elongation at break increases due to loss of cross-linking tie-chains and the resultant decline in the tensile strength [114]. In short, while it affects the length distribution of polymer chains inside the matrix, further degradation emerges as a consequence of chain scission (see Fig. 2.1), which is regarded as a chemical alteration at the macro-molecular level [11]. The molecules that get detached from long chains could be trickled and migrated from materials by water or other solution mediums via a process termed as leaching [151].

Over the years, many researchers have focused on deformation-induced aging methodologies. In his widely acclaimed work, Struik proposed the concept of mechanical rejuvenation in response to the observed reduction in relaxation times of amorphous glass polymers subjected to large stresses

[171]. Bahrololoumi et al. have proposed a synergistic damage accumulation-based modular network concept for a micro-mechanical constitutive model [15]. In this model, the concepts of damage accumulation have been applied to describe the damage induced by thermal aging and cyclic fatigue on the constitutive response of cross-linked polymers. Mohammadi et al. proposed a model addressing network evolution in polymers [133] by introducing different decay functions dealing with deformation- induced aging phenomenon such as stress softening and permanent set.

Two of the most studied mediums for hydrolytic aging are distilled and seawater. In the study of Heshmati et al. [85], salt water degrades the mechanical properties of adhesives to a lesser degree than distilled water. A similar trend was observed in the study by Anna Rudawska et al. [155], even though salt water was compared to tap water instead of distilled water. One reason for such a phenomenon could be that distilled water is more conducive to the proceeding of swelling than salt solution owing to hydrated ions, and ionic atmospheres [42]. Liu H and Wang J [123] maintain that the diffusion of seawater is ruled by the difference in seawater chemical potential between the solution phase and the polymer solid phase. Seawater absorption equilibrium corresponds to the equal seawater chemical potentials in the two phases. The greater the difference, the faster the seawater diffuses through the polymer, and accordingly, the greater the saturated level of seawater absorption. Accelerated aging is a feasible approach to studying the aging process in a reasonable time frame. Accelerated hydrolytic aging is a degradation mechanism of hydrolytic aging under elevated temperature to achieve long-term natural environmental aging on the material under consideration. The constitutive behavior of materials in a potent manner could evaluate the level of degradation due to aging [131]. Mathew et al. demonstrated that before entering into the degradation phase, polymers are expected to undergo post-curing with cross-linking, making the samples more resilient and tough [128]. But in hydrolytic aging, even short-term aging at elevated temperatures can potentially engender an increased plasticization effect of water, thus decreasing the tensile stress and adding to the elongation at breakage. Under the presence of moisture, accelerated aging promotes the process of water penetration to cause the plasticization of materials, which leads to softening behaviors [181]. The relative rate of polymer chain scission, sorption, and resulting cross-link density determines the subsequent hardening or softening of the material. While these rates may be variable depending on material chemistry, aging condition, etc., it is expected that the resulting changes in cross-link density will demonstrate an exponentially decreasing toughness in the material matrix.

Aging at elevated temperatures might change the cross-link density inside PDMS [38], the network would be re-arranged and optimized to reach equilibrium in physical alteration [116, 19]. It

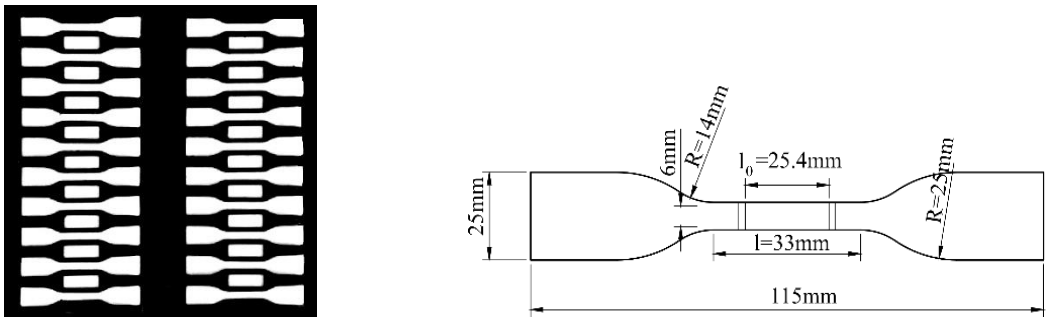

(a) (b)

Figure 2.2: Sample preparation for (a) customized mold and (b) detailed sample dimensions.

is worth mentioning that hydrolysis of PDMS could create an oligomeric product in alkaline solutions to form the denser colloidal aerogel, which attributes to chemical changes [182, 8]. During aging at elevated temperatures, PDMS deteriorated by inter-molecular de- polymerization reactions, named back-biting [115, 75]. Those chemical changes decrease the molecular weight to promote the constitution of volatile materials, which could have been broken by chain scission reactions [191]. Nevertheless, PDMS-based adhesive possesses the same characteristics as PDMS. But, they are required to show higher resistance to the harsh environment in case of sudden breakage of sealing. The contribution of physio-chemical changes induced by hydrolytic aging on the constitutive behavior of PDMS remains a challenge that has been barely studied before. The study on curing kinetics of DOWSIL-7091 adhesive by Nassiet et al indicates the susceptibility of this silicone adhesive to increasing temperature and relative humidity [142]. Especially in high temperature environments, the potential vulnerability of volatile components resulting in retardation of the expected cross-linking reactions merits consideration. Nassiet et al, also expressed the need to carry out a durability assessment for future works in order to evaluate the chemical resistance of this silicone adhesive in different aggressive media such as humidity [142] and submerged conditions.

Therefore, this study aims to investigate the correlation between mechanical damage and hydrolytic decay mechanisms on silicone adhesives exposed to seawater and distilled water. To this end, we first studied each damage mechanism separately, namely (i) damage induced by accelerated hydrolytic aging and (ii) damage induced by cyclic deformation. For hydrolytic decay, aging tests were carried out under controlled lab conditions. Temperatures 60°C, 80°C, and 95°C were utilized for accelerated aging in distilled water and seawater spanning up to 30 days. Gravimetric measurements, tensile failure and cyclic tests were performed on unaged and aged specimens to investigate the deterioration of mechanical properties. Fourier Transform Infrared (FTIR) spectroscopy, Dynamic Mechanical Analysis (DMA), Scanning Electron Microscopy (SEM), and cross-link density (CLD)

analysis were utilized to trace physical and chemical alterations induced by hydrolytic aging. Inelastic characteristics such as relative stress softening and relative residual strain were studied to investigate the correlation between deformation-induced and environment- induced damage. The paper is outlined as follows. After discussing the experimental method in section 2.2, the results and discussion are presented in section 2.3. Finally, section 2.4 includes the summarized concluding remarks for this experimental effort.

2.2 Experimental Procedure

2.2.1 Material

The research objective is to investigate the characterization of silicon-based adhesives. For this experimental study, we have used Dow Corning 7091 Adhesive/Sealant. It is an RTV (room-temperature-vulcanizing) silicone adhesive [142] which cures at room temperature into a flexible rubber material with durometer hardness, Shore-A-32 [7]. Dow Corning 7091 is used as a Formed-in-Place Gasket (FIPG) material in the automotive industry. It consists of the following components [142].

i. An alkoxy (here CH_3)-terminated PDMS of average molecular weight M_n=63,000g.mol^{-1}.
ii. Low molecular weight trimethylsiloxy-terminated PDMS of M_n = 5,000g.mol^{-1}.
iii. A mixture of silanes and titanates to enhance adhesion and allow cross-linking.

2.2.2 Sample Preparation

Dimensions The sticky adhesive was cast into a customized mold with 20 dumbbell-shaped and 18 rectangular samples for each plane with a thickness of 3.175mm shown in Fig. 2.2a. The adhesive above the mold surface was removed to assure similar dimensions in all samples (see Fig. 2.2b). The dimensions were selected in accordance with ASTM D412: "Standard Test Methods for Vulcanized Rubber and Thermoplastic Elastomers - Tension" [48]. For specimens with an overall length of 115 mm, ASTM D412 calls for a thickness of 3 mm with ± 0.3mm accuracy. Furthermore, some recent investigations on RTV silicone rubbers have also considered similar sample dimensions for studying material behavior. Using similar sample thickness provides suitable grounds for comparison of results [5, 22]. Dumbbell-shaped specimens were used for tensile tests, while rectangular samples (35 × 12 × 3.175 mm) were cured and aged for DMA testing.

Curing RTV (room-temperature-vulcanizing) adhesives cure at room temperature by cross-linking. This cross-linking process is responsible for improving the mechanical properties of the material. As

long as this cross-linking process continues, it is considered a 'curing period.' While the adhesive can gain serviceable bond strength per the 'minimum' curing period mentioned in the manufacturer's specification sheet, the material continues to cure much later. While preparing the samples for this aging study, preliminary test results showed that material samples were not 'fully-cured' at room temperature. Resultantly, material reflected curing behavior during the initial hours of aging. If *"fully-cured"* state is achieved before starting the aging process, it is termed as 'over-cured'; whereas, if "fully-cured" state is achieved after the aging process begins, it is termed as 'post-cured.'

Many recent investigations have shown that silicone elastomers, when aged, show an improvement in mechanical and thermal properties. This behavior has been attributed to post-curing phenomenon in high temperatures shortly after aging begins (initial 4 to 10 hours) [80][196][28]. In fact, it was recommended that commercial silicone elastomers should undergo short-term post-curing for mechanical, thermal, and electrical stability before being applied in service conditions [154]. Therefore, for this study, we have considered the over-curing of specimens as a pre-requisite before initializing the designed aging experiment. Conventionally, the post-curing phase is followed by the degradation phase [181]. Initial over-curing ensures that there is no post-curing during aging, and the only outcome of aging is seen in terms of degradation of the material matrix. In this study, for reference, we have implied aging up to 24hrs as 'short-term,' whereas 10 and 30 days of aging is referred to as the 'long-term' aging period.

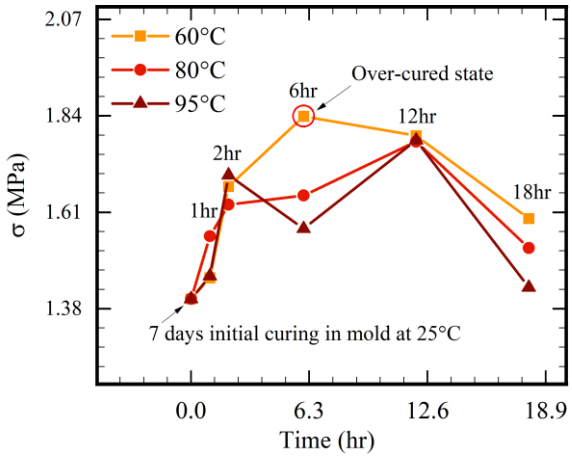

Figure 2.3: Stress variation during post-curing in 60°C, 80°C and 95°C after initial-curing at room temperature.

To study hydrolytic aging, the over-curing should be removed by the short-term aging under the same temperature of aging. The peak of material strength presents after the 6hrs aging at 60°C (see Fig. 2.3). In order to make sure that the material specimens were fully cured before aging began,

we conducted a short over-curing study on samples cured for 7 days at room temperature. After that, tensile strength declines, so 60°C 6hrs aging of PDMS-based adhesive is regarded as the over-cured state Samples were exposed to 60°C, 80°C, and 95°C for 1, 2, 6, 12, and 18 hours. Tensile failure test was carried out, and the time when test samples reflected peak stress was considered for preparing fully-cured samples. We considered a fully-cured state achieved after 6 hours in 60°C when the material reached the stress peak (see Fig. 2.3). For this study, fully-cured samples were considered un-aged, and the material behavior after subjecting the samples to hydrolytic environmental aging was considered for analysis as aged samples.

2.2.3 Aging procedure

To simulate actual long-term weathering conditions, we have resorted to the accelerated aging technique by time- temperature superposition. We conducted hydrolytic aging in laboratory controlled environment at elevated temperatures (i.e., 60°C, 80°C, and 95°C) to investigate the environmental damages incurred by the aged material. Plastic buckets were utilized as containers for aging in 60°C and 80°C. However, for 95°C, aluminum cooking pots were utilized. The temperature inside the containers was periodically checked using Fisher-brand digital thermometer model 15-077-9E (see Fig. 2.4). The thermometer has a water-proof thermo-probe with a 0.1°C accuracy. When checking the inner temperature, a special lid was used with an opening for the temperature-probe to hang inside (see Fig. 2.4b and c). The temperature was always found to be within ±2 of the desired temperature condition. In this regard, distilled water (i.e. distilled water with pH = 7) simulates high-humidity environments, and seawater (i.e. sea-salt solution with pH=8.2 [47]) imitates marine environment. Desired aging periods were 1 day, 10 days, and 30 days. Batches of ten specimens for each condition were immersed in aqueous solutions in sealed plastic buckets. Grit guards were placed under the specimens to ensure that the specimens were evenly exposed to the conditions from all sides (see Fig. 2.4). Samples were aged in ovens without light, so the effects of UV radiation could be excluded from the degradation of materials. Five samples were tested immediately after desired aging time finished.

2.2.4 Gravimetric measurement

To be able to interpret and better understand the dynamics of hydrolytic degradation, water absorption and resulting weight changes of test specimens were investigated at every critical stage of the experiment. Before submerging, the weight of each specimen was measured and recorded using an electronic scale with a precision of 0.1mg. At desired aging times, samples were removed from

containers and immediately blotted with tissue paper; after that, the weight of wet specimens was measured by the same scale. In this regard, we disregard the "typically" used mathematical expression for calculating the percentage of the water-uptake W_C, i.e.,

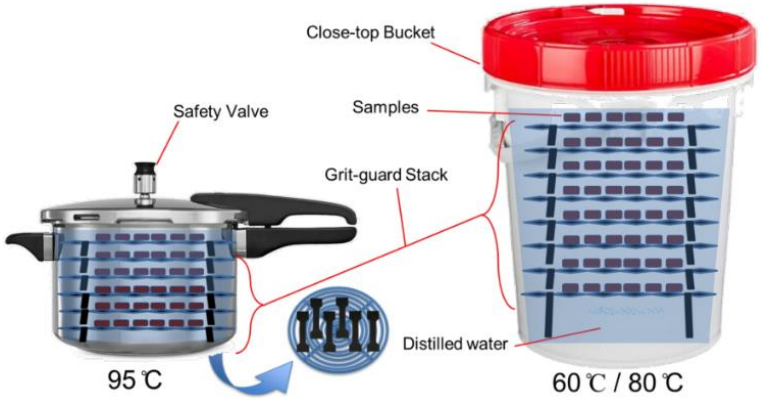

(a) Aging set-ups for 60°C, 80°C, and 95°C

(b) Special container lids for temperature check

(c) Temperature check in 60°C oven

(d) Temperature check in 95°C oven

Figure 2.4: Sample loading setup and temperature checking procedure.

$$W_c(\%) = \frac{W_t - W_0}{W_0} \times 100 \quad , \qquad , \qquad (2.1)$$

where W_t and W_0 are the sample weights at time t and unaged state, respectively. In this context, it is very critical to understand that the weight difference between starting weight (W_0) and the final weight (W_t) does not truly represent the amount of water absorbed. At best, it can be termed as an increase in weight due to water absorption only. This is an erroneous approach, especially in the case of hydrolytic aging since we are ignoring the mass-loss phenomenon due to thermal aging and the

leaching effect. For this reason, we consider that water-uptake W_C and mass loss (M_L) are closely related. For each aging condition, 10 specimens were used to allow for a reliable statistical depiction. For Wt, 5 specimens were weighed directly after removing from aging chambers. These were referred to as wet state samples, while the remaining 5 samples were referred to as dry after being dried in the vacuum oven. The dry weight is referred to as W_d. Samples were dried in a vacuum oven at 40°C at 700mmHg vacuum for 24 hours. Drying in vacuum oven was done to evaporate the absorbed water at a much lower temperature without adding further thermal fatigue to aged samples. This way, we could accurately measure the weight/ mass variations due to water absorption during aging. If a percentage of absorbed water shows a linear increase with the increase in temperature and time, it shall be considered in agreement with Fick's second law of diffusion, [87]. Through these gravimetric measurements, we probed relevant phenomena like mass-loss and absorption-desorption trends. The percentage weight of Water absorbed by specimens W_c was calculated using the following mathematical expression:

$$W_c(\%) = [\frac{(W_t - W_d)}{W_0}] \times 100 \quad , \qquad (2.2)$$

where W_t is the weight of the aged sample at time t, W_d is the dry weight after removing all water content, and W_0 is the weight of the unaged specimen. Samples generally maintained a similar dry weight, but it is possible that some water may remain confined within the matrix due to the interaction of functional groups with water molecules [173]. The mass loss (M_L) in the sample was measured by comparing the weight difference between the unaged specimen's weight with the weight of the aged sample after drying. The following mathematical expression was used to calculate the % M_L:

$$M_L(\%) = [\frac{(W_0 - W_d)}{W_0}] \times 100 \quad , \qquad (2.3)$$

where W_d is the weight of the aged sample in dry state, and W_0 is the weight of the unaged sample before placing in aging conditions.

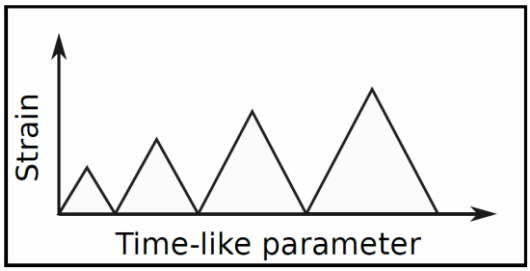

Figure 2.5: A schematic curve for cyclic tensile tests.

2.2.5 Mechanical test

A uni-axial universal testing machine (Test Resources 311 Series Frame) was used for quasi-static tensile tests of wet samples. All tests were displacement controlled with a crosshead speed of 50mm/min. The distance between the extensometer grips was set to 25.4mm and all the experiments were performed in room conditions (i.e., 27 ± 2°C, 50 ± 3% RH). Uni-axial tensile testing was done with 5 specimens each for reliability control. In monotonic failure tests, 3 samples were stretched until breakage. While in the cyclic test, 2 samples were continuously loaded by being stretched to preset amplitudes of 45%, 87.5%, 125% and 175% of elongation at the breakpoint of unaged samples. Due to aging effects, aged specimens may break before completing the desired cyclic amplitudes depending on the degree of damage. Each sample was subjected to a non-relaxing cyclic test with increasing amplitude, where the samples were loaded 3 times at each amplitude (see Fig. 2.5). During deformation, elongation of the central zone of 25.4mm (see Fig. 2.2b) has been measured by an external extensometer. The cyclic experiment was designed to illustrate the evolution of the permanent set and stress softening during the primary loading for both unaged and aged samples.

2.2.6 FT-IR

Various aging conditions inducing chemical alterations could be detected by FT-IR Spectroscopy on the specimen's surface. One sample per condition was tested by using Jasco FT/IR-4600 spectrometer; spectra were detected from 4000 to 500cm^{-1} at a resolution of 4cm^{-1} and an accumulation of 64. The angle of the incident was set at 45° with the monolithic diamond as the ATR prism.

2.2.7 DMA

Rectangular specimens (35 × 12 × 3mm) were customized and immersed in distilled water and seawater for 1 day, 10 days, and 30 days. After carrying out the visual inspection, one of the aged samples from each condition was selected and tested. Single cantilever tests to record storage modulus and Tan δ were performed on the TA Instrument DMA Q800 machine from −150°C to −70°C with a speed of 3°C per min. The test has been performed in the linear viscoelastic region (LVR) using strain amplitudes of 15% and a frequency of 1.0 Hz.

2.2.8 SEM

Morphology of unaged and 30-day immersed specimens was inspected by a scanning electron microscope (Zeiss EVO LS 25) with an accelerating voltage of 3.0kV. distilled water aging for 30 days was gauged by various micro-graphs on the tensile fracture surfaces of specimens.

2.2.9 Cross-Linking Density

The changes in cross-link density due to aging were observed by employing the equilibrium swelling method [89, 3, 170, 143, 55]. We used Toluene (molar volume 106.3mL/mol) as solvent to immerse unaged and aged rectangular specimens (0.4in × 0.3in × 0.12in). The test was performed with two samples submerged in the solvent for twelve hours. The sample weights were monitored and recorded every hour until a constant weight was reached, indicating maximum absorption of the solvent. Samples were removed from the solvent, patted to dry with paper-towel, and weighed again. The cross-link density (ν_c)(mol1/cm^3) and average molecular weights between the chains (M_c) were estimated using the following equations, introduced by Paul C. Hiemenz, Flory, and Rhener [86, 158, 64].

$$ln(1-\phi_e)+\phi_e+X\phi_e^2 = n_e\frac{V_1}{V_0}(\frac{\phi_e}{2}-\phi_e^{1/3}) \quad , \qquad (2.4)$$

$$\frac{n_e}{V_0} = \frac{ln(1-\phi_e)+\phi_e+X\phi_e^2}{V_1(\frac{\phi_e}{2}-\phi_e^{1/3})} \quad , \qquad (2.5)$$

where X is the solvent-polymer interaction parameter, and V_1 is the solvent's molar volume (106.3mL/mol). From equation 2.5, we can further derive equation 2.6,

$$\frac{n_e}{V_0} = \frac{\rho}{M_x}(1-\frac{2M_x}{M}) \quad , \qquad (2.6)$$

where ne is the molar cross-linking, V_0 Is the volume of the silicone adhesive samples before swelling, ϱ is the density of the solvent, M_x is the molar mass of the solvent, and M is the molar volume of the polymer. The measurement should not exceed ± 0.1 percent of the constant measurement, thus, maintaining high accuracy levels for elastomer density [57].

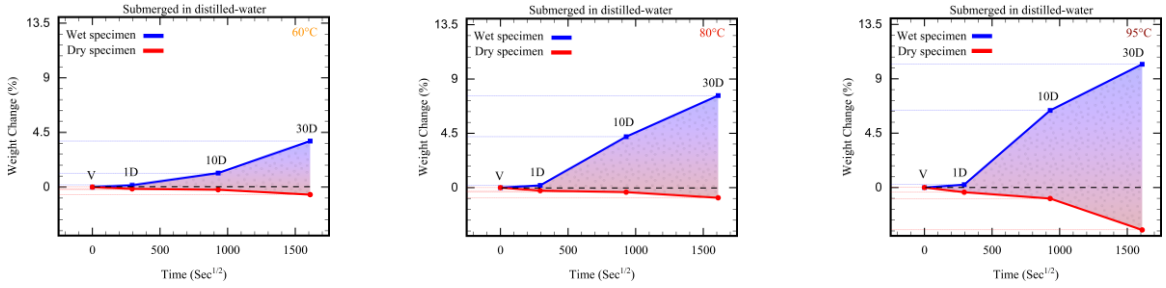

(a) Water up-take at 60°C (b) Water up-take at 80°C (c) Water up-take at 95°C

Figure 2.6: water-uptake of specimens aged in distilled water at (a) 60°C, (b) 80°C and 95°C.

2.3 Results and Discussion

2.3.1 Water-uptake

Fig.2.6 and Fig.2.7 show the gravimetric changes taking place during the aging of adhesive specimens due to water-uptake (absorption) and mass-loss (leaching effect). We compared water-uptake and mass-loss of specimens aged in distilled water vs those aged in seawater (see Fig. 2.8). It was observed that water-uptake in distilled water was much higher than in seawater, especially under high temperatures and longer aging duration (see Fig. 2.8a). We know that seawater, due to the presence of salts, is much denser than distilled water. The naturally occurring voids within the polymer matrix provided more accessible sites to distilled water for reaching deeper layers of polymer resin. However, the high density of seawater limited the water-uptake and gradually formed a protective salt barrier on the outer layer of specimens slowing down the water absorption process as aging proceeded (see Fig. 2.8b).

Since distilled water had deeper ingress and access to the polymer matrix, specimens aged in distilled water were subjected to aggressive water attack and plasticization. High water-uptake is expected to cause higher degradation in the polymer matrix. Therefore, in terms of mechanical behavior, it can be expected that specimens aged in distilled water shall endure a relatively higher degree of damage compared to the samples aged in seawater. Higher temperature caused an increase in water absorption, which resulted in higher mass loss due to the leaching effect [52]. The results also show a simultaneous mass-loss effect which is also attributed to the leaching effect. Higher water-uptake is expected to cause higher leaching as well. Fig. 2.8b shows a higher degree of mass-loss in distilled water which is proportional to the trend observed in water-uptake (see Fig. 2.8a).

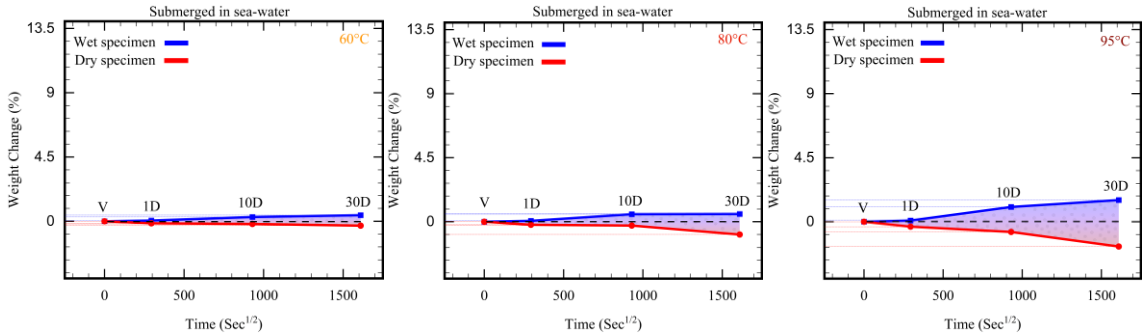

(a) Water up-take at 60°C (b) Water up-take at 80°C (c) Water up-take at 95°C

Figure 2.7: water-uptake of specimens aged in seawater at (a) 60°C, (b) 80°C, and (c) 95°C.

Data shows that water-uptake in the case of the specimen being submerged in distilled water and seawater. is linearly correlated with the square root of aging time (i.e., $W_c \propto \sqrt{t}$), representing that

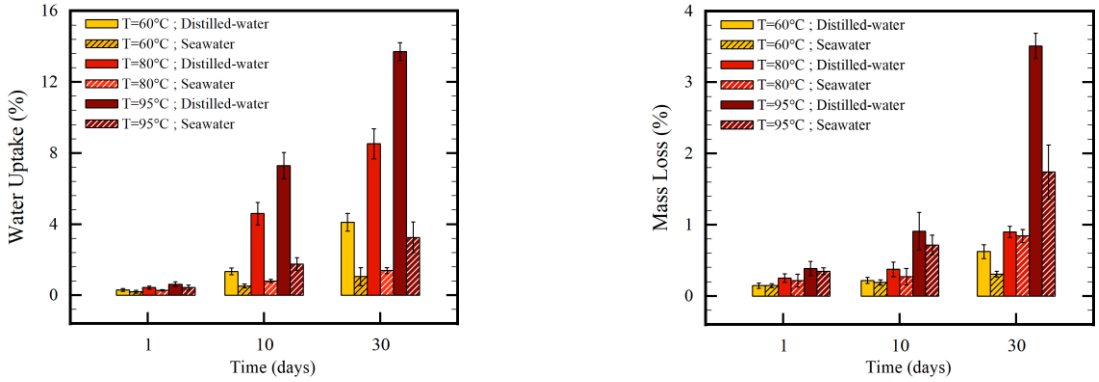

(a) water-uptake (b) Mass loss

Figure 2.8: The comparison of (a) water-uptake and (b) Mass loss for specimens in distilled-water.

it follows Fick's second law [142]. In this respect, Crank and Park [45] provide an analytical solution to characterize the water-uptake of a thin plate sheet

$$\frac{M_t}{M_\infty} = 1 - \sum_{j=0}^{\infty} \frac{8}{(2j+1)^2\pi^2} \exp\left[-\frac{D(T)(2j+1)^2\pi^2 t^2}{4h^2}\right] \quad , \qquad (2.7)$$

where D(T) is the diffusion coefficient factor which itself is a function of temperature T , M∞ and Mt are the mass uptake of the sheet at saturation and time t, respectively, and h is the sample thickness. For super-thin samples (i.e., $D_t/h^2 < 0.05$), the Eq. 2.7 can be reduced to

$$\frac{M_t}{M_\infty} = \frac{4}{h}\sqrt{\frac{D(T)t}{\pi}} \quad , \qquad (2.8)$$

From Eq. 2.8, the diffusion coefficient D can be found by calculating the slope of water-uptake versus the square root of time (see Fig. 2.9a). The amount of equilibrium water content M∞ and diffusion coefficient D for different aging temperatures in distilled water are listed in Table 2.1. As it can be seen, raising the temperature accelerates the diffusion of water molecules into the polymer matrix which causes both parameters of Fick's diffusion law (i.e., D and M_∞) to increase.

By representing the evolution of the diffusion coefficient factor by the Arrhenius function [54], one can write D(T) as:

$$D(T) = D_\infty \exp\left(-\frac{E_a}{\mathcal{R}T}\right) \quad , \qquad (2.9)$$

where E_a is the activation energy, and R = 8.314[J]/[mol][K] the gas constant. By substituting D(T) in Eq. 2.8, one can rewrite Fick's diffusion law as follows:

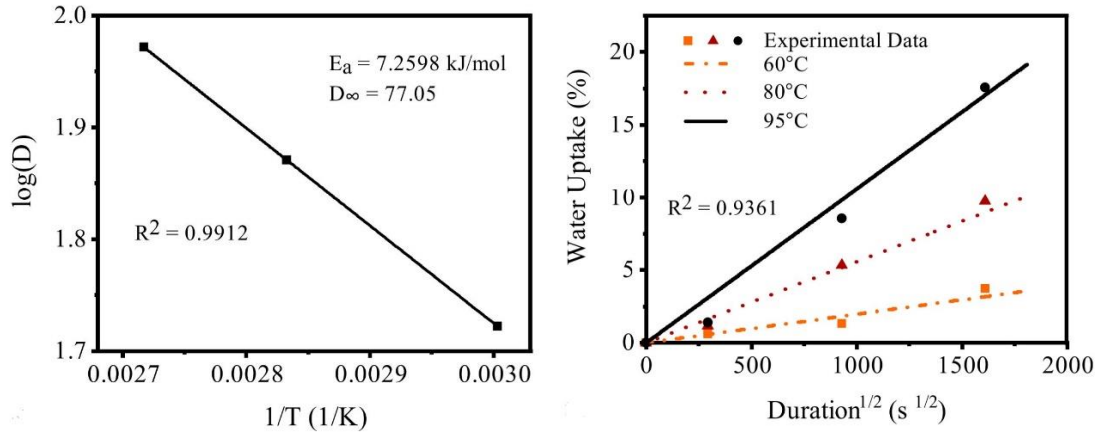

(a) (b)

Figure 2.9: Prediction of (a) the diffusion coefficient factor, and (b) the water-uptake for a different amount of aging time and temperatures.

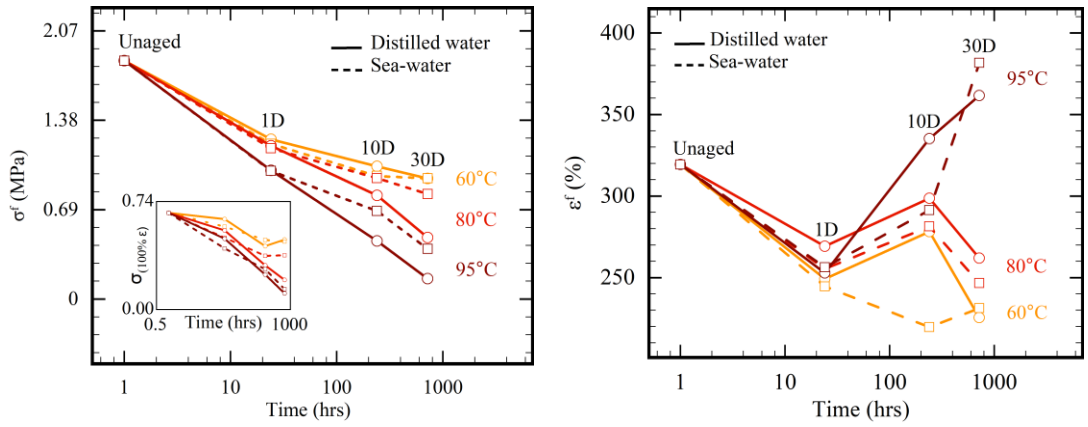

(a) Failure Stress σ_f variation against time (t) (b) Failure strain ϵ_f (%) variation against time (t)

Figure 2.10: The (a) stress and (b) strain comparisons of specimens aged in distilled water and seawater.

$$\frac{M_t}{M_\infty} = \frac{4}{h}\sqrt{\frac{D_\infty \exp\left(-\frac{E_a}{RT}\right) t}{\pi}} \quad , \qquad (2.10)$$

To assess the capability of the proposed method, its predictions were bench-marked against our experimental results, which were mainly designed to show the effects of water-uptake. To this end, the Levenberg -Marquardt algorithm was used to minimize the least square error function R2. The prediction of the diffusion coefficient factor is plotted versus its experimental values in Fig. 2.9a, while the prediction of the water-uptake against the experimental diagrams for a different amount of aging times and temperatures are plotted in Fig. 2.9b.

2.3.2 Damage

In this section, we shall perceive degradation in the polymer matrix with respect to two different damage mechanisms induced by i) mechanical, and ii) environmental stresses.

a. During mechanical damage which mostly encompasses physical changes, the continuous loading can lead to the detachment of chains from either cross-linked or aggregate surfaces and reform the composition of the polymer matrix with a longer chain.
b. In the course of environmental damage in absence of the deformation-induced damage, aging occurs mostly as a chemical process by reducing the polymer active agents which are directly involved in the rubber elasticity.

Generally, environmental elements along with the mechanical loads will contribute to chemo-physical deterioration that will eventually lead to showing decay in the mechanical behavior of the material. Understanding the correlation between environmental-induced damage and decay in mechanical performance is critical for the prediction of cross- linked polymers. Hereafter, we investigated the accumulative contribution of mechanical and environment-induced damage to silicone adhesives, by performing cyclic tensile tests on aged specimens.

Table 2.1: The coefficient of diffusion D and the equilibrium water absorption content M∞ of the silicone adhesive in three different aging temperatures.

Parameter	60°C	80°C	95°C
$M_\infty(\%)$	3.7175	9.7438	17.5761
$D \times 10^7 (mm^2 s^{-1})$	5.569	6.554	7.1501

Environment induced damage

The variation of tensile strength σ_f, as well as elongation at break ϵf versus time t in the case of distilled water and seawater are given in Fig. 2.10. The tensile strength of silicone-based adhesives (σ_f) decreases over time for both distilled and seawater (see Fig. 2.10a). The temperature of 95°C proved to be too aggressive for RTV silicone adhesive such that the specimens after 30-days aging could barely sustain any load while exhibiting high elongation. This is due to the fact that high temperature causes water to act as a plasticizer which caused chain scission and engendered low-molecular-weight chains [113]. The ϵf (see Fig. 2.10b) has been equally influenced by both distilled and seawater aging media. Seawater, being more corrosive in nature, inflicted a higher loss of σ_f during the first 24 hours in all temperatures (see Fig. 2.10a). But this phenomenon was soon reversed due

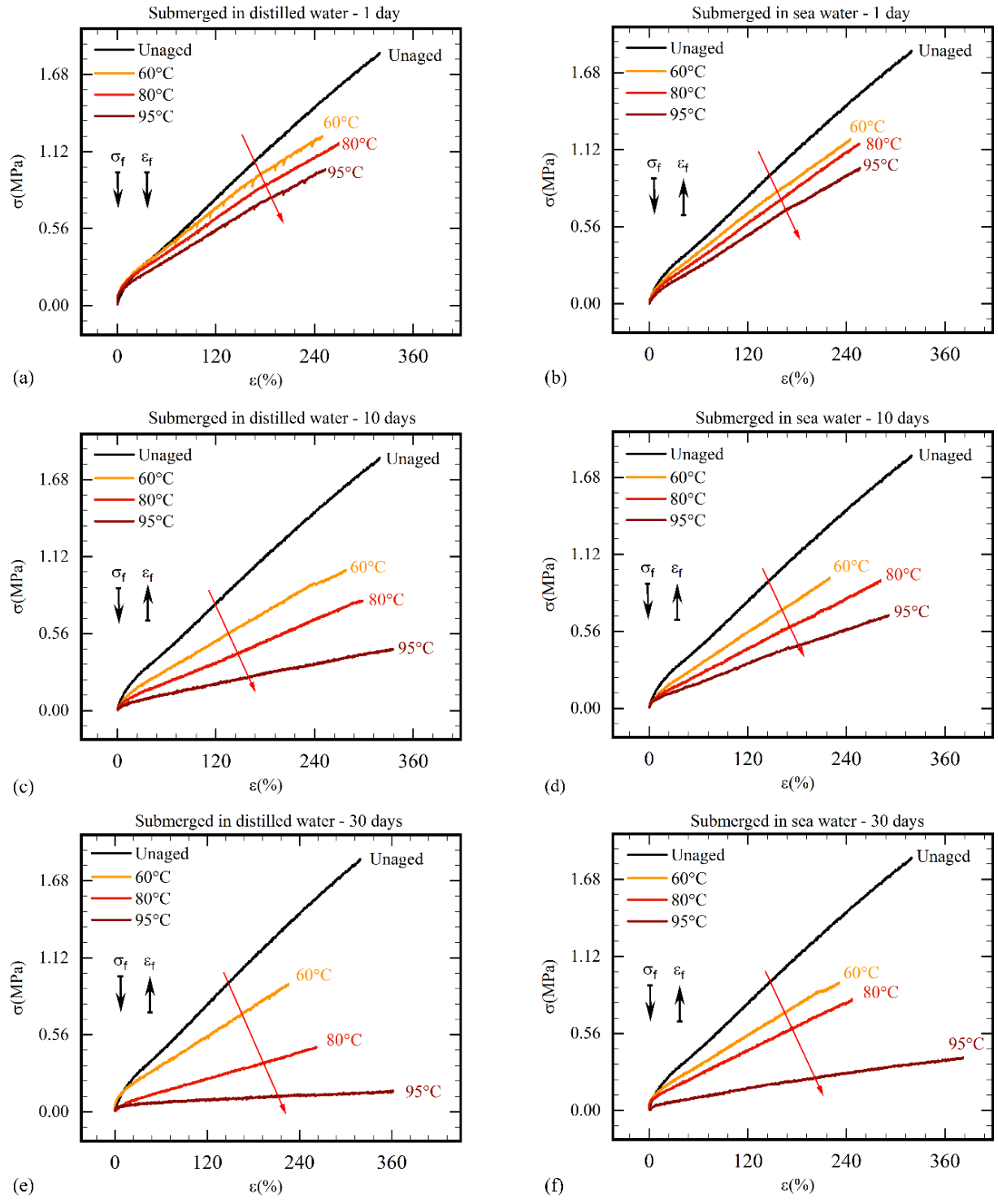

Figure 2.11: Stress vs strain curves for specimens submerged in distilled and seawater at (a)(b) 60°C, (c)(d) 80°C and (e)(f) 95°C, respectively.

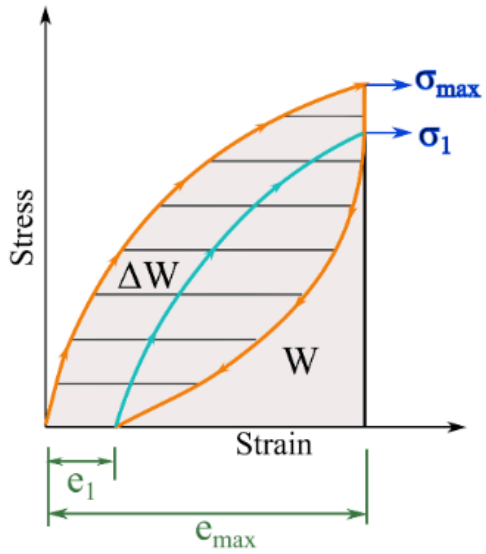

Figure 2.12: Schematic representations for relative stress softening, relative residual strain, and hysteresis loss.

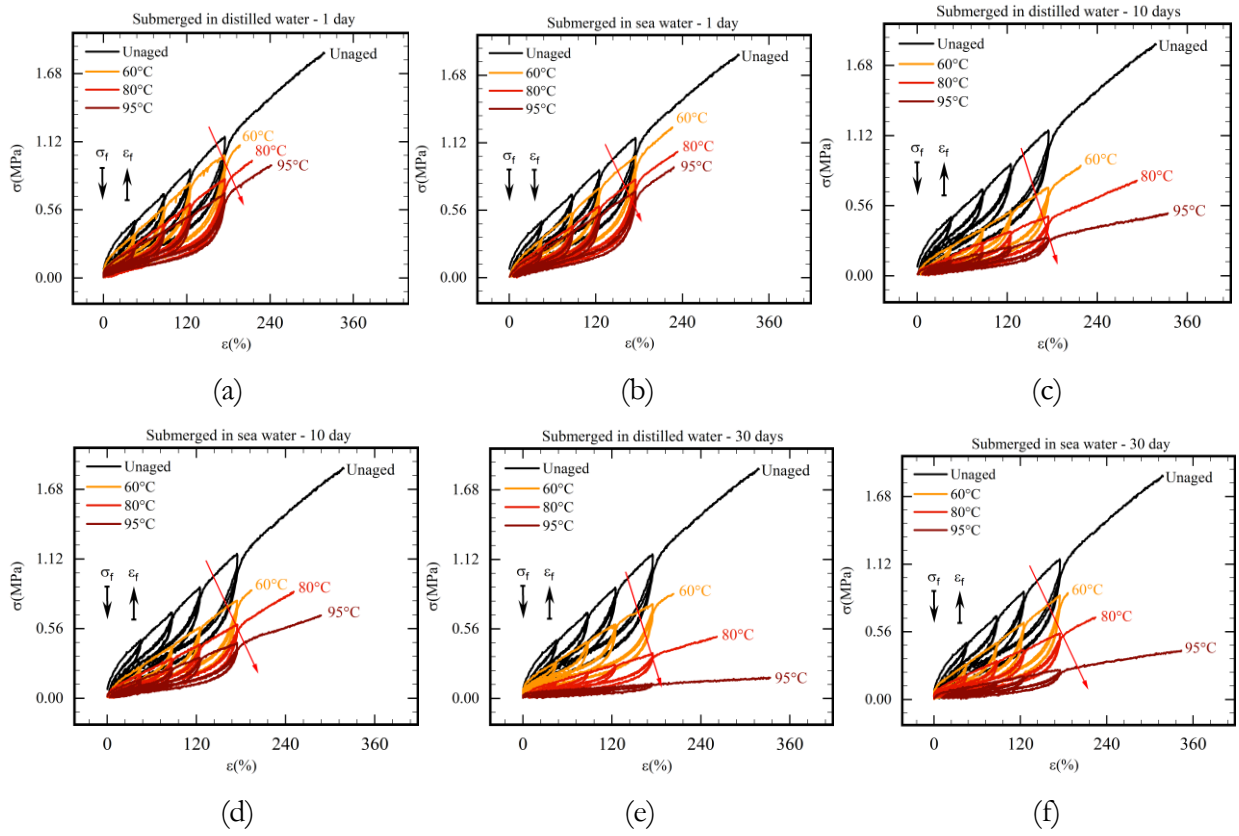

Figure 2.13: Comparison of stress strain behavior between distilled water aging and seawater aging, (a,b) 1-day, (c,d) 10 days, and (e,f) 30 days.

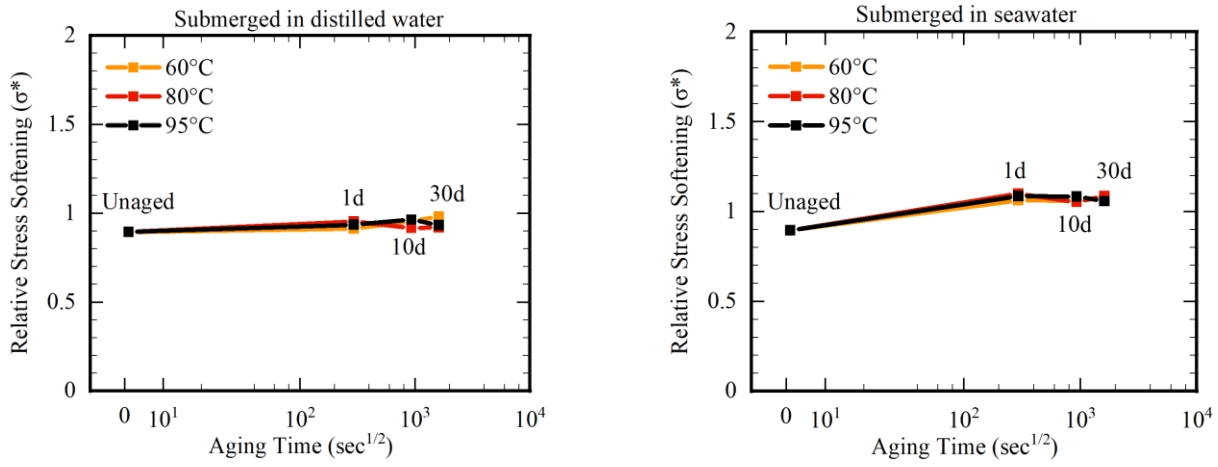

(a) (b)

Figure 2.14: Relative stress softening for (a) distilled water, and (b) seawater in 45% strain.

to slower diffusion of seawater owing to higher density and formation of salt barrier at vulnerable gaps in the polymer matrix.

The constitutive behavior of unaged and aged specimens is shown in Fig. 2.11. Specimens show elastic behaviors, despite going through various aging conditions. Softening behaviors and less ductility are attributed to hydrolytic aging. 95°C 30-days aging caused specimens to be more stretchable and sustain lower loads.

Deformation-induced damage

To isolate the effects of hydrolytic aging from those of mechanical damage in silicone adhesive, cyclic tensile tests have been performed on aged samples. Therefore, relative stress softening σ^*, relative residual strain e^*, and hysteresis loss W^* are utilized to eliminate the effect conducted by the assigned strain for each cycle.

Firstly, relative stress softening $\sigma*$ is defined as the ratio of the stresses at the maximum strain of second cycle σ_1 (see Fig. 2.12) to the stress at the same strain value of the first cycle σ_{max} (i.e., $\sigma^*=\sigma_1/\sigma_{max}$) both referred to the same aging condition.

The relative stress softening has not been altered by hydrolytic aging within either distilled water (see Fig. 2.14a) or seawater (see Fig. 2.14b) at the strain of 87.5%. In other words, relative stress softening is the stress comparison between loading and reloading periods. During loading, fillers would be oriented along applied force and entangle with polymer chains. After that, the entanglements prevent the fillers from retracting fully to the initial state due to the presence of knots [65]. When reloading presents, less stress value is required to re-orient and re-entangle fillers and

polymer chains. Hydrolytic aging under intense heat scarcely influenced the ratio of the reloading stress to the loading stress in 87.5%.

Secondly, relative residual strain e* can be interpreted by residual strain after the first cycle e_1 (see Fig. 2.12) over the maximum strain e_{max} (i.e., $e^* = e_1/ e_{max}$). During aging in temperatures 60°C and 80°C, both distilled and seawater mediums could not exert overt changes in material properties (see Fig. 2.15). The formation of entanglements during the loading phase may constrain the retraction of fillers, which is depicted in the form of residual strain. Hydrolytic aging in lower temperatures likely caused the specimens to generate chemical cross-links, which may have impeded the materials' reverse motion. However, in 95°C, especially in distilled water (see Fig. 2.15a), accumulating time effects caused a considerable increment of relative residual strain. For all aging conditions, except 30 days in 95°C, environmental damage and mechanical damage are separable with little error (acceptable error 10%). But in the case of 95°C for 30 days in hydrolytic aging, aging conditions

Lastly, the relative hysteresis loss W* is written as the ratio of the dissipated energy in the first cycle ($\Delta W = \int_{loading}\sigma de - \int_{unloading}\sigma de$) to the whole work input $W = \int_{loading}\sigma de$ which is depicted in Fig. 2.12 (i.e., $W^* = \Delta W/W$). In fact, the relative hysteresis loss reflects how much energy is dissipated due to bond breakage during cyclic tensile tests in each aging condition. The variations are shown in hysteresis loss for distilled water (see Fig. 2.16a) and seawater (see Fig. 2.16b). Besides, the increment of hysteresis loss at 95°C is a reflection of breaking chemical bonds owning to loss of chain mobility, corresponding to decreasing peak of Tan δ shown in Fig. 2.18, which is in agreement with the study of Abd-El et al. on filled silicone rubbers [1].

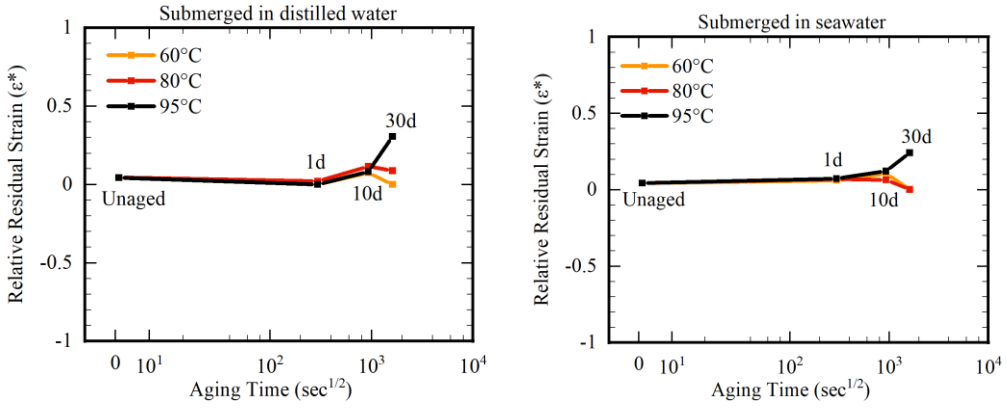

(a) (b)

Figure 2.15: Relative residual strain for (a) distilled water, and (b) seawater in 87.5% strain.

95°C proved to be too harsh for the material and the material matrix can be considered as fully annihilated. This high degree of damage to the material matrix is the main cause for an unusual increase in residual strain after aging at 95°C after 30 days.

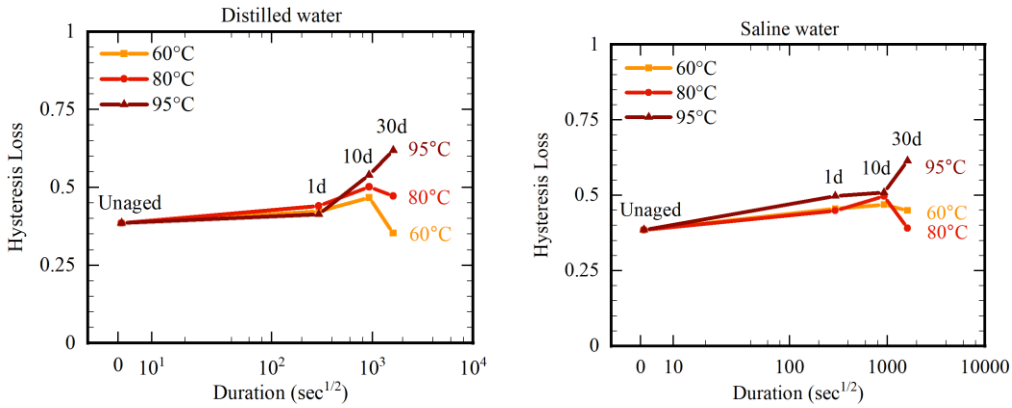

(b) (b)

Figure 2.16: Hysteresis loss for (a) distilled water, and (b) seawater in 87.5% strain.

From another perspective, the relative stress softening, residual strain, and hysteresis loss of PDMS-based adhesives eliminated the softening behaviors induced by hydrolytic aging. Moreover, the structural changes that occur during hydrolytic aging are capable of being decomposed by cyclic loading. Therefore, the constant values shown in Fig. 12-14 between unaged and aged adhesives indicate the independent nature of deformation induced damage from aging degradation effect. Specimens aged at 95°C for 30 days are regarded as annihilated.

Table 2.2: Assignments and wave range corresponding to FT-IR spectra peaks.

Peaks in cm^{-1}	Range in cm^{-1}	Assignments
3386	3400-3200	Si−OH
2965 & 2911	3000-2840	CHst
2847	2840	$Si-OCH_3$
1577 & 1539	1610-1550	Ringskeleton
1410	1410	$Si-CH=CH_2$
1258	1275-1260	CH_3
1082 & 1007	1130-1000	Si−O−Si
868	900-800	Si−OH
786	865-750	$Si-CH_3$

Distilled water penetrated silicone adhesive and gradually generated chemical reactions with material molecules. At the wave number of 1410 cm^{-1}, in most of the aging conditions, spectra are slightly curtailed after desired aging periods under high temperatures (see Fig. 2.17a). Yet, 95°C 30-days hydrolytic aging with an increment of absorbance could result from re-crosslinking. Immersion

medium with pH = 7 barely caused chemical reactions of silicone adhesive, which is in agreement with the studies by Alok et al. [179] and Liao et al. [121, 120], showing that silicone elastomers are largely stable w.r.t time and temperature. On the contrary, it has also been reported that silicone degradation is higher in submerged medium [188] depending upon the type of filler used. While silicone is known for its stability and hydrophobic nature, if the filler used is hydrophilic, it contributes to adverse degradation effects on the material's sustainability and performance in a hydrolytic environment [180]. Although the manufacturer did not release information about the filler used in Dow Corning 7091, looking at the water-uptake, physical changes, and mechanical test data, it can be deduced that the filler used in this silicone adhesive developed an affinity for hydrophilic reactions at the higher temperature.

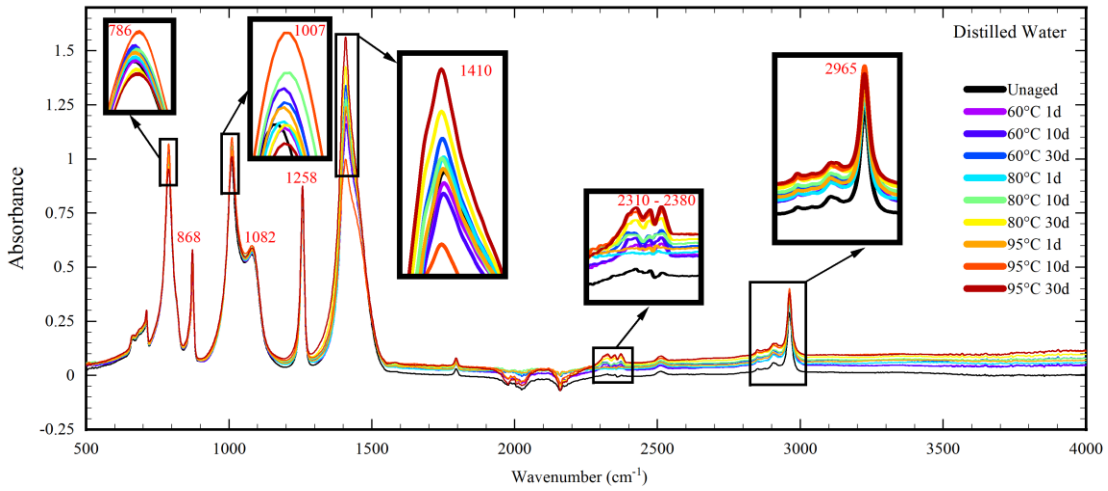

(a)

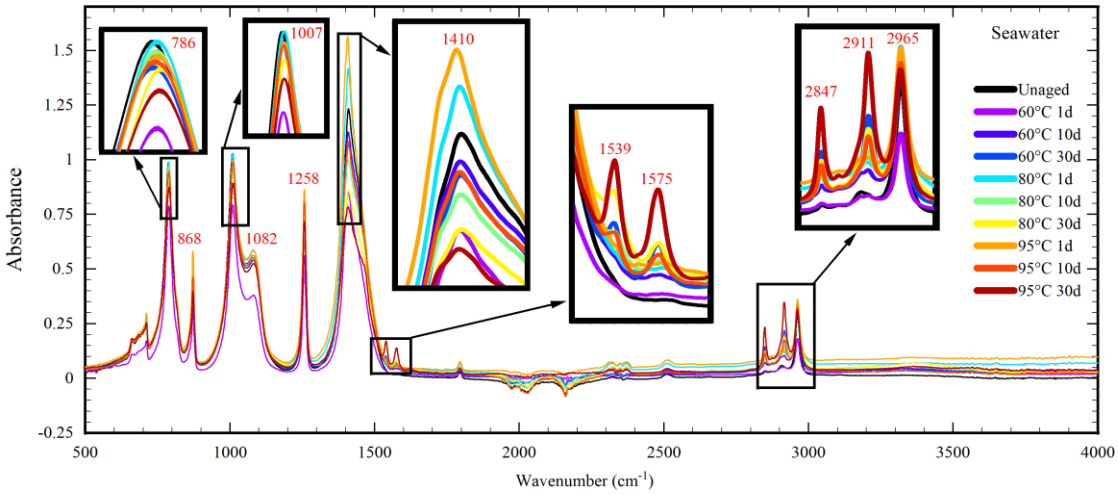

(b)

Figure 2.17: The FT-IR spectra of unaged and aged specimens through various durations and temperatures within (a) distilled water and (b) seawater.

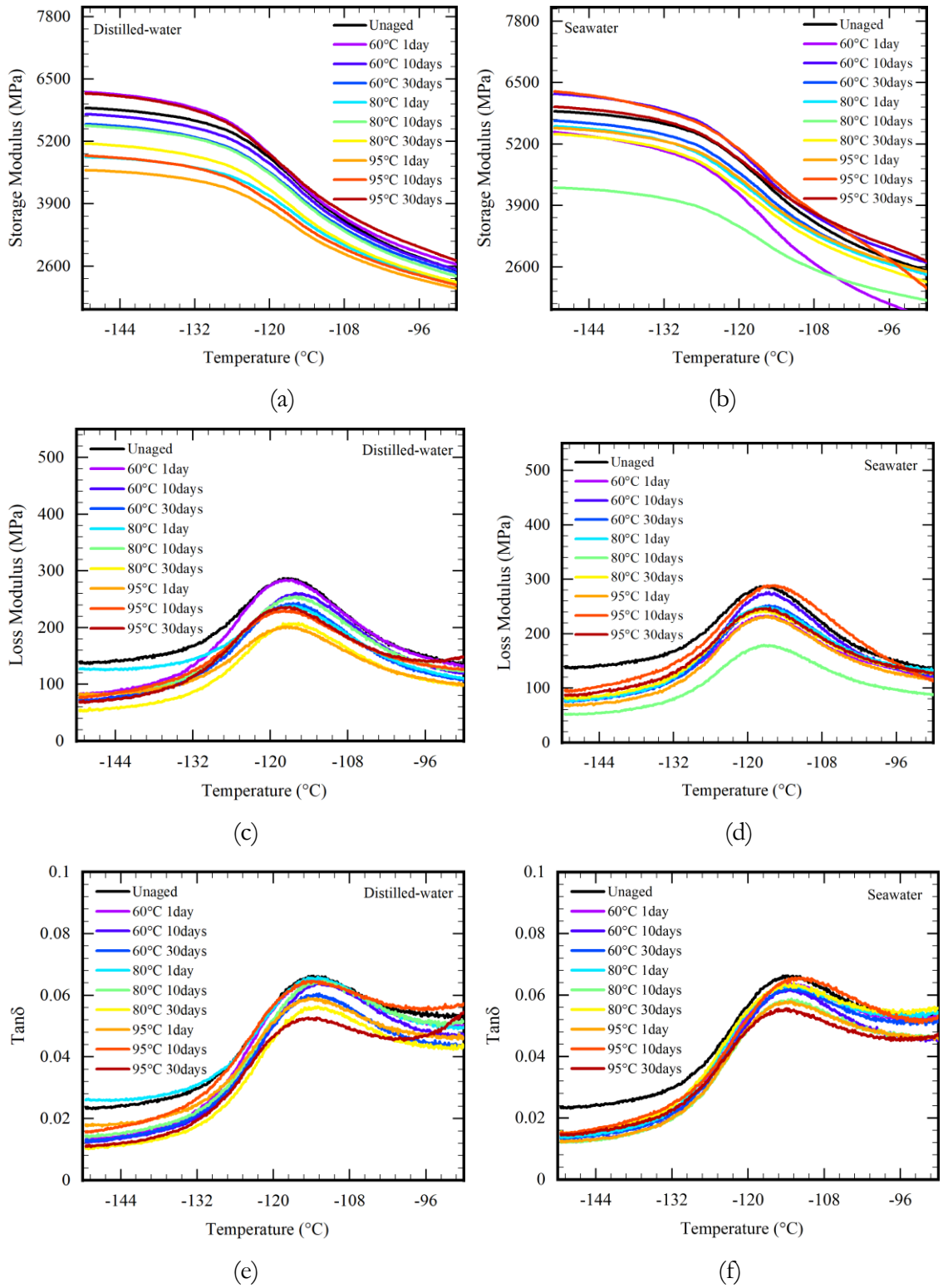

Figure 2.18: Storage modulus variation aged within (a) distilled water and (b) seawater, loss modulus changes of (c) distilled water and (d) seawater, and Tan δ changes due to (e) distilled water and (f) seawater aging.

In this regard, at the wave numbers 786 cm^{-1}, ($Si-CH_3$), 868 cm^{-1}, (Si−OH), and 1007 cm−1, (Si−O−Si) the absorbance has been reducing with increase in severity of aging condition. These are all main functional groups indicating loss of cross-links subsequently removed through leaching process and possible chain scission.

Degradation in the main-chain elements is visible in mechanical test results with a prominent drop in failure stress parameter (see Fig. 2.10). For specimens submerged in seawater (see Fig. 2.17b), the peak at 1410 cm^{-1} exhibits a wider range of intensity than spectra from specimens aged in distilled water. The band of 2847 cm^{-1} indicates $Si-OCH_3$ is present inside the adhesive after aging. The increased quantity of $Si-OCH_3$ combined with Si−OH caused new cross-links. Now considering the peaks that increased while the adhesive was exposed to seawater, the salt contaminants show escalated intensity at 2911, and 2965 cm^{-1} which represent C−H stretching vibrations in methyl group [111][23]. Besides that, the new structure, named ring skeleton, generated in seawater aging is in accordance with the bands appearing at 1539 and 1575 cm^{-1} [9]. The absorption peaks at 1539 cm^{-1} are assigned to the stretching vibrations of C=O in -COO- [149]. It must be given due consideration that the increase in the peaks is, in other words, related to a decrease in the value of transmittance. Thereby implying that the chain density within the matrix became dense with new functional groups showing presence. Compared with specimens aged in distilled water, seawater-aged specimens displayed relatively better mechanical properties (see Fig. 2.10a).

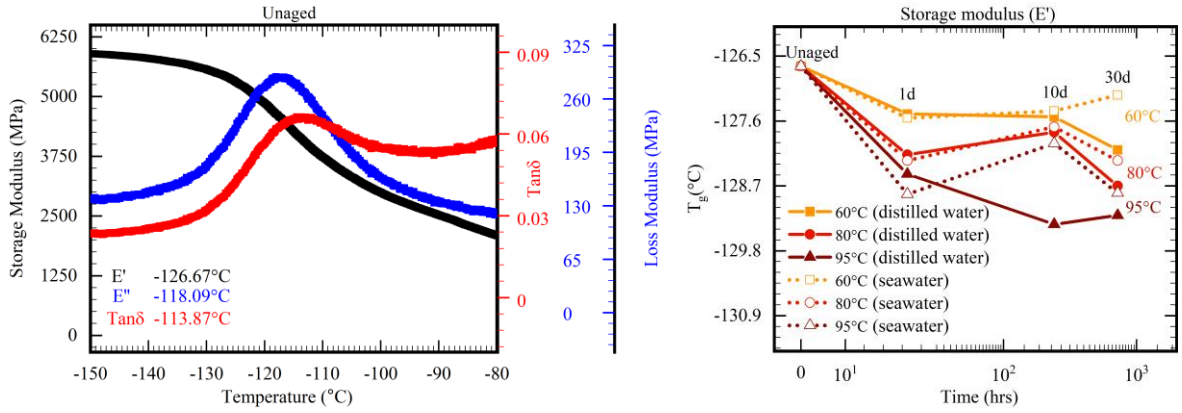

(a) (b)

Figure 2.19: Glass transition temperature from DMA testing (a) Un-aged specimen, and (b) Comparison of T_g calculated from storage modulus (E') of samples aged in distilled water and seawater.

2.3.4 DMA analysis

Fig. 2.18 shows DMA results of unaged and aged specimens with distilled and seawater. The storage modulus E', the loss modulus E" and the phase lag Tanδ of specimens aged in distilled and seawater are compared in Fig. 2.18 a-f, respectively. Storage modulus curves characterize the transition from glassy to rubbery behavior of materials and obtained glass transition temperature T_g as a significant factor, which is displayed in Fig. 2.19. Loss modulus is the dissipated energy switched to heat for each cycle of sinusoidal deformation. Tan δ, which reflects the molecular level changes, is the ratio of loss modulus to storage modulus E"/E'. The peak height of Tanδ reduced due to the decline of molecular mobility [161, 60]. Hydrolytic aging plays a significant role in the hindrance of chain motions.

T_g of unaged and aged specimens was determined by the onset point of storage modulus. The left-shifted onset points of storage modulus represent the reduction of T_g. Meanwhile, the peak of loss modulus and Tanδ, the other manners of measuring T_g, shifted left. In general, for the specimens submerged within distilled water, declining of T_g from −126.67°C to −128.09°C, −128.70°C, and −129.20°C proves the plasticization in materials during hydrolytic aging, which coincides with tensile properties of materials (see Fig. 2.19 and Fig. 2.10).

Table 2.3: The water-uptake and T_g of specimens for distilled water under various temperatures.

Aging condition	Aging time (days)	water uptake(%)	T_g (°C)
60°C & distilled water	0	0	−126.67
	1	0.23 ± 0.045	−127.48
	10	1.15 ± 0.253	−127.53
	30	3.79 ± 0.223	−128.09
80°C & distilled water	0	0	−126.67
	1	0.18 ± 0.024	−128.17
	10	4.22 ± 0.427	−127.79
	30	7.62 ± 0.585	−128.7
95°C & distilled water	0	0	−126.67
	1	0.15 ± 0.075	−128.5
	10	6.38 ± 0.202	−129.35
	30	10.20 ± 0.452	−129.2

It is known that the absorbed moisture in the matrix can impact the material's thermo-mechanical properties, and the variations in glass transition temperature are attributed to the resulting changes in the chemical structure of the resin [26, 148, 162, 187, 189]. Hence, aging under elevated temperatures results in promotion of water absorption and consequently reduction of T_g (see Fig. 2.19b). Table 2.3 summarizes the values of T_g and water content for various aging conditions in distilled water. Fig. 2.19b also highlights an interesting decrease-increase-decrease trend in T_g which resonates with the trend observed in failure strain variation as well (see Fig. 2.10b). We interpret the

decrease-increase-decrease trend in T_g as three stages of aging that the adhesive matrix undergoes, namely (i) plasticization, (ii) leaching, and (iii) degradation. During stage-1 of aging, water acted as a plasticizer and depressed the T_g (see Fig. 2.19b) [181]. In stage 2, once sufficient water was absorbed by the polymer matrix, small material fragments acting as matrix plasticizers began to leach out. This leaching resulted in reduced mobility of the main chain, thus causing an inverted or increasing trend of T_g [31]. Beyond a certain point, the final degradation process begins, which is considered stage-3, in which plasticization appears dominant. At this stage, multiple hydrolytic damage mechanisms are simultaneously involved in severe degradation and loss of integrity within the polymer matrix, ultimately resulting in the decrease of T_g (see Fig. 2.19b) and increase of failure strain (see Fig. 2.10b).

2.3.5 SEM analysis

SEM analysis has been done to study the failure type of samples after aging in both seawater and distilled water environments. Fig. 2.20 shows the failed samples with their respective SEM images after uni-axial tensile tests have been conducted on unaged and aged specimens after 30-days of aging at temperature 95°C in seawater and distilled water. Scope of 10μm and 2μm on the tensile fracture surfaces was analyzed to study the detrimental effect induced by hydrolytic aging. As depicted, the unaged sample failed with an approximate 45° inclination which is one of the characteristics of soft material's failure (see Fig. 2.20a). SEM figures confirm this observation by presenting a high volume of microparticles on the failed sample surface (see Fig. 2.20b, c). These micro-particles are fillers added to the resin to improve the adhesion of glass surfaces with plastic, metal, and ceramic surfaces.

While the nature and type of filler have not been disclosed by the manufacturer, the agglomerated matrix appearance in SEM figures shows their hydrophilic nature, which is in agreement with the gravimetric analysis showing water-uptake during the aging process. Furthermore, distilled water caused the material to move even further in the direction of soft failure. As it can be seen, in the most extensive case, the material almost lost its structural integrity, became like gum, and then failed due to rupture. On the other hand, seawater interestingly shifted from the failure type to fracture type failure. One of the most essential characteristics of this failure type is that the failure surface is like a clean-cut perpendicular to the loading direction, which is almost the case in Fig. 2.20g. Furthermore, SEM pictures of the failed surface also add more certainty to this observation as they have relatively fewer surface particles than unaged and distilled cases. This observation also can be concluded from the fact that elongation at breaks tends to increase in distilled water, while their trend is almost the opposite in a seawater environment. This trend agrees with SEM observations.

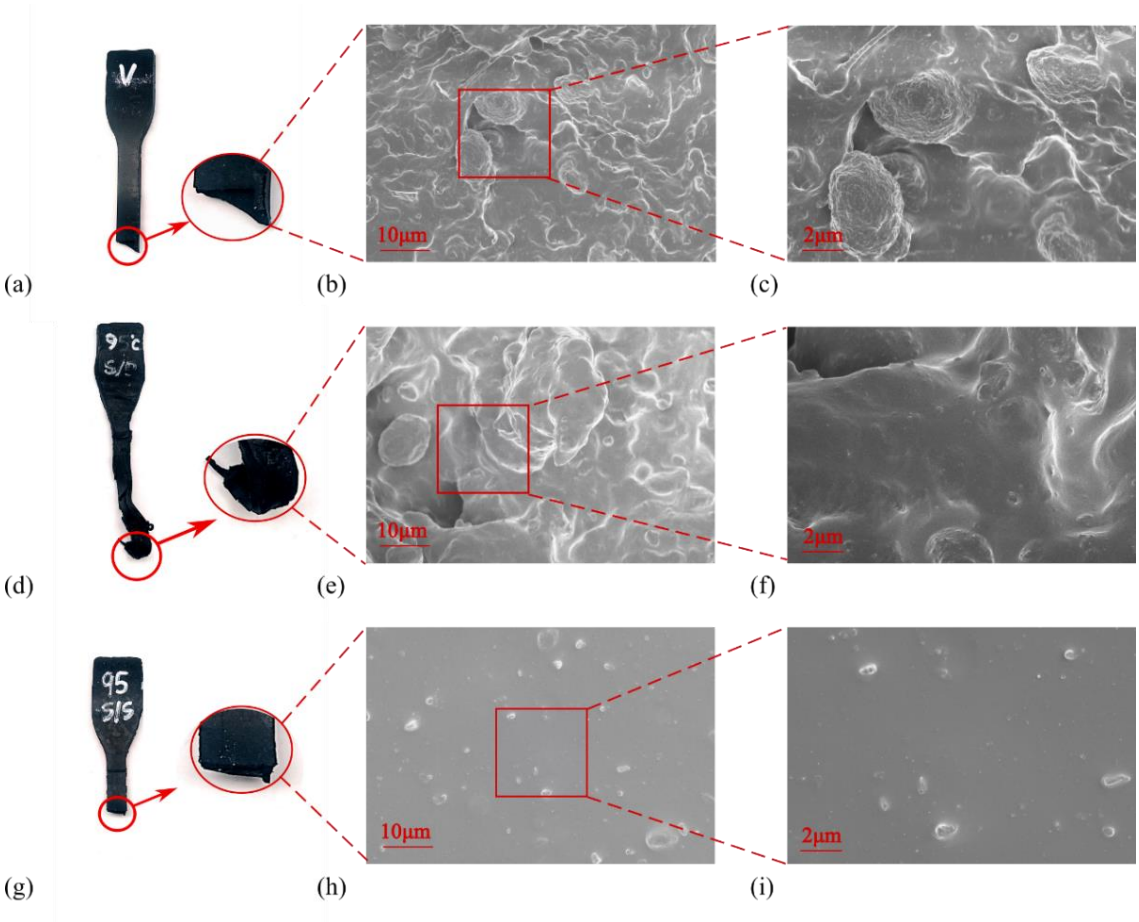

Figure 2.20: Failure samples and SEM micro-graphs of tensile fracture surfaces of (a), (b), and (c) unaged specimens, (d), (e), and (f) specimens aged within distilled water at 95°C for 30 days, and (g), (h), and (i) specimens aged within seawater at 95°C for 30 days.

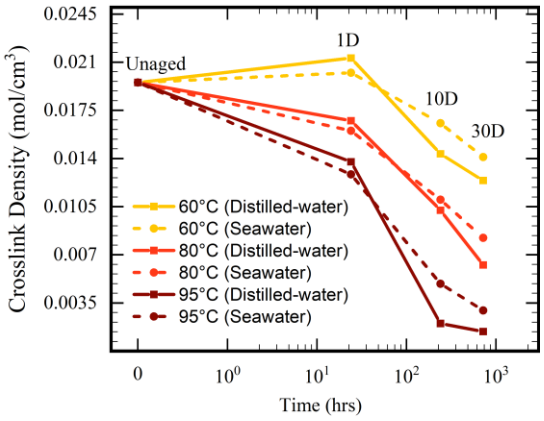

(a) Cross-link density variation in silicone adhesive specimens submerged for aging in distilled and seawater at 60°C, 80°C, and 95°C

(b) Specimen in Toluene during cross-link density testing.

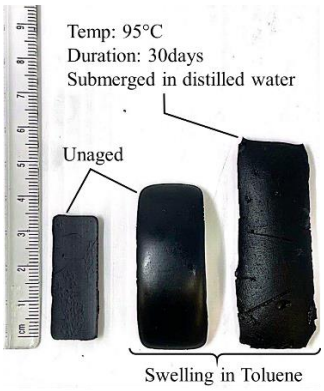

(c) Swelling comparison of unaged and aged samples

Figure 2.21: Cross-link density analysis.

2.3.6 Cross-link density analysis

Before immersing the samples in Toluene for carrying out cross-link tests (see Fig. 2.21b), all aged specimens were dried because the presence of water within the polymer matrix can be misleading by demonstrating relatively lower and incorrect solvent absorption. False weight change in specimens can give an impression of higher cross-link formation resulting from a low solvent absorption rate. Tensile tests depicted higher degradation in specimens with an increase in severity of aging conditions (see Fig. 2.10). A similar phenomenon was observed in cross-link density testing, i.e., cross-link density decreased with an increase in aging time and temperature (see Fig. 2.21a). Specimens displayed higher swelling as the aging temperature and duration increased (see Fig. 2.21c). On average, equilibrium weight was gained after 5±1 hours, and equilibrium weights were recorded at least for another 4-5 hours to calculate cross-link density accurately.

The results showed an interesting resemblance with the trend seen in stress decline (see Fig. 2.10a and Fig. 2.21a). All aging conditions after day 1 show a higher loss of cross-link density for specimens aged in seawater compared to the ones aged in distilled water. This shows that seawater is more corrosive due to a higher concentration of salts. Still, the higher density of seawater complemented by the formation of a protective salt layer on the samples' outer surface slowed down seawater's ingress into the matrix. Therefore, in cases of 10 and 30 days of aging, we observed a relatively higher cross-link density loss in samples aged in distilled water. Cross-link density variation was found to agree with trends observed in tensile tests, confirming that material degradation is higher in the case of distilled water in the long term.

2.4 Conclusion

This research investigated the accumulated damage during hydrolytic aging in the distilled and seawater in silicone-based adhesives. We observed that mechanical and environmental damage are independent by doing multiple mechanical and chemical tests and analyses. The material behavior was characterized by water-uptake, failure/ cyclic tensile tests, FT-IR spectroscopy, DMA, SEM, and cross-link density analysis. Multiple characterization methods helped us understand the mechanisms involved in material degradation and damage during the aging process.

Gradual increment of water-uptake causes an increase in elongation at break and reduced tensile strength of aged specimens. This increase in elongation at break results from the consistent expansion of the plasticization phenomenon, which has been verified by decreasing T_g and morphological graphs. On the other hand, in seawater, water-uptake started decreasing after a specific

aging time. This could be considered the effects of protection barriers by precipitation of sea salt and leaching due to cross-link and chain scission. It is noteworthy to mention that in the seawater solution, due to its higher pH value, degradation of materials is more overt in one-day aging and comparatively gentle in its reduction during further aging than in distilled water, which further augments the protective barrier theory.

Chapter 3:

Investigation of hygrothermal aging on the polyurethane-based (PUB) adhesive: substantiating competition scenario between sub-aging thermal oxidation and hydrolytic phenomena

3.1 Introduction

Polyurethanes are a special type of polymers that exhibit a wide range of mechanical properties [3], and there are several published references that describe their physical and chemical behavior [99, 84]. Due to their flexible application, high reactivity, superior mechanical and adhesive properties, and weathering resistance, polyurethane resins have always been a popular choice in industries [157, 27]. In particular, polyurethane is utilized in the automotive industry for joining components since the obtained joints are resistant to petrol, oils, greases, and water [183, 136]. Among a widespread population of elastomers [43, 137, 121], polyurethanes are prominently regarded as a material of choice because, over the period, it has proved to be a versatile and sustainable problem solver for the challenges of modern age [176, 53, 67]. These materials are currently finding increasing applications both on land and in marine environments. For both the automobile [122, 56, 78] and offshore industries, this includes seals, protection, and fluid flow line coatings [104, 58, 177, 25]. Regardless of these structural applications being intermittent or long-term in nature, the selected material must be able to deliver long-term sustainability in terms of output and physical properties.

There are many notable studies about the long-term durability of polymers in hygrothermal conditions. For instance, Burns et al. followed the bulk modulus of elastomers, including natural rubber, synthetic rubber, and polyurethanes exposed to hydrolytic aging for up to two years in the water. They found the stiffness properties to be quite stable over the period under study [30]. Gutierrez correlated data from accelerated aging in the laboratory with specimen results from ship structures submerged in seawater for over 20 years [79]. Bowditch explained the behavior of polymer deliberated upon the hydrolytic resistance of polyurethanes and illustrated the significance of the diol chemistry on molecular weight stability in water [139]. Damage parameters have been used to evaluate the influence of water aging on PDMS containing multi-block polyurethanes [36]. Le Gac proposed

a model for the urethane hydrolysis reaction that predicts the degradation of polymers used as thermal insulation materials [108]. Somarathna's state-of-the-art review covers the hyper-viscoelastic mechanical response of polyurethane for structural and infrastructural engineering applications [169]. Jingxin Na et al. have deliberated upon the mechanical behavior of polyurethane adhesive bonded joints as a function of temperature, and humidity [141]. Joshi studied about the sustainability of polyurethane membranes in artificial weathering [92]. Bardin et al. developed a hydrolytic kinetic model predicting embrittlement due to chain-scissions of a polyurethane elastomer containing an anti-hydrolysis agent [17]. Recently LR Bhagavathi et al. have shown that cellulosic-particle-reinforced (CPR) polyurethane adhesive joints demonstrate excellent aging resistance and stability in hygrothermal aging environment [21]. W Tan et al. have explored the characteristics of inter-facial cohesive failure and fatigue performance of polyurethane adhesive joints affected by a wide range of service temperatures [174]. Most of the above-mentioned works encompass the adhesive properties of the material. It is felt that the studies related to the cohesive properties of polyurethane-based adhesives (PUB) are still limited. This study is a step towards understanding the behavioral variations in PUB when exposed to hygrothermal conditions in comparison with other environmental agents. This particular study is an effort to investigate and evaluate the effect of thermo-oxidation, hydrolytic and hygrothermal aging through the characterization of the mechanical behavior of polyurethane-based (PUB) adhesive with rubber-like properties. Our goal is to distinguish material behavior with respect to aging environments. The influence of aging is often followed by the measurement of tensile properties. In addition to mechanical tests, we have applied various simultaneous methods, including DSC, DMA, FTIR, cross-link density (CLD) analysis, and SEM to characterize as-received and aged samples. In the current work tensile testing was the main technique employed, supported by the above-mentioned chemical and thermal analysis methods. The paper is outlined as follow. After discussing the experimental method in section 3.2, the results and discussion are presented in section 3.3. Finally, section 3.4 includes the summarized concluding remarks for this experimental effort.

3.2 Methodology

The research objective was to characterize a flexible polyurethane adhesive in competing environmental conditions. The thermal, mechanical and surface properties of the aged adhesive were evaluated and followed testing methods elaborated in relevant ASTM standard [6]. Laboratory aging was performed in thermo-oxidation at 0% RH; hydrolytic aging specimens were submerged in distilled water and hygrothermal aging was conducted in 80% RH at 60◦C, 80◦C and 95◦C. Aging

durations were set as 1, 10, 30 and 90 days. Sealed containers (see Fig. 3.2) with multiple layers of grit guards were used to age samples in desired conditions. Effort was made to minimize errors/ variations in aging conditions. A summary of methods used to maintain required environmental conditions is shown in Table. 3.1. For hygrothermal aging, salt solutions were used as standard method for achieving humidity fixed points by binary saturated aqueous solutions [76].

In order to maintain constant humidity level, all the vessels were briefly opened on weekly basis to replace distilled water and salt-solutions. While it ensured that desired submerged condition and relative humidity was constantly maintained, the oxygen level inside sealed container condition was also kept from falling below critical level.

Table 3.1: Summary of methods used to maintain desired environmental conditions.

Environmental condition	Temperature	Method
	Thermo-oxidation	
0%RH	60°C, 80°C, 95°C	Molecular sieves
	Hygrothermal	
80 ± 3%RH	60°C, 80°C, 95°C	Potassium Chloride
	Hydrolytic	
Submerged	60°C, 80°C, 95°C	Distilled water

3.2.1 Material The material studied here is 3M™ 590 Polyurethane Glass adhesive sealant. It is a rubber like flexible polyurethane-based adhesive used in automobile industry as glass sealant and also for some prototype parts, particularly where abrasion resistance is required. The material subsequently described as flexible PUB adhesive is nominally of hardness 60-65 Shore-A.

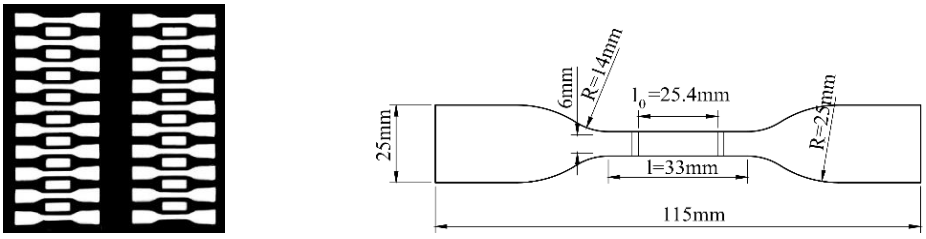

(a) Casting mold (b) Dimensions of cured adhesive specimen

Figure 3.1: Sample preparation and dimensions.

3.2.2 Sample Preparation A customized mold was designed for preparing dumbbell shaped and rectangular samples (see Fig. 3.1a). Dumbbell shaped samples were used for tensile tests while rectangular samples (35 × 12 × 3.175mm) were cured and aged for DMA test. The adhesive paste was cast into the 3.175mm thick mold with an injector gun (for sample dimensions see Fig. 3.1b).

The curing kinetics of the adhesive were analyzed before starting the aging process, and the conditions for obtaining the completeness of the curing reaction were established. Specimens were

allowed to cure in room temperature for four days and then over-cured in 60°C for 12 hours before starting the accelerated aging process.

3.2.3 Gravimetric measurements To show the effect of temperature-time duo on the moisture-uptake and mass changes, weights of PUB specimens were recorded at every critical stage of the experiment. For each environmental aging condition, an average of 10 specimens were used to allow for a good statistical representation. It is expected that if material displays Fickian behavior, a percentage of absorbed water should linearly increase with increase in temperature and time [87]. Absorbed water in outer layers is expected to be lost after drying, while a small percentage of trapped water or moisture may remain within the specimens. Comparison of the recorded weights revealed two types of phenomena taking place in case of PUB material i.e., moisture uptake and mass-loss (ML).

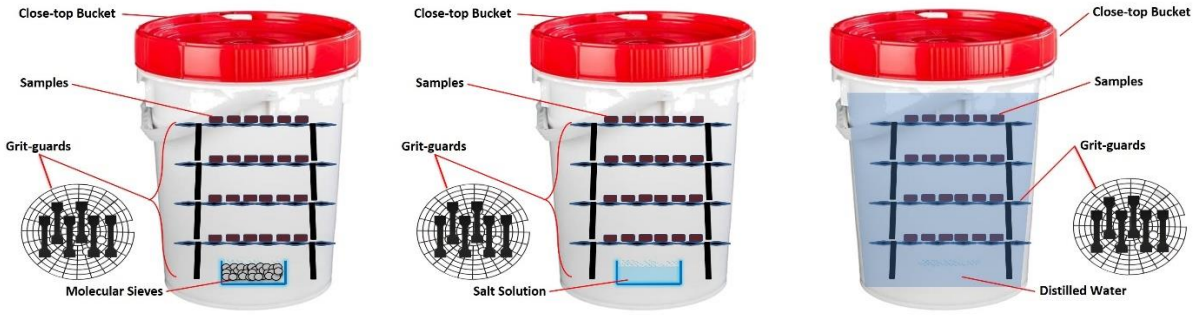

(a) (b) (c)

Figure 3.2: Loading set-ups used for specimens during aging in different temperature conditions, (a) Schematic showing sample loading, (b) Schematic showing sample loading, and (c) Schematic showing sample loading.

3.2.4 Moisture-uptake To carryout water-uptake, unaged PUB samples were individually weighted on an electronic balance (0.01mg accuracy) before being placed in 80%RH or submerged in distilled water. Sample containers were then placed for aging in designed humidity and temperature conditions for planned aging durations. Immediately after aging, the samples were carefully dried with tissue paper and weighed on the same electronic balance. The water content W_c in the sample was measured as the % weight increase in the sample at completion of aging when sample was considered wet. The percentage water-uptake was calculated using equation,

$$W_c(\%) = [\frac{(W_t - W_0)}{W_0}] \times 100 \quad , \qquad (3.1)$$

where W_t is the weight of aged sample at time t and W_0 is the weight of unaged sample before placing in aging conditions.

3.2.5 Water Desorption and Mass Loss Aged samples were dried in vacuum oven at 40°C for 24hrs at 700 in-Hg. Although samples maintained a steady dried weight, we do not rule out the possibility of some water still retained due to the formation of strong interaction of functional groups with water molecules [173]. The desorption or mass loss (M_L) in the sample was measured by comparing the unaged specimen weight with the % weight of aged sample after drying. The percentage water-uptake was calculated using following equation:

$$M_L(\%) = [\frac{(M_0 - W_d)}{W_0}] \times 100 \quad , \qquad (3.2)$$

where M_d is the weight of aged sample in dry state and W_0 is the weight of unaged sample before placing in aging conditions. All the weights were then compared with original weight of the sample. All weight changes (%) were then plotted to see the water-uptake and mass loss in the PUB specimens. For simplification and understanding, weight % above average unaged sample weight is considered as water/ moisture uptake and the weight % below the same is taken as mass loss.

3.2.6 Uni-axial Tensile Test The effects of exposure on tensile characteristics were assessed through the use of dog-bone shaped specimens following ASTM D412 as standard guideline. A uni-axial universal testing machine (Test Resources 311 Series Frame) with 5kN load cell (Test Resources SM-5000N-294 force transducer) was used for quasi-static tensile tests using which all specimens were stretched until breakage. All tests were displacement controlled with a crosshead speed of 50 mm/min. The starting distance between the extensometer grips was set to 25.4mm and all the experiments were performed at room conditions (i.e., 22 ± 2°C, 50 ± 3% RH). A minimum of four failure tests were performed for each time period and exposure condition for reliability control.

3.2.7 Differential scanning calorimetry (DSC) For the unaged adhesive specimens glass transition temperature (T_g) was measured using DSC analysis and was found to be −62.51°C. The experimental device used for this measurement is a Q2000 series machine from TA Instruments™. All DSC measurements were performed in standard aluminum pans with lids containing an average sample mass of 10 ± 3mg under an inert Nitrogen atmosphere (50ml/min). Dynamic scans were performed at a heating rate of 10°C/min with a temperature scan between −80°C and 350°C.

3.2.8 Dynamic Mechanical Analysis (DMA) Rectangular specimens (35mm × 12mm × 3.175mm), unaged and aged were subjected to DMA analysis. After carrying out the visual inspection, one representative sample from each condition was selected and tested. Single cantilever tests to record storage modulus, loss modulus and Tan δ were performed on the TA Instrument

DMA Q800 machine from −70°C to 10°C at a temperature rate of 3°C per min. The test has been performed in the linear viscoelastic region (LVR) using strain amplitudes of 15% and a frequency of 1.0 Hz.

3.2.9 Cross-Linking Density (CLD) The cross-link density of PUB adhesive was determined by employing the equilibrium swelling method as described in the literature [90, 143, 55]. The rectangular specimens with average dimensions of 0.4in × 0.3in × 0.12in were immersed in three different solvents namely hexane, toluene and pentane (molar volumes, 130.7mL/mol, 106.3mL/mol and 115.2mL/mol respectively). The reason for using three different chemical solvents is to see which one of these solvents has the most effect on the cross-linking bonds of the PUB. The test was performed with three samples in each solvent. The samples were weighed every 3 hours at the room temperature to find out when a constant weight was reached, indicating maximum absorption of the solvent. For PUB, the equilibrium point was approximately obtained after 6 hours, then they were removed from the solvent, patted with paper and weighted again. The cross-link density and average molecular weights between the chains were estimated using calculations introduced by Flory, and Paul C. Hiemenz [158, 64, 86].

$$ln(1-\phi_e)+\phi_e+X\phi_e^2=n_e\frac{V_1}{V_0}(\frac{\phi_e}{2}-\phi_e^{1/3}) \quad , \qquad (3.3)$$

$$\frac{n_e}{V_0}=\frac{ln(1-\phi_e)+\phi_e+X\phi_e^2}{V_1(\frac{\phi_e}{2}-\phi_e^{1/3})} \quad , \qquad (3.4)$$

where X is the solvent-polymer interaction parameter and V_1 is solvent molar volume. From equation (3.4) we can further derive equation (3.5),

$$\frac{n_e}{V_0}=\frac{\rho}{M_x}(1-\frac{2M_x}{M}) \quad , \qquad (3.5)$$

where n_e is the molar cross-linking, V_0 is the volume of the PUB samples before swelling, M_x is the molar mass of the solvent, and M is the molar volume of the polymer. ϱ is the density of the solvent. The density of the elastomers, such as a rubber-like polymer, should be at a high accuracy level. The measurement shouldn't exceed within ±0.1% of the constant measurement [57].

3.2.10 Fourier Transformation Infrared (FTIR) The chemical structure evolution of the specimen during aging is characterized by FTIR on an IR Affinity-1S Shimadzu model. The spectra

were measured in the wave number range of 4000 − 600cm−1 with 64 scans and a resolution accuracy of 4cm−1.

3.2.11 Scanning Electron Microscopy (SEM) Morphology of unaged PUB and specimens aged in thermo-oxidation, hydrolytic and hygrothermal conditions for 90 days has been inspected by a scanning electron microscope (Zeiss EVO LS 25) with an accelerating voltage of 3.0 kV. Effects of the aging environment on samples were gauged by various micro-graphs on the cured and tensile fracture surfaces of specimens.

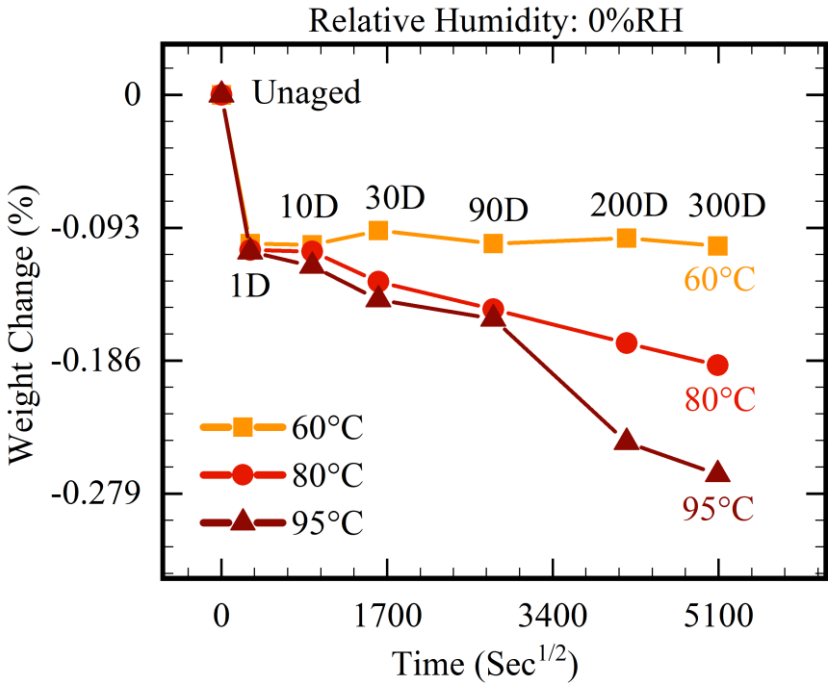

Figure 3.3: Weight changes (%) during thermo-oxidation aging (0%RH) in 60°C, 80°C and 95°C.

3.3 Results and Discussion

In this section, tensile tests of specimens aged in each environment are first analyzed in isolation. Stress-strain behavior of specimens aged in thermo-oxidation (0%RH) are presented in Fig. 3.6, while the relation of stress (σ_f) and strain (ϵ_f) against time is plotted as shown in Fig. 3.7. Similarly, stress-strain behavior and their trend against time for submerged state aging and hygrothermal aging (80%RH) are presented in Fig. 3.8, Fig. 3.9 and Fig. 3.10, Fig. 3.11 respectively.

Thermo-oxidation involves the degradative effects of high temperature in the presence of oxygen; hydrolytic aging considers the effect of water and temperature; and hygrothermal aging combines all of the above sub-phenomena of oxygen, heat, and moisture movement in competition with each other. First, we want to emphasize the types of collaborations that may take place between

two or more environmental factors. Next, we will highlight water absorption, followed by the consequences of the presence of water on both tensile behavior and T_g changes. While the aged samples do reflect changes in constitutive behavior, ultimate failure points of the specimens demonstrate uncertainty due to errors during casting, the presence of voids within the material matrix or axial misalignment during testing, etc. In order to have a better understanding of the constitutive behavior, we also looked at stress (σ) at 50% strain ϵ (see Fig. 3.7a, Fig. 3.9a, and Fig. 3.11a).

(a) Swelling in each temperature after aging in submerged condition for 90 days

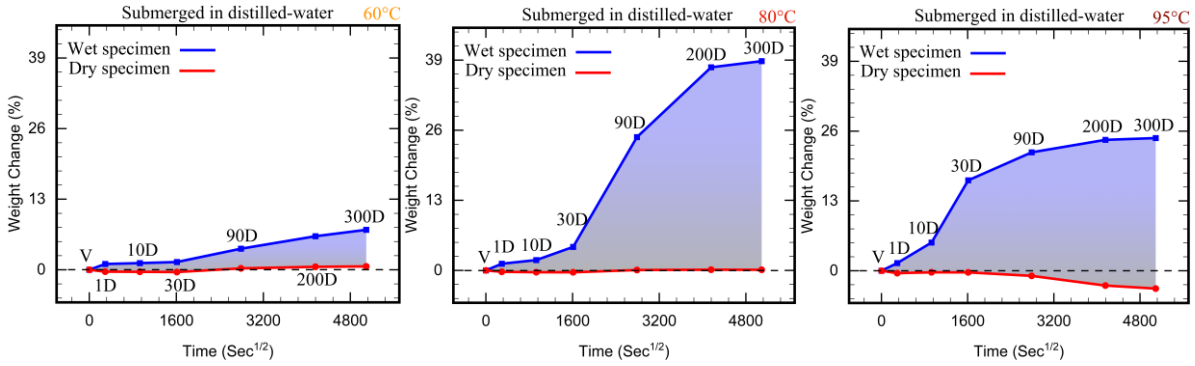

(b) Water up-take at 60°C (c) Water up-take at 80°C (d) Water up-take at 95°C

Figure 3.4: Water up-take and weight (%) changes during hydrolytic aging (submerged) in 60°C, 80°C and 95°C.

3.3.1 Types of collaborations When we have multiple phenomena/ environmental factors acting on the material, and we want to see the combined effect on its properties, the question is how their contribution is co-related and added up towards the resulting effects. We have subdivided these contributions into the following categories,

a. Collaborative contribution When we add up two phenomena, A and B, sometimes it is simply a superposition of both, which means that, A + B = collaborative contribution

b. Competitive contribution When two mechanisms are competitive, it means that if A is gaining, then B is at a loss, indicating the opposite direction of effect. In this case, the result is always between contributing phenomena. It is explained as, A + (-B) = competitive contribution.

c. Additive contribution Additive contribution is that A will result in +B, and their contribution will be added together. It means that if one of them is zero, we will still have something else.

d. Multiplicative contribution In this type of contribution, either one or both A and B will act as a catalyst. It means that in the absence of B, the effect of A will be super slow, and in the presence of B, the effect due to A is enhanced significantly. Based on the results achieved in this particular study, the nature of collaboration by contributing environments is observed to be competitive and addictive. Point out in discussion where the contribution is collaborative instead of competitive.

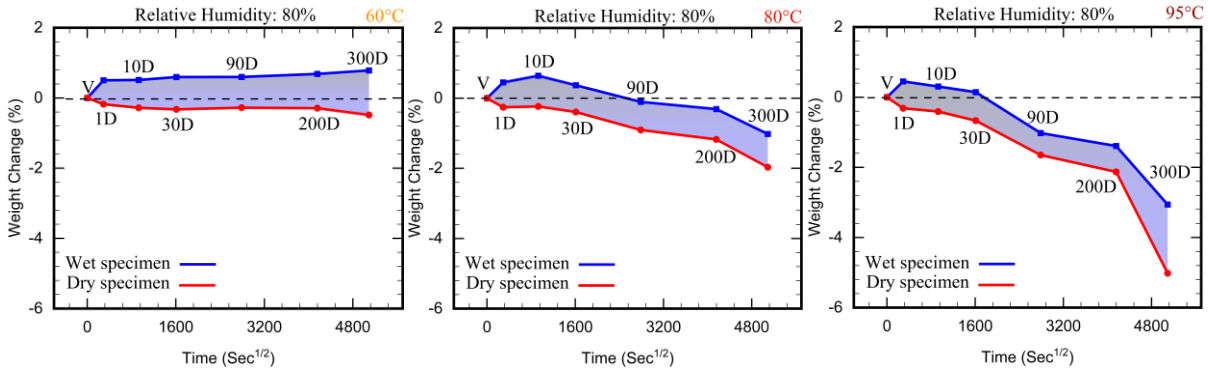

(a) Moisture up-take at 60°C, (b) Moisture up-take at 80°C (c) Moisture up-take at 95°C

Figure 3.5: Moisture up-take and weight (%) changes during hygrothermal aging (80%RH) in 60°C, 80°C and 95°C.

These collaborations are dictated by material responses to a single or a combination of multiple environmental sub-phenomena during aging. By expanding the characterization methods and aging period, future studies can further elaborate on this effect. While this study will keep PUB in focus, it will be interesting to see in follow-up studies if some other material shows different responses to the collaboration effects. The following characterization methods will reveal that PUB fits into the competitive collaboration scenario.

3.3.2 Moisture Absorption and Weight Changes

Moisture absorption increases linearly with the square root of aging time during aging in submerged condition. In order to ascertain whether PUB follows Fick's second law of diffusion, we needed to expand the aging span and allow the material to demonstrate the saturation plateau.

The PUB material shows consistent mass loss during thermo-oxidative aging and this phenomenon is amplified with the higher storage time and temperature (see Fig. 3.3). During hydrolytic aging, the material shows a large amount of water-uptake which follows the second Fickian law. In all hydrolytic aging cases, weight change representing water-uptake linearly increased and reached the plateau when plotted against the square-root of the aging time.

In the case of hygrothermal aging, very interestingly, we have a combination of both water-uptake and mass loss. Similar to hydrolytic aging, the water sorption reached the plateau which is maintained concurrently throughout hygrothermal aging duration along with the mass loss. This mass loss is primarily seen as a collaborative effect of thermo-oxidation in the presence of water molecules. These results confirm that hygrothermal aging environment can be considered as an actor between the other two sub-aging mechanisms.

Samples in 80%RH did not show any visible swelling, however, an irreversible mass loss depicted through weight changes was noted. Although mass loss is documented for some construction composites (FRP) [74] due to chemical decomposition; there is a need to further explore the cause behind this phenomenon in PUB adhesive.

Results showed that exposure to water molecules in both humid and submerged environments adversely affected the elastic modulus and tensile strength. Furthermore, a large degradation was noted with exposure to high temperatures while the plasticity became notable simultaneously. In both hydrolytic (submerged) and hygrothermal (80%RH) aging environments we observe plasticization phenomena during the very initial phase of aging i.e., around 24hrs. But soon after moisture and water began to ingress the polymer matrix, this behavior takes a rapid U-turn due to moisture attack as we observe consistent decrease in strain indicating chain scission with increase in both time and temperature. The first category is more vividly noticeable with a thermal upsurge and is customary for flexible adhesives while the second phenomenon comes into play with an increase in the factors responsible for shaping the aging conditions i.e., temperature, humidity, and duration.

As already mentioned, the hygro-thermal and hydrolysis damages are a consequence of prevailing temperature and water absorption by the samples. Data recorded and compared from hydrolytic aging (see Fig. 3.4) and from hygrothermal aging (see Fig. 3.5) clearly shows very high water-uptake for PUB in submerged conditions specially in higher temperatures. In short, while plasticization affects the length distribution of polymer chains inside the matrix, further degradation results from chain scission which is considered as a chemical alteration at the macro-molecular level. The molecules that get detached from long chains could be trickled and migrated from material

matrix by water or other solution mediums via a process termed as leaching [151]. Leaching is considered as main contributor of mass loss during aging in submerged state.

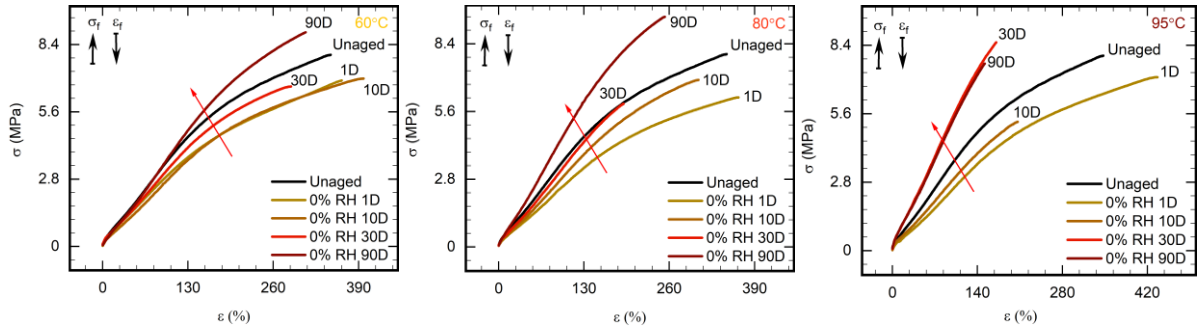

(a) (b) (c)

Figure 3.6: Stretch to failure tests of specimens showing σ_f and ϵ_f variation of specimens aged in 0%RH (a) 60°C (b) 80°C (c) 95°C.

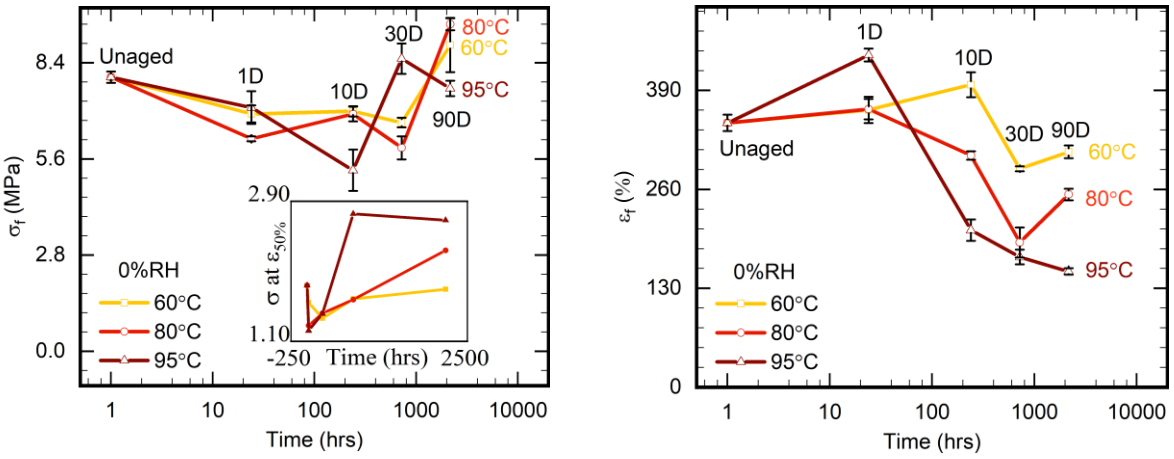

(a) (b)

Figure 3.7: Stress and strain variation of specimens in 0%RH plotted against time (a) σ_f (b) ϵ_f (%).

In the following paragraphs, we will compare these observations through mechanical tests to try and understand what may have been happening inside the polymer chains. Despite being the opposite phenomenon, chain scission and cross-link development take place simultaneously which further complicates the characterization process. For simplification we will consider the dominating factor only when necessary.

3.3.3 Thermo-oxidation In thermo-oxidative aging, σ_f and ϵ_f trend emerging from uni-axial tensile tests for thermo- oxidative aging of PUB have been plotted against time (see Fig. 3.7). We observe two simultaneous processes i.e., chain scission and cross-link formation (see Fig. 3.13) [12]. Initial softening is attributed to chain scission. Later on, there is a consistent stress hardening and ϵf

reduction which are indicative of the dominant cross-link formation mechanism in presence of oxygen and heat. Cross-link phenomenon dominates chain scission during thermo-oxidative aging.

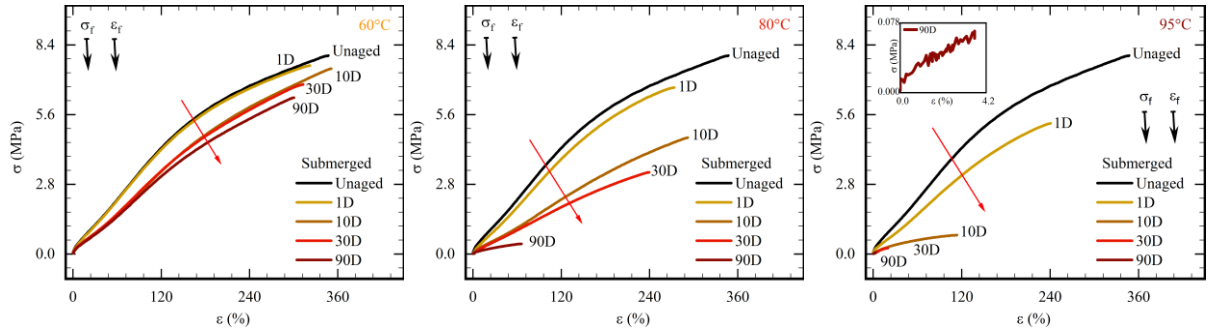

(a) (b) (c)

Figure 3.8: Stretch to failure tests of specimens showing σ_f and ϵ_f variation of specimens aged in submerged condition (a) 60°C (b) 80°C (c) 95°C.

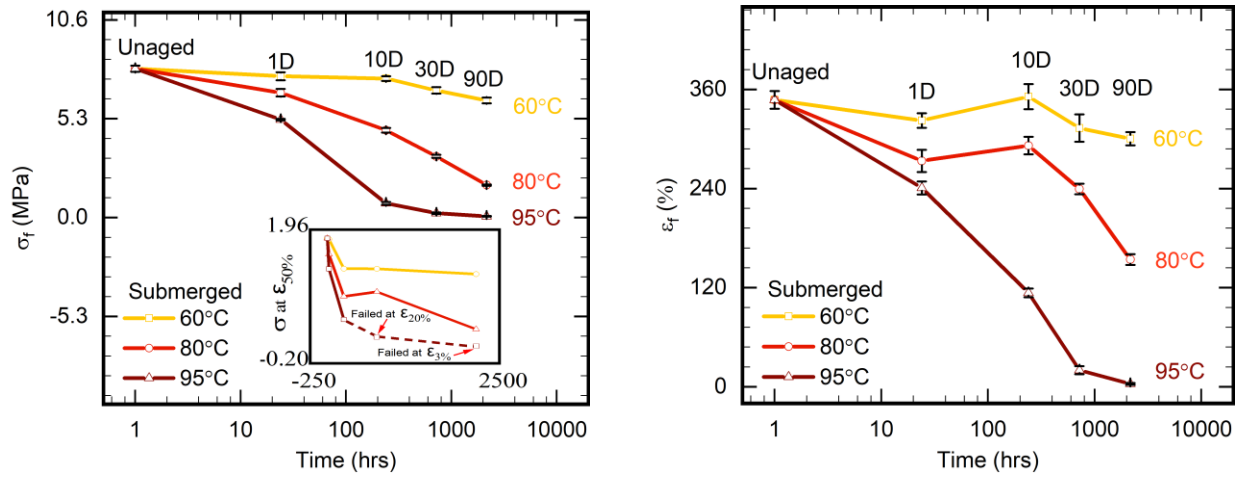

(a) (b)

Figure 3.9: Stress-strain variation in submerged state plotted against time (a) σ_f (b) ϵ_f (%).

3.3.4 Hydrolysis When aging the specimens in submerged state; it is seen that stress behavior of the PUB consistently degrades with increase in temperature and aging duration. This happens due to cross-link reduction and hydrolytic chain-scission taking place simultaneously due to water attacking the polymer matrix [13]. σ_f and ϵ_f variations emerging from uni-axial tensile tests for hydrolytic aging of PUB have been plotted against time (see Fig. 3.9). In the presence of water molecules, the chain scission reactions take place more aggressively as compared to other conditions [14], it can be clearly seen by comparing hydrolytic aging versus the thermo-oxidation and hygrothermal aging. In the beginning, higher plasticization is notable which is followed by a severe degradation phase in longer aging durations. Chemical tests to analyze changes in cross-linking density measurements are

conducted to further support this argument. Wet specimens were stabilized at room temperature for two hours before being subjected to uni-axial tensile tests.

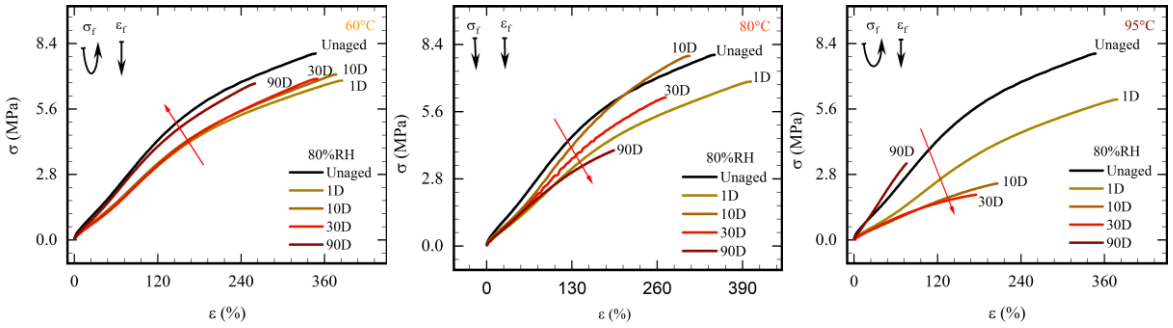

(a) (b) (c)

Figure 3.10: Stretch to failure tests of specimens showing σ_f and ϵ_f variation of specimens aged in 80%RH (a) 60°C, (b) 80°C, and (c) 95°C.

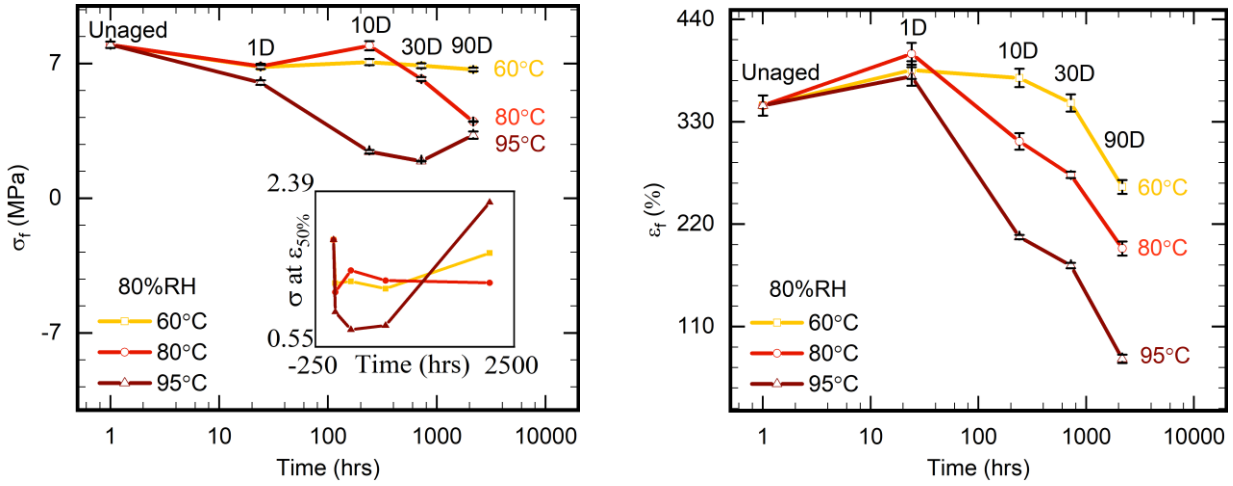

(a) (b)

Figure 3.11: Stress and strain variation of specimens in 80%RH plotted against time (a) σ_f (b) ϵ_f (%).

3.3.5 Hygrothermal Aging Hygrothermal aging can lead to degradation of both chemical and mechanical properties of polymeric adhesives [81]. σ_f and ϵ_f behavior emerging from uni-axial tensile tests for hygro-thermal aging of PUB have been plotted against time (see Fig. 3.11). Tensile tests show chain scission to be dominant as temperature and aging duration reach the maximum limits set under the experiment design. While it is a competitive damage scenario [192] between thermo-oxidation and hydrolytic environment; chain scission due to water attack always dominated any cross-link development due to oxidation reactions [33].

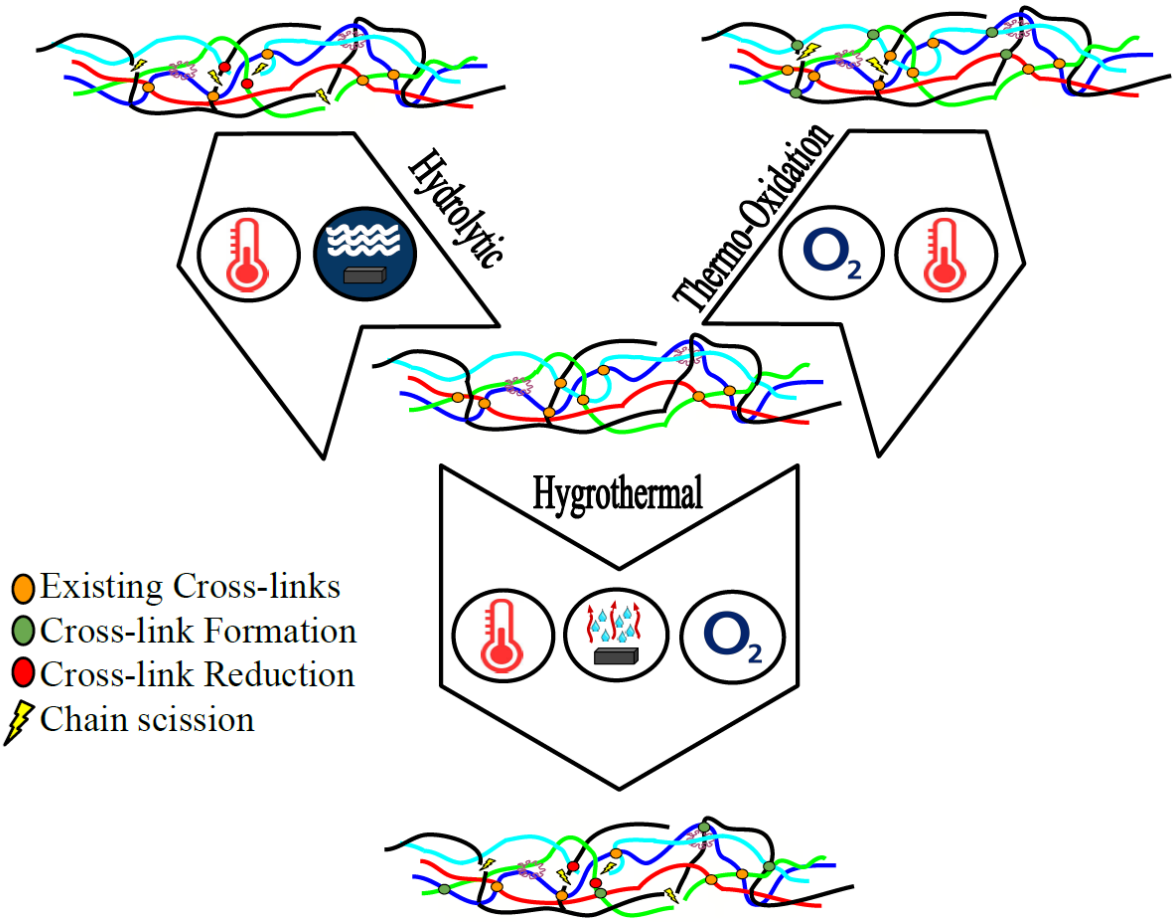

Figure 3.12: Schematic comparing the effects of all aging environments on the micro-structure.

As already mentioned above, thermo-oxidation as a process is dominated by formation of cross links; hydrolytic aging affiliates with chain scission being dominant; while for hygrothermal aging we consider both phenomena, (i) cross-link development due to oxidation, and (ii) chain scission attributed to oxygen, water molecules, and high temperature. It appears that effects of heat, oxygen, and moisture act simultaneously yet independently. Independently, because we observe stress increase like thermo-oxidation and decline in failure strain attributed to chain scission in presence of water molecules. Both effects are competing, and the overall degradation is likely to be the combined effect of damage imparted through oxidation and moisture effect variations in different temperatures. While chain scission dominates in most conditions; 80% relative humidity at 60°C and 80°C initially showed increased cross-linking density within the polymer matrix under favorable oxidation conditions (see Fig. 3.14a,c). With the increase in time, cross-link density gradually drops when water molecules diffuse into the material. But it deteriorates aggressively once the temperature is increased to 95°C in 80% RH (see Fig. 3.14e). The loss of cross-links and chain scission is due to the presence

of heat and water molecules, whereas; the increase in cross-links is due to heat and oxygen. The total loss of stretchability indicates chain scission to be dominating the cross-linking phenomena [194].

3.3.6 Environmental degradation Here, we studied damage in the polymer matrix in context of different agents responsible for inducing environmental stresses. In the following paragraphs we have compared test results from specimens aged in thermo-oxidative, hygrothermal and hydrolytic aging conditions. Results include mechanical test data and chemical test outcomes. On similar lines as already mentioned in beginning of Sec. 3.3, here as well, we have compared stress variation at 50% stain for inter-environmental comparison to have a better understanding of the constitutive behavior (see Fig. 3.13a, Fig. 3.13c, and Fig. 3.13e).

The variation of tensile strength σ_f, as well as elongation at break ϵf plotted against time in the case of thermo- oxidation (0%RH), hydrolytic aging (submerged in desalinated water), and hygrothermal aging (80%RH) are given in Fig. 3.7, Fig. 3.9, and Fig. 3.11, respectively. In thermo-oxidation the specimens undergo initial softening possibly due to chain scission causing some cross-link reduction mechanism but there-on we observed consistent hardening behavior due to oxidation reactions.

In hydrolytic conditions, plasticization effects degrade the tensile strength and deterioration of the polymer matrix with the diffusion of water molecules into the structure [40, 190]. Considering all aging conditions, we observe indications of plasticization initially in both 60°C and 80°C. Whereas, in 95°C (see Fig. 3.8 and Fig. 3.9), degradation phase begins much sooner in water at higher temperatures [18]. The hydrolytic damage is mainly due to the effect of water and temperature; both combine to do maximum damage to the polymer matrix. Hydrolytic damage is the most detrimental to the material among all three aging phenomenon in consideration. Introducing thermo-oxidation alone to hydrolytically aged specimen will remove water molecules from system and partly revive the damage by initiating cross-link development, but most damage shall be non-reversible considering its magnitude.

Regarding aging in hygrothermal aging condition the plasticization effects are visible during initial phase of aging process where we saw σ_f decreasing and ϵ_f increasing in three temperatures [181]. Later, once aging reaches the mid-term phase, the retention of the tensile strength is found to be inversely correlated with temperature. At high temperatures, adhesive tensile strength (σ_f) sharply decreases in longer aging spans (see Fig. 3.13a, Fig. 3.13c, and Fig. 3.13e). σ_f decrease also intensifies with increase in temperature. At the same time, the ϵ_f (see Fig. 3.13b, Fig. 3.13d, and Fig. 3.13f) also

follows an almost identical behavior pattern signifying harsher degradation in presence of water with increasing temperature. Considering stress-strain tendency from constitutive behavior in each environment, let σ_1, σ_2, σ_3 and ϵ_1, ϵ_2 and ϵ_3 represent stress and strain of samples aged in thermo-oxidation, hydrolytic and hygrothermal aging conditions respectively. The general behavior falls in place as $\sigma_1 > \sigma_3 > \sigma_2$ and $\epsilon_3 > \epsilon_1 > \epsilon_2$. Whereas, in context of time (t) and temperature (T), results dictate two tendencies, (i) in thermo-oxidative aging $\sigma_f \propto$ T, t and $\epsilon_f \propto 1/T, 1/t$, and (ii) in hygrothermal/ hydrolytic aging $\sigma_f \propto 1/T, 1/t$ and $\epsilon f \propto 1/T, 1/t$.

Fig. 3.13 compares the deterioration mechanism of diverse conditions affecting adhesive specimens under identical temperatures and aging spans. Under comparatively low temperature (i.e., 60°C); all environments i.e., heat (0%RH), desalinated water, and humidity (80%RH) reflect an identical response of material during initial aging phase (see Fig. 3.6, Fig. 3.8 , and Fig. 3.10). After 30-days, PUB shows prominent hardening in thermo-oxidation but σf and ϵf are reduced in other two environments. The temperature 95°C proved to be very aggressive for PUB adhesive, hence we see exaggeration in degradation trend (see Fig. 3.13e, and Fig. 3.13f). In submerged state there is total loss of elasticity due to water attack causing high chain scission and it results into low-molecular-weight chains. This can be ascertained by comparing sheer drop of σ and ϵ with loss in cross-link density (see Fig. 3.13e, Fig. 3.13f , and Fig. 3.14e) [114]. Whereas, in thermo-oxidation aging (0%RH) loss of strain is attributed to increased cross-linking (see Fig. 3.13b,d,f and Fig. 3.14a,c,e). Loss of ϵf is in both cases but due to different reasons. However, in case of stress behavior; thermo-oxidation shows increase in stress while submerged condition shows significant stress decrease.

Constitutive behavior comparison for unaged and aged samples in 60°C, 80°C and 95°C are shown in Fig. 3.6, Fig. 3.8 and Fig. 3.10. In 0%RH specimens show initial softening followed by hardening in all temperatures. In 80%RH, while the specimens showed consistent decrease in elongation till the maximum aging duration; the stress loss shows softening till 30-days only and displayed hardening behavior thereafter. At the same degree, prolonged aging durations impelled specimens to descend their ductility and load sustainability.

Especially, for immersion in 95°C after 30-days and beyond, specimens barely sustained any load and can be referred to as annihilated. But when we compare all aging environments against each other, it is clear from Fig. 3.13 that while thermo-oxidation causes hardening and water induces softening behavior; this competition in opposite directions can be seen in stress variation of hygrothermal aging results which are falling between thermo-oxidation and hydrolytic aging.

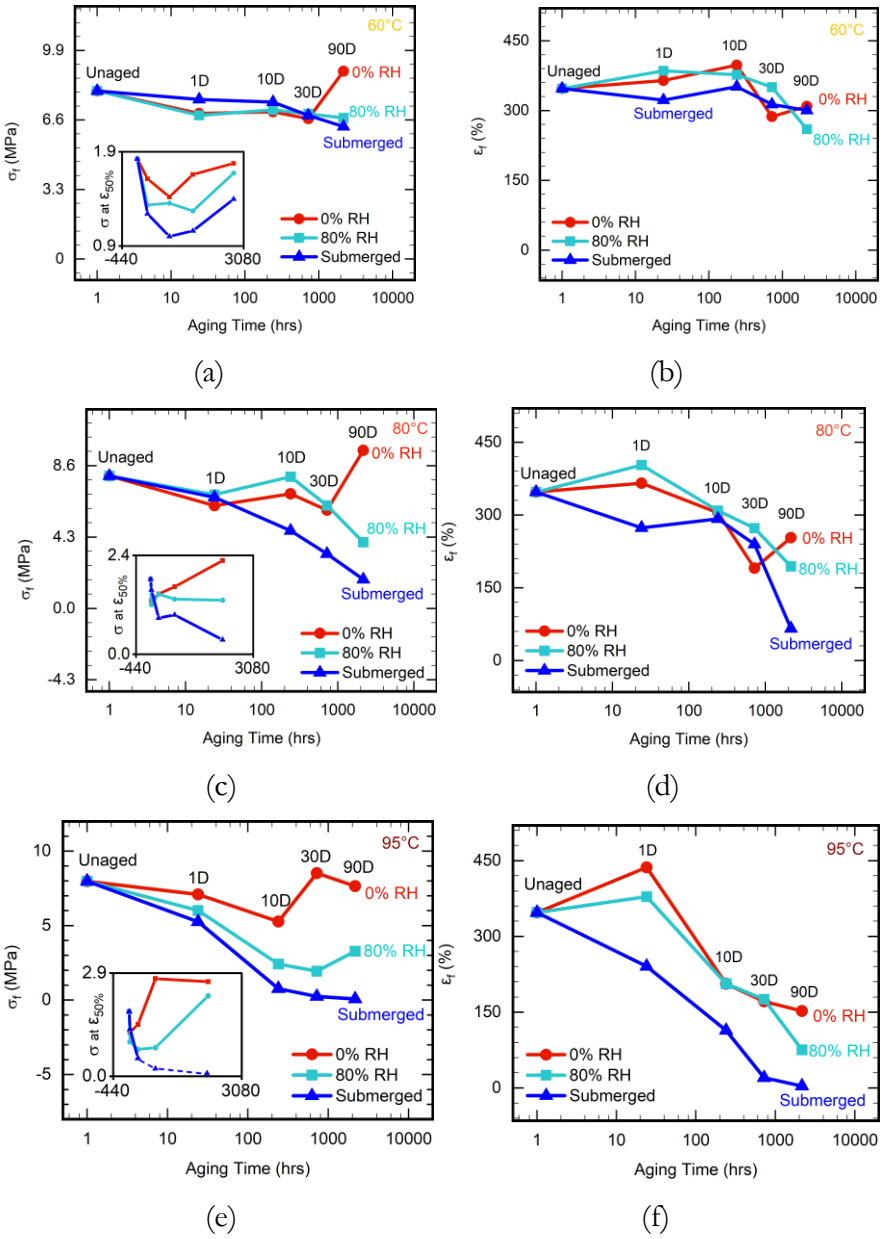

Figure 3.13: Comparison of failure stress, σf [(a) 60°C,(c) 80°C, and (e) 95°C] and failure strain, ϵ_f [(b) 60°C,(d) 80°C and (f) 95°C] between specimens aged in thermo-oxidation, hydrolytic and hygrothermal environments.

3.3.7 Cross-Linking Density All cross-link tests were carried out on dry samples since presence of water within polymer matrix can be deceiving by demonstrating low solvent absorption. Small weight change in PUB specimens would give a false impression of higher cross-link formation because of low solvent absorption rate. Among the three solvents used for this test, maximum fluid absorption and swelling was noted in case of toluene between first 3-6 hours, whereas there was negligible absorption observed in case of hexane and pentane.

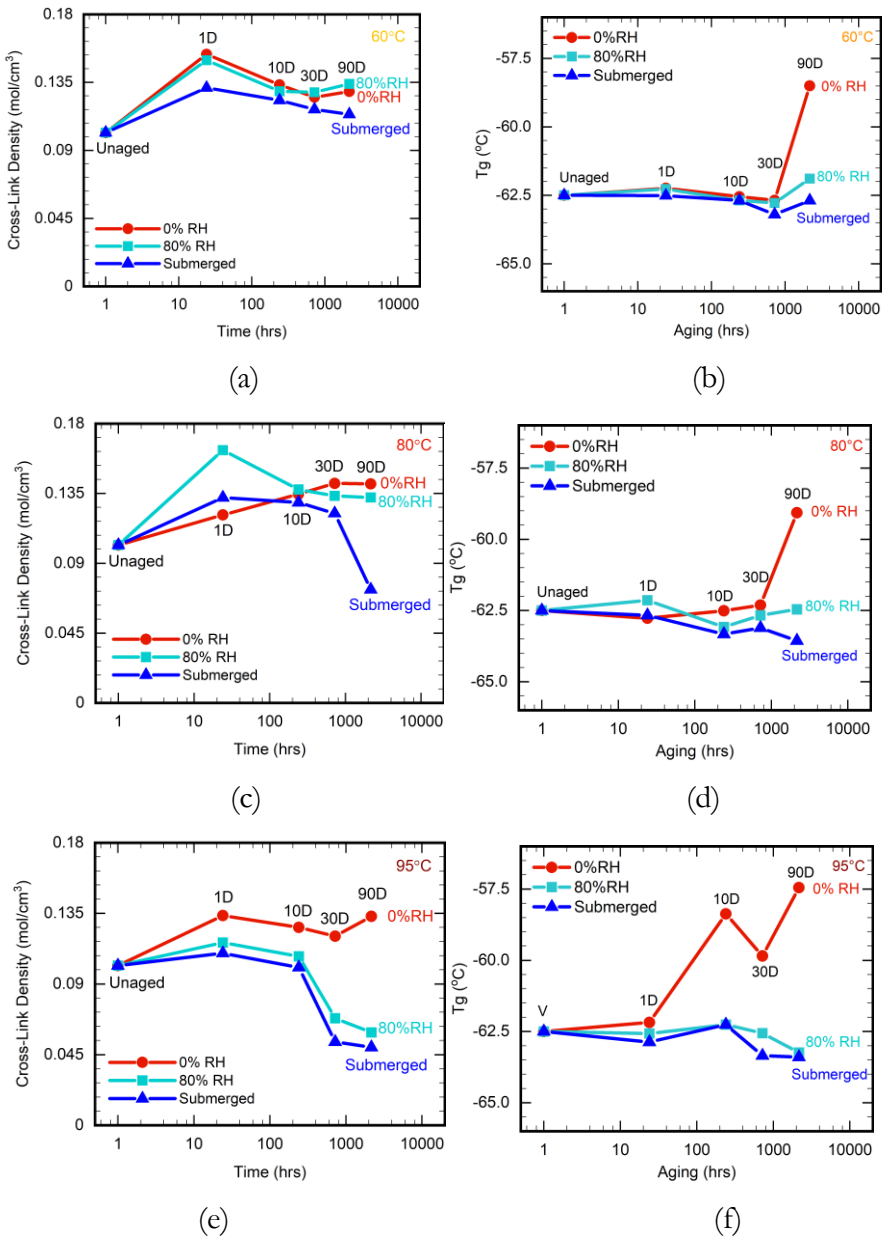

Figure 3.14: Comparison of cross-link density, (a) 60°C,(c) 80°C, and (e) 95°C and T_g obtained from DSC (b) 60°C,(d) 80°C and (f) 95°C between specimens aged in thermo-oxidation, hydrolytic and hygrothermal environments.

The results, specially in higher temperatures (see Fig. 3.14e and Fig. 3.14f) are in agreement with tensile test results (see Fig. 3.13e and Fig. 3.13f) and confirm our hypothesis that humidity is a result of two competing environments i.e., heat and water. In 60°C, specimens show identical behavior for thermo-oxidation and hygrothermal aging at start and end of aging (see Fig. 3.10a).

3.3.8 DSC Analysis DSC was performed to compare changes in Tg for different conditions to validate our hypothesis by the variation observed in Tg. Due to thermo-oxidation, the Tg can be seen

increasing while the same is decreasing in case of samples aged in submerged state. All the mechanical and chemical results are in agreement here. As we can see in Fig. 3.6, the thermo-oxidation reaction shows a hardening effect with aging. It is indicative of higher cross-link formation (see Fig. 3.14a,c,e) which caused increase in σf and thus the reduction in ϵf (see Fig. 3.13). It is also confirmed with the increase in Tg (see Fig. 3.14b,d,f). Likewise, we observe Tg decreasing in case of hydrolytic aging which indicates softening and loosening in polymer matrix. This can be attributed to softening behavior due to plasticization and high chain scission (see Fig. 3.13) attributed to water attacking and degrading the polymer chains severely. Apropos, we observe steep drop in both σf and ϵf values. As expected, for hygrothermally aged specimens, Tg can be seen in between other two conditions (see Fig. 3.14b,d,f) in agreement with the argument presented.

3.3.9 DMA Analysis DMA has been done for all aging conditions. However, to see the exaggerated environmental effect, we are presenting data from the most extreme aging condition (95°C, 90 days) in this section. Fig. 3.15 shows DMA results of virgin and aged specimens (95°C, 90 days) from all the aging environment conditions.

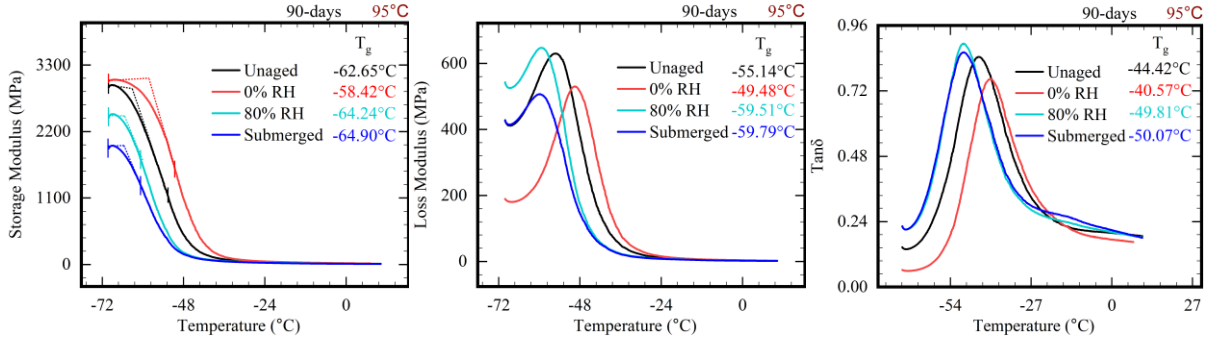

(a) Storage Modulus, E (b) Loss Modulus, E (c) Tan δ, E /E

Figure 3.15: Storage modulus, loss modulus and Tan δ variation between thermo-oxidation (0%RH), hydrolytic aging (submerged), and hygrothermal aging (80%RH) environments.

The storage modulus E' , the loss modulus E" and the phase lag Tan δ of specimens aged in thermo-oxidation (0%RH), hydrolytic aging (submerged), and hygrothermal aging (80%RH) environments are compared in Fig. 3.15 a-c, respectively. Storage modulus curves characterize the transition from glassy to rubbery behavior of materials and obtained glass transition temperature T_g as a significant factor. Loss modulus is defined as the dissipated energy, switched to heat, for each cycle of sinusoidal deformation. Tan δ which reflects the molecular level changes is the ratio of loss modulus to storage modulus E" /E' . Based upon DMA test data, the glass transition (T_g) range of unaged PUB spans between -62.65°C to -44.42°C.

For thermo-oxidation aging, (see Fig. 3.15a, b and c) the Tg increased in thermo-oxidative aging. This is in confirmation with the cross-link density analysis and tensile test results. Also, the peak height of Tan δ reduced due to decline in molecular mobility attributed to increase in cross-link density (see Fig. 3.14e) [161, 60]. Same is also reflected as hardening behavior in tensile test results (see Fig. 3.13e).

In case of hydrolytic aging the T_g reduced the most. It is in agreement with the plasticization effect (see Fig. 3.13e,f) in tensile tests as well as the cross-link density analysis (see Fig. 3.14e).

Regarding hygrothermal aging, we can see that the T_g of PUB specimen aged in 80%RH is between T_g of specimens aged in thermo-oxidation (0%RH) and hydrolytic (submerged) aging conditions. This result is in complete agreement with the discussion presented in the study.

3.3.10 FTIR A side-by-side comparison of FTIR spectra obtained from thermo-oxidation (0%RH), hydrolytic (submerged), and hygrothermal aging (80%RH) of 90-days is shown for 60°C in Fig. 3.16a and b, for 80°C in Fig. 3.16c and d, and for 95°C in Fig. 3.16e and f, respectively. Since the chemical composition of the material is not disclosed by the manufacturer, we based our analysis on FTIR spectra bands shown in Table. 3.2 compiled from [97], [10], [150] and [178].

In terms of chemical changes, there is no significant reaction observed in thermo-oxidation aging. Thermo-oxidation FTIR spectra generally show similar peaks in all aging temperatures (see Fig. 3.16). While no new peak appears, some variation in absorbance is observed in 60°C at wave number 2360 cm^{-1} associated with [O=C=O] bonds (see Fig. 3.16a,b).

For hygrothermal aging in 80%RH, only significant change is highlighted in 80°C pertaining to C-H bonds around wavelengths 817-910 cm^{-1} and 2855-2930 cm^{-1} (see Fig. 3.16c,d).

Regarding hydrolytic aging, the FTIR spectra of the sample aged at 60°C reveal the most absorbance in [O=C=O] bond region (wave-number 2360 cm^{-1}) compared with 0%RH and 80%RH FTIR spectra. For samples aged in distilled water, we observed very high water-uptake at high temperatures, i.e., 80°C and 95°C (Fig. 3.4). As a result of high water present inside the polymer matrix, loss of elastic properties is seen in tensile tests at longer aging spans (Fig. 3.13). In 95°C (see Fig. 3.16e,f) prominent peak appeared at wave number 3321 cm^{-1} associated with [O=H] in Polyol. At wave number 3080 cm^{-1}, a new peak showing a decrease in transmittance appeared after aging in a hydrolytic environment; it represents [=C-H] bond stretch. The hydrogen-bonded urethane group at peak 1726 cm^{-1} and [C=O] of urethane at peak 1735 cm^{-1} also show an increase in transmittance under hydrolytic aging.

Table 3.2: Assignment of FTIR bands for some major peaks of PUB.

Peak Location	Associated Functional Group
3321	(O=H) in Polyol
3080	=C-H bond stretch
2855 and 2930	C-H in CH_2
2360	O=C=O
1726	H-bonded Urethane
1735	C=O of urethane
1535	C=N
1510	$H-N-C=O$ Amide II
1174	$C-O-C$
817, 910	C-H

3.3.11 SEM Analysis SEM revealed some variation in damage mechanisms between unaged, hygrothermal aging, and hydrolytic aging effects on cured samples as they aged. Fig. 3.17, and Fig. 3.18 show the SEM images reflecting changes in surface morphology. The left column contains the SEM graphs with a larger scope of the specimen. In contrast, the right column corresponds to their smaller scope images with more detailed information regarding morphological changes.

Fig. 3.17 contains SEM images of the cured unaged surface along with the specimen aged in a thermo-oxidation environment. There is no prominent damage seen on the surface after aging in thermos-oxidation. As shown, the surfaces of unaged specimens are relatively smooth and compact with no loose particles or cracks (see Fig. 3.17a,b). For humid and submerged conditions, we have Fig. 3.18 containing SEM images of hygrothermally and hydrolytically aged (in 95°C) specimens, respectively. For the aged cases, there are a host of cracks and swollen agglomerated particles in the surfaces (see Fig. 3.18c-f), derived from the degradation of the polymers due to humidity and water attack in the presence of high temperature. Specifically speaking, in the submerged condition, we see much higher damage propagation to the polymer surface morphology (see Fig. 3.18c). Deeper layers from the cross-section show effects of plasticization with swollen agglomerated appearance in deeper layers (see Fig. 3.18d). In high humidity (80%RH), tiny nodules and crack propagation are observed, which is believed to get exploited by moisture by allowing the ingress of water molecules in deeper layers.

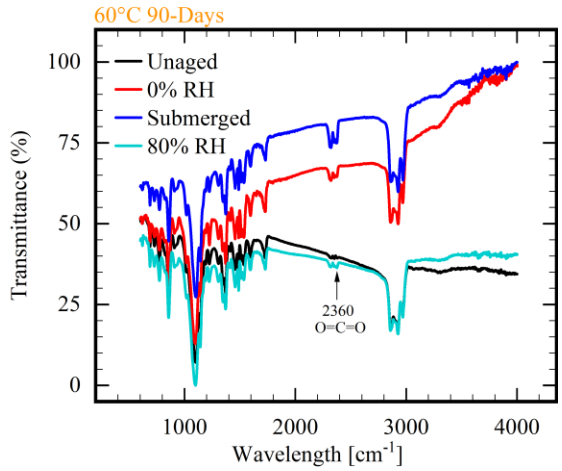

(a) Complete FTIR spectra: 60°C 90 days

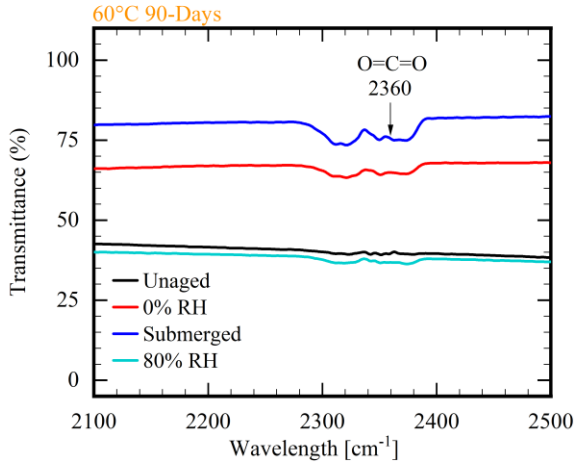

(b) O=C=O functional group after aging at 60°C

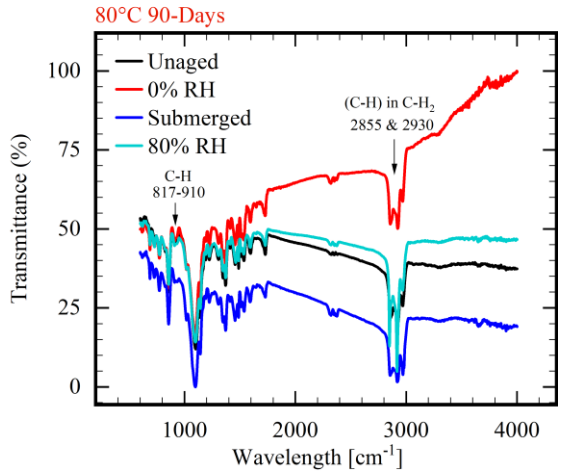

(c) Complete FTIR spectra: 80°C 90 days

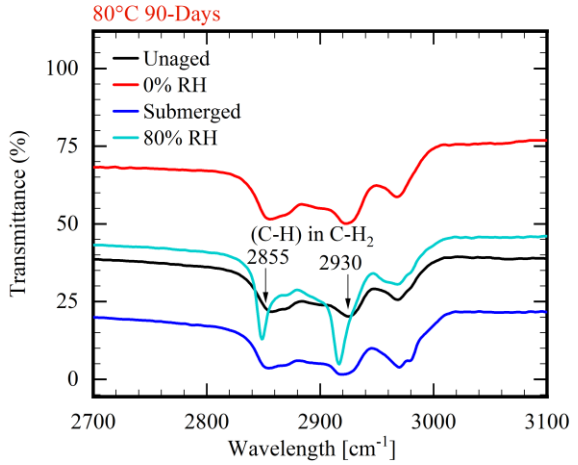

(d) C-H functional group after aging at 80°C

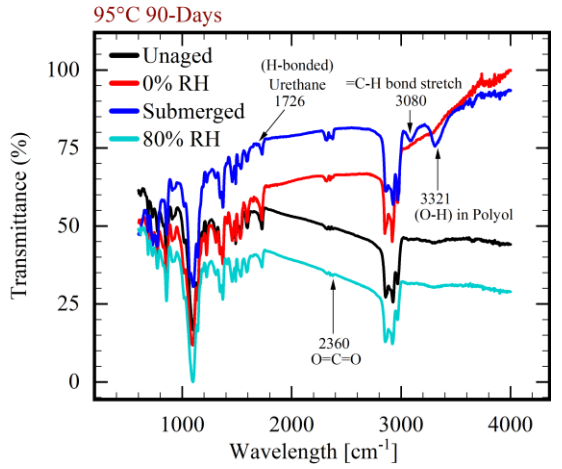

(e) Complete FTIR spectra: 95°C aged for 90 days

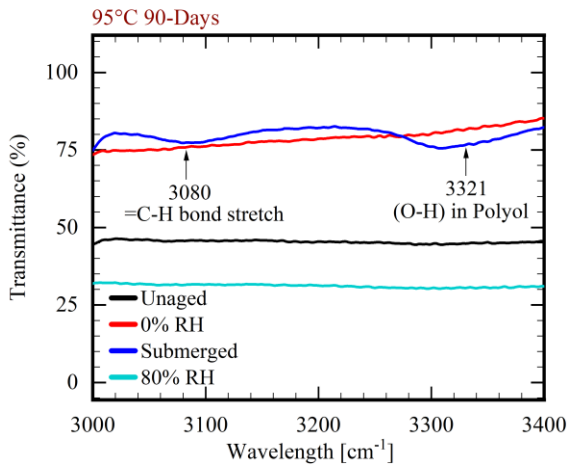

(f) C-H and O=H groups after aging at 95°C

Figure 3.16: Changes observed in FTIR spectra after aging at (a,b) 60°C, (c,d) 80°C, and (e,f) 95°C.

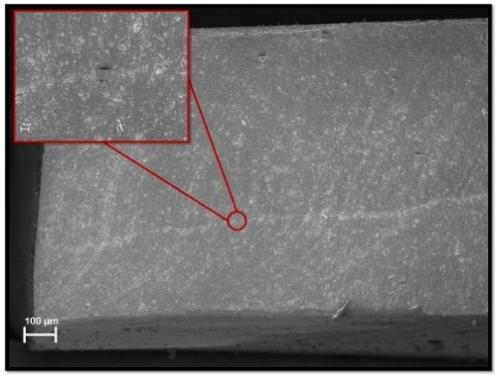

(a) Large scope cross-section view (100µm−10µm) of cured (unaged) sample showing firm polymer chain matrix

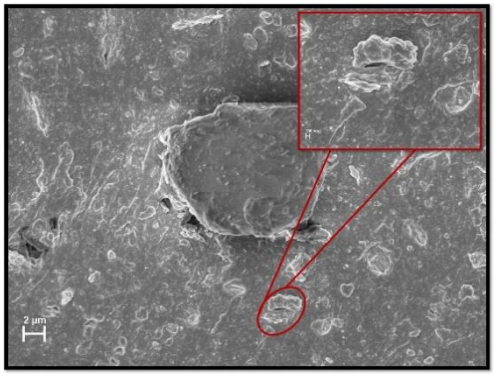

(b) Small scope cross-section view (2µm − 200nm) of cured (unaged) sample revealing vulnerable pockets that can store moisture or act as sites for crack initiation

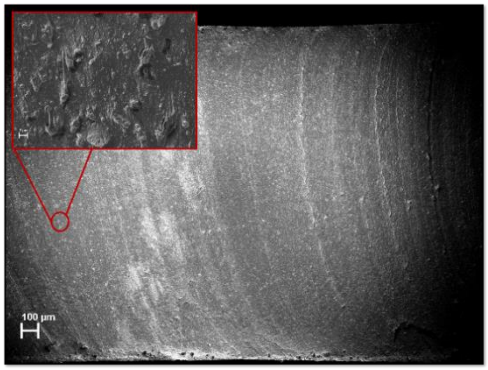

(c) Large scope cross-section view (100µm − 1µm) of sample aged in thermo-oxidative condition showing dry and dense polymer matrix

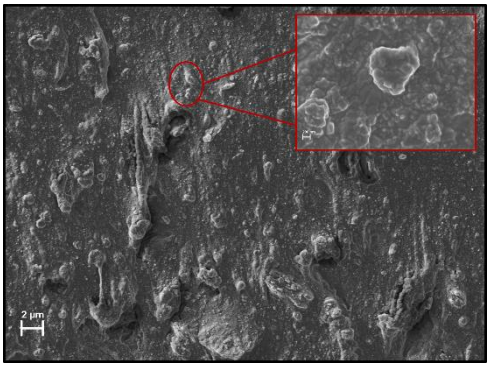

(d) Small scope cross-section view (2µm − 200nm) of sample aged in thermo-oxidative condition revealing compact polymer structure resulting in hardening behavior in tensile tests

Figure 3.17: SEM images of unaged cured specimen surface and surface aged in thermo-oxidation environment.

While moisture in the presence of heat will be responsible for the decomposition and deterioration of the resins, much of the surface appears firm without direct water attack (see Fig. 3.18a). We can see the surface aged in 80%RH showing similarities borrowed from other aging conditions, i.e., thermo-oxidation (compact surface) and hydrolysis (moisture absorbance). Overall, SEM image results are in conformation with gravimetric changes, tensile test results, and the changes observed in other chemical tests.

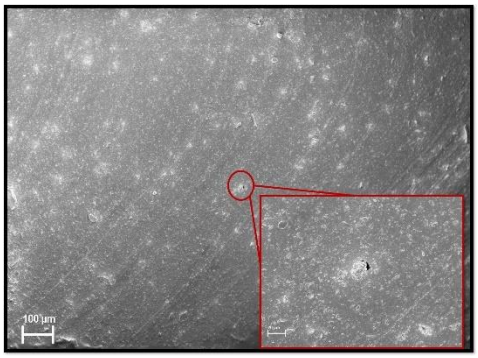

(a) Large scope cross-section view (100µm−20µm) showing effects of hygrothermal aging

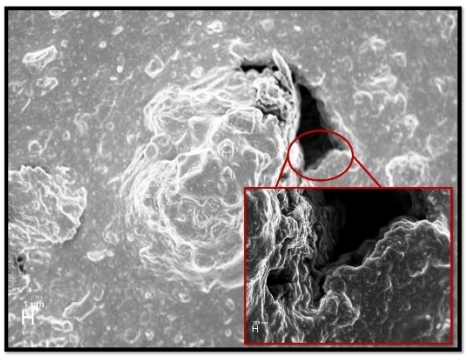

(b) Small scope cross-sectional view (1µm − 200nm) of hygrothermally aged sample revealing an agglomerated polymer lump being pulled off the surface as a result of the softened surface due to humidity

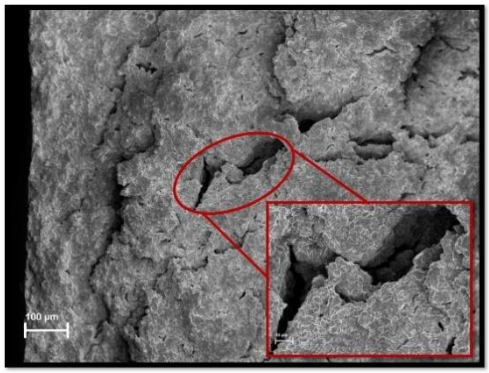

(c) Large scope cross-section view (100µm−20µm) showing high damage effects of hydrolytic aging

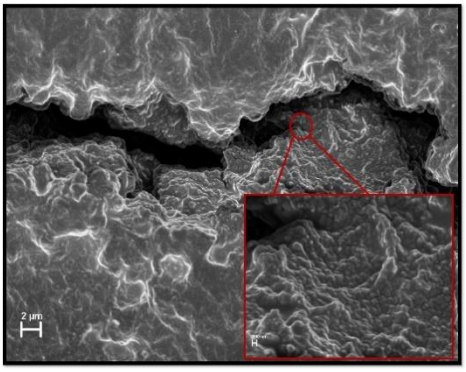

(d) Small scope cross-sectional view (2µm − 200nm) of hydrolytic aging effects on PUB revealing deep cracks and gelled micro-particles as a result of water attacking the polymer chains

Figure 3.18: SEM images showing extent and type of damage due to accelerated aging in hygrothermal and hydrolytic environments.

3.4 Conclusion

The damage-driven kinetics of accelerated hygrothermal aging has been established by comparing it with two sub- aging processes, namely thermo-oxidation and hydrolytic aging. During thermo-oxidative aging, two microstructural phenomena, (i) chain-scission and (ii) cross-link formation, happen, while during hydrolytic aging, (i) chains-scission and (ii) reduction of cross-links are generally observed. A hygrothermal aging environment combines all of the above, i.e., chain

scission and cross-link formation/ reduction. In each aging condition, high temperature contributes to higher damage accumulation. When compared astride each other, thermo-oxidation had higher cross-link density, T_g, failure stress σ_f, and failure strain ϵf out of the three, and hydrolytic aging reflected the minimum values for each of these characteristics. Our experimental results show that these quantities in the case of hygrothermal aging are between the other two aging phenomena. The cross-linking due to oxidation reactions effectively helped reduce the effect of hydrolytic chain scission. Thus, it is concluded that the damage in hygrothermal aging is a resultant effect between thermo-oxidation and hydrolytic aging environments. All mechanical and chemical test results are in good agreement.

Chapter 4:

Experimental Study of Damage Evolution in Polyurethane Adhesives: Independence of Mechanical and Environmental Damage

4.1 Introduction

Polyurethane (PU) is one of the most utilized polymers, exhibiting various structural and non-structural applications [169]. They form one-fifth of the resin markets for sealants, coatings, and adhesives [72]. Many recent works emphasize polyurethane's chemical and physical behavior [103, 84]. One primary usage of PUs includes their application as elastomers and adhesives. These applications are enabled by hydrogen bonding and micro-phase separation between urethane linkages. It is also reported that in some cases, adhesion is aided by hydrogen bonding between urethane linkages and functional groups on the substrate [112]. Polyurethane resins are widely applied in the field of sealants and adhesives due to their highly flexible options in application technologies, mechanical and adhesion properties, and weathering resistance [176]. PU adhesives have large-scale applications in the automotive industry for joining components since the obtained joints are substantially resistant to oil, gasoline, grease, and water [62, 185]. Polyurethanes are evidently considered a material of choice because they have proved to be an all-round and sustainable problem solver for the present-day industry requirements [61]. From an application standpoint, their demand is increasing in both land and marine environments. Automobile and shipping industries, in particular, include seals, protection, and fluid flow line coatings [104, 58, 177]. In the fishing industry sorting and selectivity, polyurethane grids have been proposed for their durability and elastic properties [50, 147], while oceanographic applications include sub-water antenna coatings and tubing [110] on submarines. Regardless of these recurrent structural applications, the chosen material must be sustainable in terms of physical characteristics and serviceability.

There have been many studies about the underwater sustainability of polyurethane adhesives. For instance, Li et al. have investigated cross-link enhancement of polyurethane adhesives to improve their cohesion properties underwater [118]. Joshi investigated polyurethane membranes for their endurance in artificial weathering conditions [92]. Davies has explained the effects of accelerated

aging of polyurethanes for marine applications and helped to understand the durability of PU underwater [50]. These include plasticization, swelling, hydrolysis, and re-bonding of fillers. Sharifi et al. investigated polyurethane elastomers' underwater sound absorption, and damping properties [168].

Fiber-reinforced composites (FRCs) are also receiving considerable attention for their use in marine applications. A fascinating insight is provided by the correlation of data from accelerated aging in the laboratory with specimen results from ship structures submerged in the sea for over 20 years [79]. Damage parameters have been used to evaluate the influence of water aging on PDMS containing multi-block polyurethanes [36].

Data based on time-temperature superposition have also been used to estimate the evolution of the mechanical behavior of composites in water [93]. Prior studies include discussions on factors influencing the serviceable age of elastomers [159]. Burns et al. studied the bulk modulus of elastomers, including PUs and rubbers exposed to hydrolytic aging for up to two years. They found the stiffness properties stable over the studied period [30]. Murata et al. explained the significance of diol-chemistry on PU's hydrolytic resistance through molecular weight stability [139]. Rutkowska et al. examined polyester and polyether-based PU in seawater for a year. They explained how the polyether-based PU retained its properties while the other material degraded significantly [156].

While some studies have interpreted and examined the effects of mechanical deformation on material, others have focused on decay mechanisms through aging environments. We feel there is a need to compare both degradation mechanisms and see if they act independently or in conjunction with each other and whether they are separable or not. The most commonly used approach to accelerated environmental aging is through exposure to elevated temperatures for a sustained period combined with the Arrhenius expression to relate the resulting evolution to material properties conducted at a longer time or lesser temperatures, for instance. This is embodied in some recent works as well [41], but there is considerable discussion over the validity of this approach. One limitation to consider is that testing at elevated temperatures assumes that only the kinetics of the aging mechanisms are modified in the temperature range employed, not the mechanisms themselves. Celina's work on thermal exposure of materials investigated the Arrhenius approach for various materials and emphasized the validity of linear extrapolation. [33]. They concluded that non-Arrhenius behavior might be expected regarding the interaction of confronting mechanisms. Another critical study of polychloroprene aged for 24 years in service by Gillen also argued the invalidity of the linear Arrhenius extrapolation [71]. One of the studies also validated the lifetime predictions by

measuring the degree of oxidation in case of thermal aging [186]. However, these are arguably not applicable to hydrolytic or hygrothermal aging.

This study is in continuation of our recent work [167], substantiating the competition scenario between sub-aging environmental conditions, where we showed that the damage in hygrothermal aging is a resultant effect between thermal- oxidation and hydrolytic aging environments. Moving further, in this work, we intend to show that damage imparted through post-aging mechanical deformation is separable from environmental damage for each aging environment. We believe this work will help develop a bi-fold understanding of material behavior: first, to examine an accelerated aging method for characterizing the selected PUB adhesive, and second, to determine if this material is suited for marine industrial applications underwater while in operation for sustained periods.
The influence of aging is often followed by the measurement of tensile properties, as this is one of the simplest tests to perform. In addition to cyclic tensile tests, we have applied various simultaneous methods, including dynamic mechanical analysis (DMA) and cross-link density analysis of as-received and aged samples. In the current work, cyclic tensile testing was the primary technique employed and supported by the above-mentioned chemical and thermal analysis methods.

The paper is outlined in the following sequence. After discussing the design of the experiment and methodology in section 4.2, the discussion on results and our analysis are added in section 4.3. Finally, section 4.4 consists of the concluding remarks for this experimental effort.

Table 4.1: Techniques used to achieve desired aging environment [167].

Environment	Temperature	Method
	Thermal Oxidation	
0%RH	60°C, 80°C, 95°C	Moisture absorbent molecular sieves
	Hygrothermal	
80 ± 3%RH	60°C, 80°C, 95°C	Binary salt solution (KCl)
	Hydrolytic	
Submerged	60°C, 80°C, 95°C	Distilled water

4.2 Methodology

The main objective of this work is to analyze a flexible polyurethane-based (PUB) adhesive and show that mechanical damage is separable from environmental degradation. The characterization methods and testing techniques were adopted as elaborated in relevant American Standards for Testing Materials (ASTM), addressing physicomechanical properties [6], CLD by swelling [46],[90], and Tg measurement of polymers [59]. Environmental aging under strictly controlled settings was performed in the laboratory for all considered environments. Thermal oxidation was conducted at

0% RH; hydrolytic aging specimens were submerged in distilled water; and hygrothermal aging was conducted at 80% RH at 60°C, 80°C, and 95°C. The experiment was designed for a range of aging durations (t) set at 1, 10, 30, and up to 90 days. Air-tight plastic buckets (see Fig.4.2) with multi-layered grit guards were used to age samples in design conditions. A summary of methods used to achieve and maintain required environmental conditions is shown in Table-4.1 [167]. For hygrothermal aging, binary saturated aqueous salt solution of Potassium Chloride (KCl) was used as the standard method for achieving humidity fixed point at 80%RH [76]. As much as possible, an endeavor was made to curtail human error during aging. In order to maintain steady humidity levels, all the containers were periodically opened to ensure that desired submerged condition and salt solution for desired RH was in sufficient quantity. In addition, this routine automatically ensured that the oxygen level inside the sealed container was kept from falling below the critical level.

4.2.1 Material For this experimental study, we have used 590 Polyurethane adhesive manufactured by the 3M™ company. It is used as glass sealant for prototype parts, particularly where abrasion resistance is required. In cured state, the material is flexible and possesses a hardness of 60-65 Shore-A. The manufacturer, in the specification sheet, has graded PUB performance in the hydrolytic condition below 100°C as excellent.

4.2.2 Sample Preparation The adhesive paste was cast into a customized mold with 20 specimens for each plane (see Fig.4.1a). The adhesive above the mold surface was removed to ensure uniform sample dimensions (see Fig.4.1b) in accordance with ASTM D412 [6]. Dumbbell-shaped samples were used for tensile tests, while rectangular samples (35 × 12 × 3.175mm) were cured and aged for DMA testing. According to instructions in the manufacturer's manual for the adhesive, the material curing time is one day at room condition (i.e., 26 ± 2°C, 45 ± 3% RH). However, for the specimen thickness (3.175mm) considered in this study, our preliminary experiments showed that the material took longer than the curing time suggested in the manual. Therefore, we allowed the specimens to cure for at least a week in room conditions, and the aging process commenced only after samples were fully cured.

4.2.3 Characterization Methods

a. Gravimetric Measurements

To better understand the dynamics of environmental damage, moisture-uptake and weight changes of PUB specimens were observed and recorded at every critical stage of the experiment. Ten specimens were used for each environmental aging condition to allow for a good statistical

representation. Five samples were weighed immediately after stabilizing at room temperature and were referred to as wet state; the remaining were weighed after drying in a vacuum oven and were referred to as dry. Samples were dried in a vacuum oven at 40°C at 700mmHg vacuum for 24 hours. Drying in a vacuum oven was done to evaporate the absorbed water at a much lower temperature without adding further thermal fatigue to aged samples.

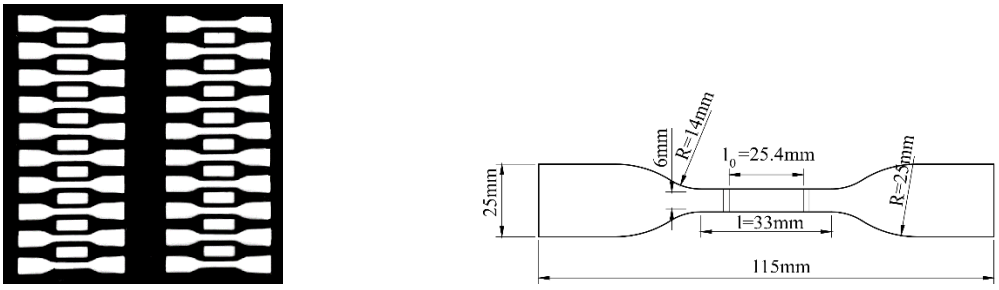

(a) Casting mold (b) Dimensions of cured adhesive specimen

Figure 4.1: Sample preparation and dimensions.

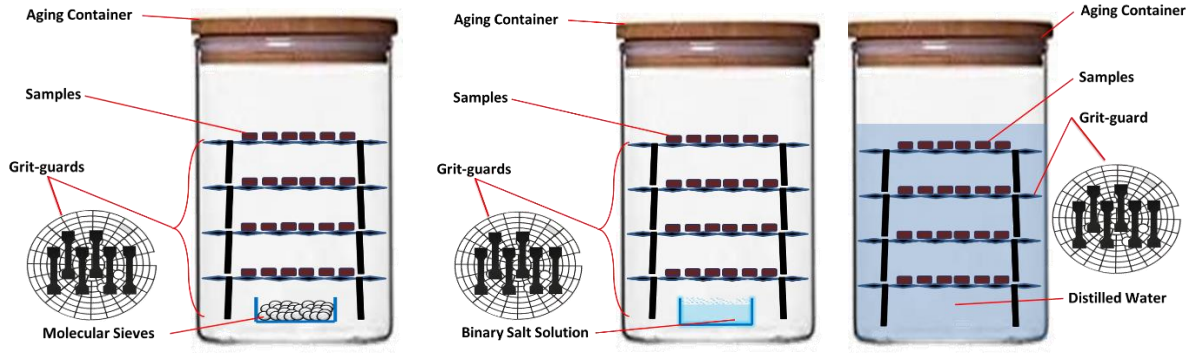

(a) Schematic showing sample loading setup for thermal-oxidation aging

(b) Schematic showing sample loading setup for hygrothermal aging

(c) Schematic showing sample loading setup for hydrolytic aging

Figure 4.2: Loading setups used for specimens during aging in different temperature conditions [167].

This way, we could accurately measure the weight/ mass variations due to water absorption during aging. If a percentage of absorbed water shows a linear increase with the increase in temperature and time, it shall be considered in agreement with Fick's second law of diffusion [87]. Through these gravimetric measurements, we further probed relevant phenomena like mass-loss and absorption-desorption tendencies.

i. **Moisture-uptake** Fully cured PUB samples were weighed on an electronic balance (0.01mg accuracy) before the commencement of aging in weathering chambers. After completion of the desired aging period, the samples were carefully dried with a paper

towel and weighed again. Immediately after removing the specimens from hydrolytic and hygrothermal aging conditions, the water content Wc absorbed by each sample was considered responsible for the % weight increase in the sample at the completion of aging. The following mathematical expression was used to calculate the percentage of moisture uptake:

$$W_c(\%) = [\frac{(W_t - W_0)}{W_0}] \times 100 \quad , \tag{4.1}$$

where W_t is the weight of the aged sample at time t and W_0 is the weight of the unaged specimen. Considering the sample dimensions, we assumed that water diffusion was unidirectional. The diffusion coefficient is determined on the initial linear part of the sorption curve; $M_t/ M_\infty \leq 0.5$, M_∞ is the mass at complete saturation after equilibrium is reached. Its value is calculated using Fick's 1st law of diffusion:

$$D = \frac{(\pi)}{16}\frac{e^2}{t} \times (\frac{M_t}{M_\infty})^2 \tag{4.2}$$

where, e is the sample thickness in mm and t is the immersion time in seconds.

ii. **Mass-Loss** Aged specimens were dried in a vacuum oven at 40°C in 700mmHg vacuum for 24 hours. Samples generally maintained a steady dried weight, but it is possible that some water may still be retained due to the formation of strong interaction of functional groups with water molecules [173]. The mass loss (M_L) in the sample was measured by comparing the weight difference between the unaged specimen's weight with the weight of the aged sample after drying. For simplification and understanding, weight % above average unaged sample weight is considered as water/ moisture uptake, and the weight % below the same is taken as a mass loss. The following mathematical expression was used to calculate the % M_L:

$$M_L(\%) = [\frac{(M_0 - W_d)}{W_0}] \times 100 \quad , \tag{4.3}$$

where W_d is the weight of the aged sample in a dry state, and W_0 is the weight of the unaged sample before placing it in aging conditions. All the weights were then compared with the original weight of the sample. All weight % were then plotted together to see the water-uptake and mass loss in the PUB specimens. For simplification and understanding, weight % above unaged sample weight is considered as water/ moisture uptake, and the weight % below the same is taken as mass loss.

b. **Uniaxial Tensile Test**

The impact of environmental exposure on the tensile property of PUB was assessed in accordance with instructions provided in ASTM D412 as a standard guideline. A Test Resources 311 Series UTM Frame with 5kN load cell (Test Resources SM-5000N-294 force transducer) was used for quasi-static cyclic tensile tests. All tests were displacement controlled with a crosshead speed of 0.83 mm/s. The distance between the extensometer grips was set to 25.4 mm, and all the experiments were performed under room conditions (i.e., 26 ± 2°C, 45 ± 3% RH).

A minimum of three cyclic tests were done for each time period and exposure condition for reliability control. Each sample was subjected to a non-relaxing cyclic test with increasing stretch, where the samples were loaded twice at each amplitude. The samples were stretched to preset amplitudes of 35%, 75%, 112.5%, and 130% of elongation at the breaking point of unaged samples, corresponding to the strain of 84%, 179%, 269%, and 311%, respectively. Due to aging effects, aged specimens might break before completing the designed stretch cycles. In the course of deformation, elongation of the central zone of 25.4 mm was measured by an external extensometer. The cyclic experiment is designed to illustrate the evolution of the permanent set and stress softening during the primary loading for both unaged and aged samples.

c. Differential Mechanical Analysis (DMA)

TA Instrument DMA Q800 machine was used to record the variation in glass transition temperature (T_g) for all specimens. Rectangular specimens (35 × 12 × 3.175mm) were used for single cantilever test to record storage modulus (E'), loss modulus (E"), and Tan δ. The test was set up to run from −70°C to 10°C at a temperature rate of 3°C per min. The test was performed in the linear viscoelastic region (LVR) using strain amplitudes of 15% and a frequency of 1.0 Hz. For the unaged adhesive specimen, glass transition temperature (T_g) from storage modulus (E') was found to be −62.51°C.

d. Cross-Linking Density (CLD)

The cross-link density variations due to environmental aging were observed by employing the equilibrium swelling method [90][3][170][143][55]. Toluene (molar volume 106.3mL/mol) was used as solvent to immerse rectangular PUB specimens (0.4in × 0.3in × 0.12in). The test was performed with three samples kept submerged in the solvent for one day. The sample weights were recorded after a regular interval of 3 hours until a constant weight was reached, indicating maximum absorption of the solvent. Samples were removed from the solvent, patted to dry with paper, and weighed till

the samples reached an equilibrium state. The cross-link density (v_c)(molcm^{-3}) and average molecular weights between the chains (M_c) were estimated using the following equations, introduced by Paul C. Hiemenz, Flory, and Rhener [86, 158, 64].

$$ln(1-\phi_e)+\phi_e+X\phi_e^2 = n_e\frac{V_1}{V_0}(\frac{\phi_e}{2}-\phi_e^{1/3}) \quad , \tag{4.4}$$

$$\frac{n_e}{V_0} = \frac{ln(1-\phi_e)+\phi_e+X\phi_e^2}{V_1(\frac{\phi_e}{2}-\phi_e^{1/3})} \quad , \tag{4.5}$$

where X is the solvent-polymer interaction parameter, and V_1 is the solvent's molar volume (106.3mL/mol). From equation (4.5), we can further derive equation (4.6),

$$\frac{n_e}{V_0} = \frac{\rho}{M_x}(1-\frac{2M_x}{M}) \quad , \tag{4.6}$$

where n_e is the molar cross-linking, V_0 Is the volume of the PUB samples before swelling, ϱ is the density of the solvent, M_x is the molar mass of the solvent, and M is the molar volume of the polymer. The measurement should not exceed $\pm 0.1\%$ of the constant measurement, thus, maintaining high accuracy levels for elastomer density [57].

4.3 Results and Discussion

Degradation The deliberation on material degradation has been straightened out, keeping in view the intent to show independence and separability of environmental aging effects from those of mechanical damage. A brief discussion about degradation mechanisms is followed by a presentation and analysis of experimental results in each case.

We studied damage in the polymer matrix with respect to chain decomposition and recreating reactions as damage mechanisms induced by i) environmental or ii) mechanical stressors. Generally, environmental elements, along with the mechanical loads, will contribute to chemo-physical damages that will eventually lead to decaying in the mechanical behavior of the material. Understanding the correlation between environment-induced damages and decay in mechanical performance is critical for the prediction of cross-linked polymers.

This work provides a better understanding of the material behavior from an application standpoint for similar adhesives. In the following sections, we will compare our observations to understand the material response as a result of environmental aging and mechanical deformation. Despite being opposite phenomena, chain scission and cross-link development take place simultaneously [167], which further complicates the characterization process. For simplification, we considered the dominating factor only when necessary.

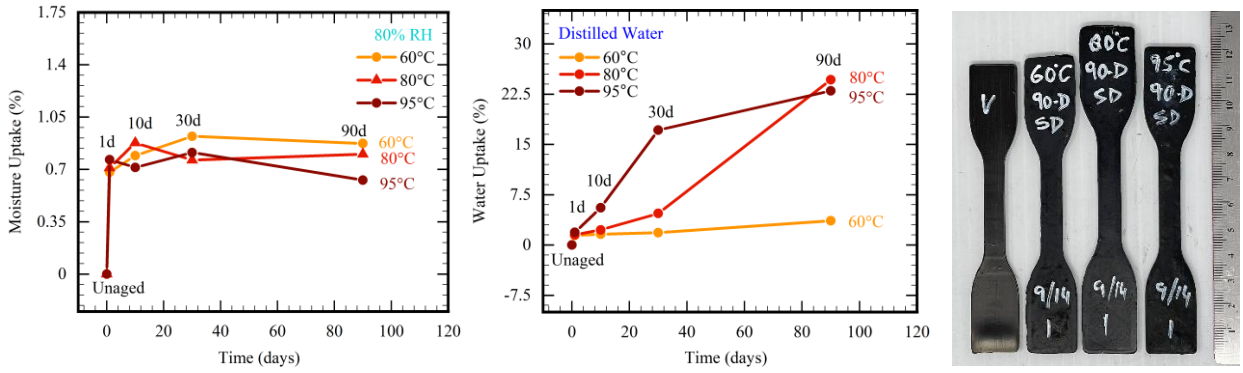

(a) Water-uptake in 80%RH

(b) Water-uptake in submerged state

(c) Swelling in each temperature after aging in submerged condition for 90 days

Figure 4.3: The comparisons of water-uptake in hygrothermal and hydrolytic aging conditions.

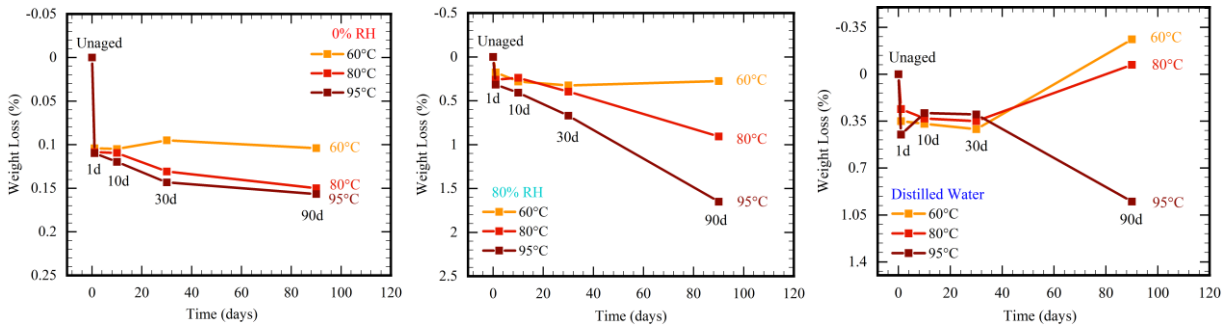

(a) Mass loss during thermal-oxidation aging in 60°C, 80°C, and 95°C

(b) Mass loss (%) during hygrothermal aging (80%RH) in 60°C, 80°C, and 95°C

(c) Mass loss (%) during hydrolytic aging (distilled water) in 60°C, 80°C, and 95°C

Figure 4.4: Mass loss in thermo-oxidative, hygrothermal and hydrolytic aging environments.

4.3.1 Environment-induced Damage

Different weathering agents, such as heat, oxygen, moisture, and water, induce certain characteristic changes in the constitutive behavior of aged materials. These changes are dependent upon the severity and time of environmental exposure. High temperature in the presence of oxygen imparts degradative effects in thermal oxidation (0%RH) aging, hydrolytic aging includes the effect of water and temperature, while hygrothermal aging (80%RH) refers to heat and moisture movement around specimens in ambient weathering conditions. It is assumed that chain decomposition and recreating reactions occur simultaneously during aging. Eventually, transforming the polymer matrix fully into a newly aged matrix compared with the unaged matrix. For environmental damage in the absence of deformation- induced damage, aging occurs mostly in the form of an irreversible chemical

process. Aging can potentially reduce the polymer's active agents, which contribute to the elastic property of the material.

Discussion on environment-induced damage shall focus on gravimetric changes after aging in each environment, along with resulting shifts in glass transition temperature (T_g) and cross-link density. However, arguments on mechanically induced damage include the effects on tensile behavior, finally leading to concluding remarks in section 4.4.

Water-uptake and Mass Loss

This part of the discussion will not cover the thermal oxidation environment due to the absence of water/moisture in that case. Water in the material matrix can exist in different forms; free water molecules (unbound), which have diffused into the 'free-volume' from the outer surface of the material, and water-bound within the chain network [200]. Therefore, with extreme care, an effort was made to record the variations in weights, water-uptake, and moisture sorption. All specimens were weighed at every critical stage of the experiment to earnestly explore and understand the complex behavior exhibited by elastomeric adhesive in humid or wet conditions. Time (t), temperature (T), oxygen, relative humidity (RH), and water not only act in isolation while competing with each other but also synergize in order to degrade the material properties. Water-uptake, mass-loss, and dimensional variations were also taken into account in this work. For polyurethane adhesive under study, the moisture absorption increases linearly with the square root of aging time, and it follows Fick's 2nd law of diffusion [167].

It is observed overall that the hygrothermal and hydrolysis damages are a consequence of prevailing temperature and water absorption by the samples. Data recorded and compiled from hygrothermal aging (see Fig. 4.3a) and from hydrolytic aging (see Fig. 4.3b and Fig. 4.3c) clearly show very high water-uptake for PUB in submerged conditions, especially in higher temperatures. It may be noteworthy that the damage decay function may not show a one-to-one correspondence to the water-uptake function. Interestingly enough, water absorption at 80°C was observed to be much higher than at 95°C, and concurrently, the degradation remains higher in 95°C. It appears that less water-uptake by specimens at 95°C is due to heat-shrink phenomena affecting the polymer chains. This counter-intuitive (heat-shrink) behavior has been reported for polymers [126] when long chains contract due to an increase in entropy as a result of high temperature. However, it is clear that the rate of water-uptake is different from the rate of damage in the polymer matrix (compare Fig.4.3 and Fig. 4.4). In submerged aging conditions, the swelling was notably high, and the samples were clearly enlarged after aging; however, all samples returned to normal size after drying except the ones aged

at 95°C, which indicates a potential loss of elastic properties at high temperatures. Nevertheless, for lower temperatures, we had desorption taking place in case of the hydrolytic aging condition. In short, while plasticization affects the length distribution of polymer chains inside the matrix, further degradation results from chain scission, which is considered a chemical alteration at the macro-molecular level [11]. The molecules that get detached from long chains could be trickled and migrated from the material matrix by water or other solution mediums via a process termed leaching [151]. Samples in 80%RH did not show any visible swelling; however, consistent mass loss depicted through weight changes was notable. With an increase in time at the higher temperature, the percentage of weight loss kept increasing. This weight loss was irreversible. Mass loss in hygrothermal and hydrolytic aging conditions generally varied within the same range, i.e., 0.3% to 1%. While the mass loss in hydrolytic conditions can be attributed to the leaching effect, weight drop during hygrothermal aging is co-related with oxidation reaction, as seen in thermo-oxidative aging (see Fig. 4.4a). Mass loss is also documented for hygrothermal aging in the wood [197], and some construction composites (FRP) [74] due to chemical decomposition; there is much room further to explore the cause behind this phenomenon in PUB adhesive.

Cross-Linking Density

For cross-link density (CLD) analysis, the presence of water within a polymer matrix can be misleading by demonstrating a low solvent absorption. Therefore, all aged specimens from hydrolytic and hygrothermal conditions were dried before being dipped in solvents. This measure was taken because even a small weight change in PUB specimens would give a false impression of higher cross-link formation as a result of a low solvent absorption rate.

As already mentioned, for the swelling test, we used toluene as a solvent. Most resulting absorption and swelling were noted within the first 3-4 hrs, and soon after, most toluene-immersed specimens reached the equilibrium state.

In all aging environments, we see a decrease in CLD since specimens generally display higher solvent absorption rates with an increase in aging duration (t) and temperature (T), thus indicating increased chain scission as environmental conditions worsened (see Fig.4.5).

Looking at the cross-link density behavior of PUB in each aging environment, we can divide it into two phases, namely, (i) cross-link formation and (ii) degradation phase. In thermal-oxidation and hygrothermal aging, in the first 24 hours, a higher cross-link formation trend is attributed to oxidation reactions. Hereafter, the degradation phase began, which continued till the completion of the designed aging process. The results of the cross-linking test for PUB adhesive were in-sync with

degradation energy analysis and uniaxial tensile tests. We observed most solvent absorption in the most extreme aging condition, i.e., 95°C, 90-days in hydrolytic and hygrothermal aging conditions (see Fig.4.5b and c). All intermediate aging durations and environments show slight variations but are generally confirmed with mechanical test results.

DMA

DMA was done for all unaged and aged specimens to ascertain the variations in glass transition temperature (T_g) of PUB when exposed to different environmental conditions. In order to highlight the effect of the environment, we selected the most extreme aging condition (95°C, 90-days) in this section.

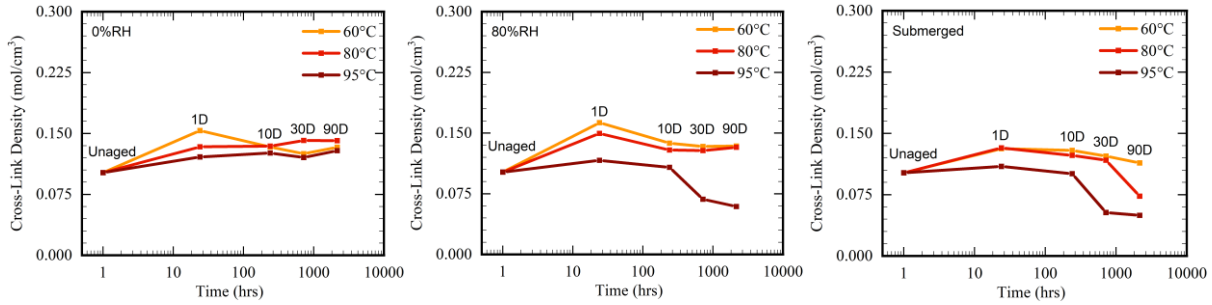

(a) Thermal-oxidation (0%RH) (b) Hygrothermal aging (80%RH) (c) Hydrolytic aging (submerged)
Figure 4.5: Cross-link density variation in thermo-oxidative, hydrothermal, and hydrolytic aging environments.

Storage modulus curves peculiarize the transition from crystal to amorphous behavior of materials and the attained T_g as a constituent factor. The loss modulus is representative of the dissipated energy, switched to heat, for each cycle of sinusoidal deformation. Tan δ presents the molecular-level changes in the ratio of loss modulus to storage modulus, i.e., E"/E'. Based on DMA test data, the glass transition (T_g) range of unaged PUB spans between -62.65°C to -44.42°C.

Fig. 4.6a-c shows the storage modulus E', the loss modulus E", and the phase lag Tan δ of specimens aged in thermal-oxidation (0%RH), hydrolytic aging (submerged), and hygrothermal aging (80%RH) environments at 95°C for 90 days.

For thermal-oxidative aging (see Fig. 4.7), the T_g increased. This is in agreement with the CLD analysis and tensile test data. Also, compared with other aging environments, for 0%RH, the peak height of Tan δ is reduced compared with other aging environments (see Fig. 4.6a). This has been attributed to a decline in molecular mobility amid an increase in CLD (see Fig. 4.5a) [161, 60]. The same explanation is also valid for hardening behavior seen in tensile test results (see Fig. 4.8).

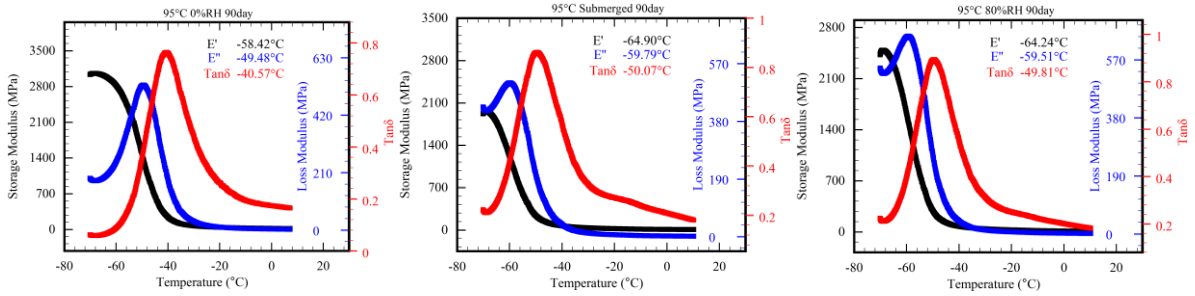

(a) Thermo-oxidative aging (b) Hydrolytic aging (c) Hygrothermal aging

Figure 4.6: Storage modulus (E'), loss modulus (E'), and Tan δ of specimens aged in 95°C for 90 days in (a) Thermal- oxidation (0%RH), (b) Hydrolytic aging (submerged), and (c) Hygrothermal aging (80%RH) environments.

During hydrolytic aging, the T_g is reduced the most. It is attributed to the softening under the plasticization effect (see Fig. 4.10) seen in tensile tests as well as the CLD analysis (see Fig. 4.5c).

Regarding hygrothermal aging, again, we observe a similar trend in T_g as we observed in the case of hydrolytic aging, i.e., decreasing trend. Fig. 4.7a-c shows that T_g of PUB specimens aged in 80%RH remained between T_g of specimens aged in thermal-oxidation (0%RH) and hydrolytic (submerged) aging conditions [167].

4.3.2 Mechanical induced damage

In the context of mechanical-induced damage, we investigated the combined contribution of mechanical and environmental- induced damages to the polyurethane adhesive by analyzing the data obtained from cyclic tensile tests on unaged and aged specimens. The continuous loading in case of mechanical damage is attributed to the detachment of chains from either cross-linked or filler surfaces and re-form the composition of polymer matrix with a longer chain. Mechanical damage is commonly perceived to be mostly an outcome of physical changes.

While the continuous deformation of specimens during cyclic tests in the form of repeated loading-unloading imparts damage as another prediction parameter; based on the nature of the material; the correlations between these two parameters are minuscule. In an attempt to carry on the study of those correlations, first, damages induced by thermal-oxidative, hydrolytic, and hygrothermal aging of PUB adhesive would be investigated from the constitutive behaviors in the direction of tensile strength, elongation at break, and elastic behaviors.

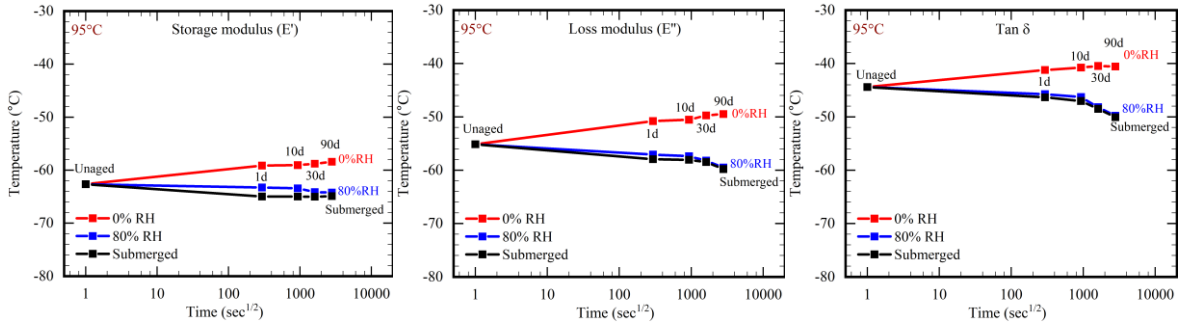

(a) Storage modulus E' (b) Loss modulus E" (c) Tan δ

Figure 4.7: Storage modulus E' , loss modulus E" , and Tan δ variation between thermal-oxidation (0%RH), hydrolytic aging (submerged), and hygrothermal aging (80%RH) environments at 95°C.

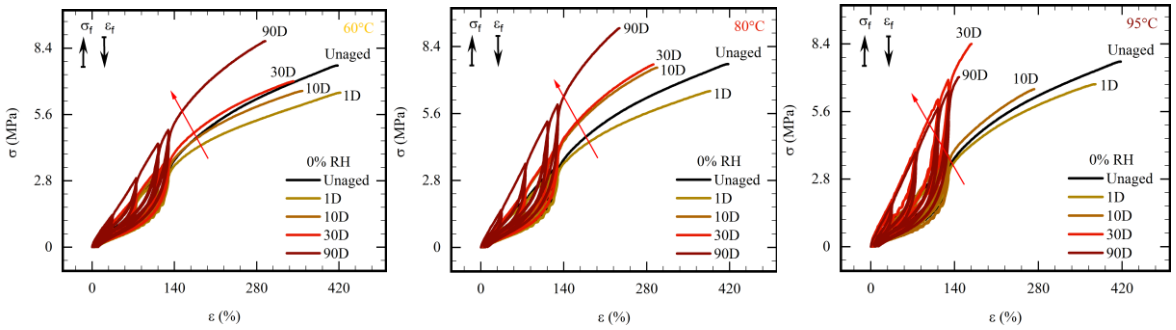

(a) Cyclic test at 0%RH 60°C (b) Cyclic test at 0%RH 80°C (c) Cyclic test at 0%RH 95°C

Figure 4.8: Cyclic tests of specimens aged in thermal-oxidation environment (0%RH) in 60°C, 80°C, and 95°C.

4.3.3 Uniaxial Tensile Test

Before and after aging, mechanical characterization was undertaken using quasi-static cyclic tensile tests to investigate the effect of aging on performance loss. We shall first discuss the σ_f and ϵ_f behavior highlighting effect of specific environment and later probe and analyze the mechanical damage leading towards segregation of environmental damage from mechanical damage. Ultimate failure points of the specimens may demonstrate uncertain fluctuations due to errors during casting, air-voids within material matrix or due to axial misalignment during testing. A conscious effort has been made to minimize these omissions through careful execution of each phase of this study.

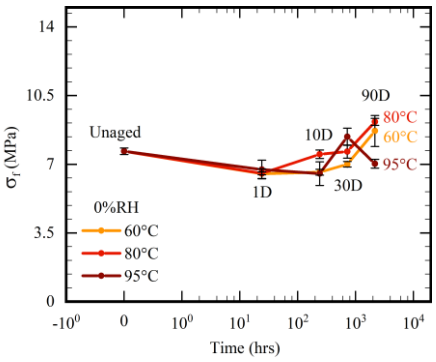

(a) Failure Stress σf variation against time (t) in thermal-oxidation (0%RH)

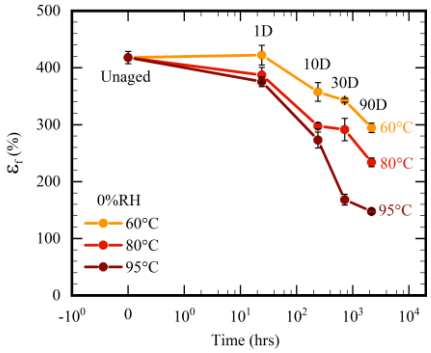

(b) Failure strain ϵ (%) variation against time (t) in thermal-oxidation (0%RH)

Figure 4.9: Ultimate stress-strain variation of polyurethane in thermal-oxidation plotted against time.

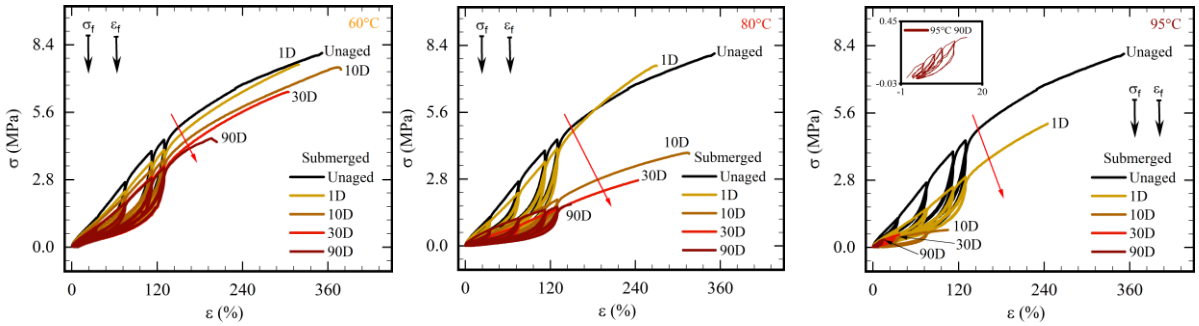

(a) Cyclic test (60°C) (b) Cyclic test (80°C) (c) Cyclic test (95°C)

Figure 4.10: cyclic tests of specimens aged in submerged state at 60°C, 80°C, and 95°C.

Thermal-oxidation In thermo-oxidative aging, the σf and ϵf values were plotted against time (see Fig. 4.9). Generally, we observe a hardening behavior with rise in σf and decrease in ϵf with increasing temperature (T) and time (t) parameters. Initial softening is attributed to chain scission followed by a consistent stress increase and reducing ϵf values which indicate dominant cross-link formation mechanism in presence of heat and oxygen (see Fig. 4.8). Hence, we can say that two simultaneous processes, i.e., chain scission and cross-link formation take place during thermal-oxidation [12]. Cross-link phenomenon clearly dominates chain scission during thermo-oxidative aging.

Hydrolysis During hydrolytic aging; water appears to damage the polymer chains aggressively. Overall, material shows softening behavior attributed to water acting as plasticizer initially [146], and later causing severe damage to material integrity in the form of chain scission [194]. It is a collaborative damage scenario between environmental agents like water, temperature and time which synergize to create ideal conditions for chain scission in the aging material [167]. From uniaxial tensile tests the σf and ϵf behavior was plotted (see Fig. 4.10). In hydrolytic aging the polyurethane specimens showed softening trend with σf and ϵf both depreciating as aging time increased. The degradation of

the tensile strength σf can be attributed to plasticization and deterioration of the polymer matrix with the penetration of water molecules into the structure [40, 190]. We observe indications of plasticization and resulting degradation very early in 95°C (see Fig.4.11). Since water ingress is more at higher temperature [18]; the water absorption in 60°C and 80°C is less than in 95°C (see Fig.4.3b). In hydrolytic damage being the synergized effect of water and temperature; the temperature seems to have an edge since we can clearly see that despite higher water-uptake and swelling in case of 80°C, the degradation is higher at 95°C with relatively lesser absorption (compare Fig.4.3c and Fig.4.5c). We can see that the degradation effect gets exaggerated as the temperature and time increase (see Fig. 4.10). At high temperature, adhesive tensile strength σf decreases over time (see Fig. 4.11a). At the same time, the ϵf (see Fig.4.11b) also follows identical behavior pattern signifying harsher degradation in presence of water with increasing temperature.

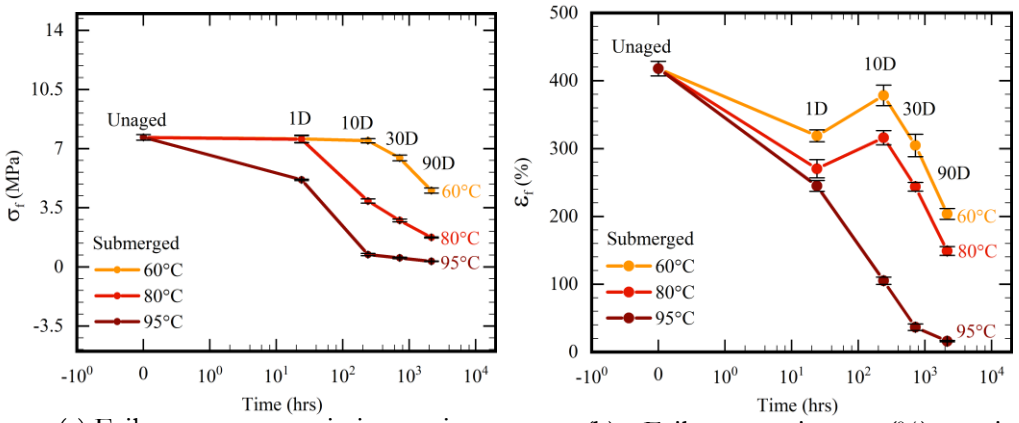

(a) Failure stress σ_f variation against time (t) in submerged condition

(b) Failure strain ϵ_f (%) variation against time (t) in submerged condition

Figure 4.11: Ultimate stress and strain variation of polyurethane in submerged condition plotted against time (t).

The temperature 95°C proved to be too aggressive for PUB adhesive such that the specimens at 30-days aging and beyond could barely sustain any load while also exhibiting inability to stretch. This is since high temperature enables water to cause excessive chain scission and engender low-molecular-weight chains [114].

Hygrothermal Aging Analysis of the hygrothermal performance loss is an important component in design of the material, especially in offshore applications. Hygrothermal effects can be categorized as both mechanical and chemical. In many cases, mechanical variations can be indicative of a chemical alteration as well [81].

As we know, during hygrothermal aging, temperature, oxygen and moisture all synergize to impart damage to the polymer chains. This synergy is competitive in nature [167]. While heat and

oxygen promote cross-link development leading to hardening behavior; temperature and moisture cause a simultaneous cross-link reduction and chain scission leading to softening in constitutive behavior. Both paired phenomenon act simultaneously yet independently during hygrothermal aging. Behavior patterns emerging through uniaxial tensile test results for hygrothermal aging of PUB have been plotted (see Fig.4.12). Uniaxial tensile test results indicate chain scission to be dominant phenomena as temperature and aging duration approach the design limits. The overall degradation is the combined effect of damage imparted through temperature, oxygen and moisture variations. While chain scission is predominant in most conditions; 80% relative humidity at lower temperature seems to present a more conducive environment for developing cross-linkages within the polymer matrix, (see Fig. 4.5b). The specimens showed a consistent decrease in elongation till the maximum aging duration (see Fig. 4.13b). Furthermore, prolonged aging durations impelled specimens to descend their ductility and load sustainability. Especially, in case of prolonged period in 95°C, specimens barely sustained any load and can be referred to as annihilated under aggressive environmental degradation. Generally, adhesives with elastic properties show consistent decline in stress at failure. New cross-link formation in case of polyurethane takes place initially due to oxidation but as aging time proceeds, we see a major decline in stretch and elasticity indicating higher chain scission attributed to moisture attack on the chains. In hygrothermal aging the polyurethane specimens showed decline in material properties as they depreciated with increase in aging time.

In hygrothermal condition the plasticization of specimens starts at the beginning of the hygrothermal aging process where we see σf decreasing and ϵf rising in all temperatures, i.e., 60°C, 80°C, and 95°C 1-day aging [181]. This initial softening is followed by hardening behavior as soon as the aging process enters degradation phase and till the end of aging. For each case, the retention of the tensile strength follows the sequence, i.e., [95°C] < [80°C] < [60°C].

Results from both hygrothermal and hydrolytic aging showed that the elastic modulus and tensile strength decreased after exposure to humidity. Furthermore, a large degradation was found with exposure to high temperatures while softening occurred due to water acting as plasticizer. In both hydrolytic and hygrothermal aging we observe plasticization phenomena in the very initial phase of aging i.e., around 24hrs. Soon after the moisture and water began to get absorbed into the material matrix, plasticization transitioned into degradation phase, and we observed consistent loss of strain indicating chain scission with increase in both time and temperature. The first category (plasticization) is more vividly noticeable with a thermal upsurge and is customary for flexible adhesives while the

second phenomenon (degradation) comes into play with an increase in the factors responsible for shaping the aging conditions, i.e., temperature (T), relative-humidity, and time (t).

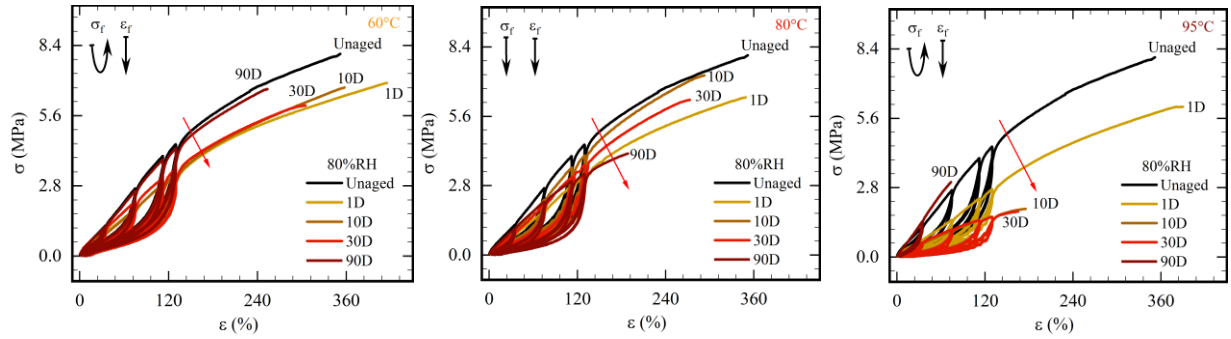

(a) Cyclic test (80%RH at 60°C) (b) Cyclic test (80%RH at 80°C) (c) Cyclic test (80%RH at 95°C)
Figure 4.12: Cyclic tests of specimens aged in hygrothermal environment (80%RH) at 60°C, 80°C, and 95°C.

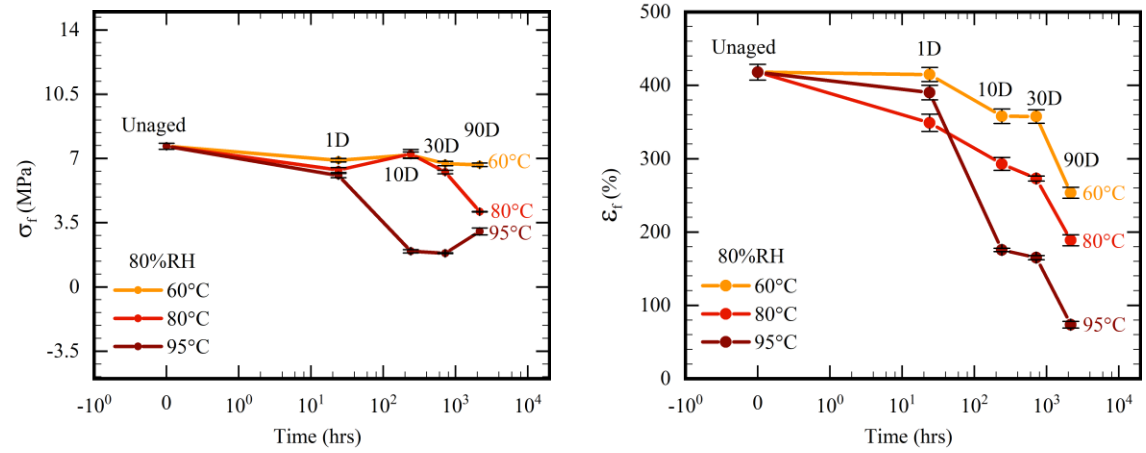

(a) Failure stress σ_f variation against time (t) in hygrothermal (80%RH) condition

(b) Failure strain ϵ_f (%) variation against time (t) in 80%RH condition

Figure 4.13: Ultimate stress - strain variation of polyurethane in hygrothermal (80%RH) condition plotted against time (t).

4.3.4 Deformation-induced damage

To isolate the effects of hydrolytic and hygrothermal aging from those of mechanical damages in PUB adhesive, tensile cyclic tests were performed on aged samples. Therefore, relative stress softening σ^*, relative residual strain e^*, and hysteresis loss W^* are utilized to eliminate the effect conducted by the assigned strain for each cycle.

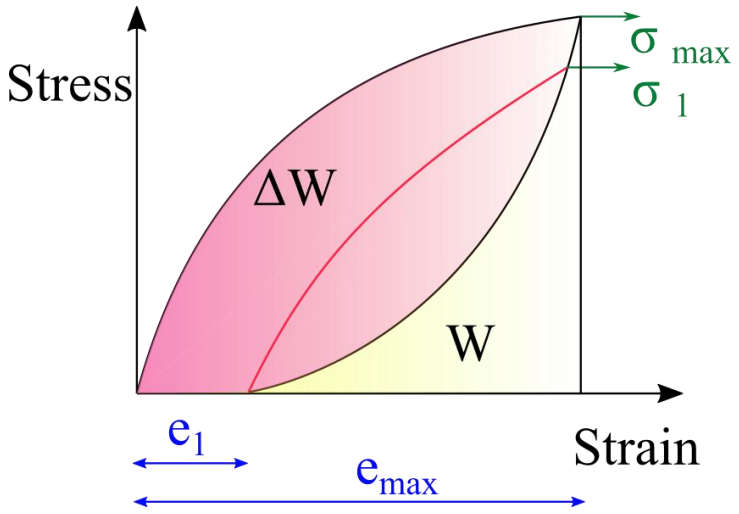

Figure 4.14: Schematic representation for relative stress softening, relative residual strain and hysteresis loss.

Firstly, relative stress softening, σ^* is calculated as the ratio of the stresses at the maximum strain of second cycle σ_1 to the stress at the same strain value of the first cycle σ_{max} (i.e., $\sigma^* = \sigma_1 / \sigma_{max}$) both referred to the same aging condition (see Fig.4.14). In other words, the relative stress softening is the stress comparison between loading and reloading periods. During loading, fillers would be oriented along applied force and entangle with polymer chains. After that, the entanglements prevent the fillers from retracting fully to the initial state due to the presence of knots [65]. When reloading proceeds, less stress value is required to re-orient and re-entangle fillers and polymer chains. Hydrolytic aging under intense heat seldom influenced the ratio of the reloading stress to the loading stress in the 75% to 85% strain. The relative stress softening has not been altered enough by thermal-oxidation and hygrothermal aging (see Fig. 4.15a, and b); however, in hydrolytic aging there are relatively more alterations visible specially in 95°C (see Fig. 4.15c).

Secondly, relative residual strain, ϵ^* can be interpreted by residual strain after the first cycle ϵ_1 over the maximum strain ϵmax (i.e., $\epsilon^* = \epsilon_1 / \epsilon_{max}$) (see Fig. 4.14). Under influence of aging in humidity and in submerged conditions, generally temperatures 60°C and 80°C were not able to exert overt changes of material properties (see Fig. 4.15). The temperature of 95°C, (see Fig. 4.15c), caused a considerable increment of relative residual strain which was noted to be higher in presence of water within the polymer matrix. As aforementioned, the formation of entanglement, during loading phase, constraints the retraction of fillers, which is depicted in the form of residual strain.

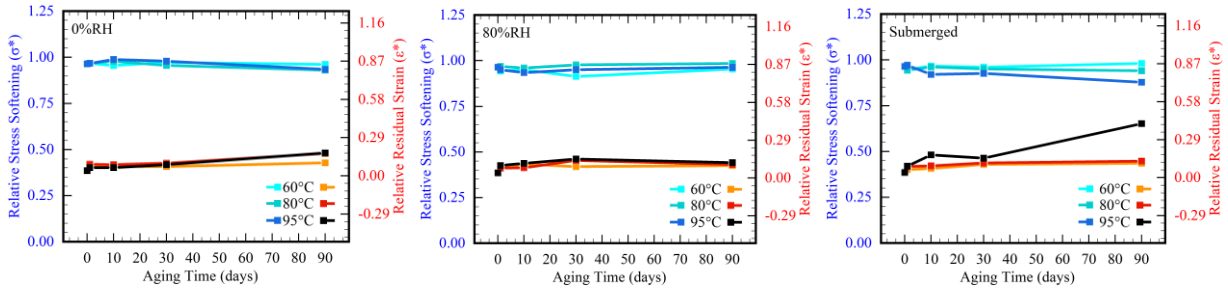

(a) Thermal-oxidation (0%RH) (b) Hygrothermal aging (80%RH) (c) Hydrolytic aging (submerged)

Figure 4.15: Relative stress softening and relative residual strain in each aging environment.

Overall, hygrothermal aging and hydrolytic aging both seemingly impelled specimens to generate chemical cross- links as well as causing simultaneous chain scission which eventually dominated the earlier cross-link effect and contributed to impede the reverse motion of materials and therefore enlarge the residual strain.

Lastly, the relative hysteresis loss W^* is written as the ratio of the dissipated energy in the first cycle ($\Delta W = \int_{loading} \sigma de - \int_{unloading} \sigma de$) to the whole work input $W = \int_{loading} \sigma de$ which is depicted in Fig. 4.14 (i.e., $W^* = \Delta W/W$). In fact, the relative hysteresis loss reflects how much energy is dissipated due to bond breakage during cyclic tensile tests in each aging condition. The variations are shown in hysteresis loss for thermo-oxidative, hygrothermal and hydrolytic aging conditions in 60°C, 80°C, and 95°C (see Fig. 4.16a-c).

By comparing the relative degradation between aging environments, it appears that the aging mechanisms work independently, and as a result, they can compete with each other. Based on the theory of network decomposition, we assume that the polymer matrix decomposes to two different networks; one of which resulted from the diffusion of oxygen to the polymer matrix, and the second one was shaped by the effect of the water on the polymer matrix. To understand the degradation imparted through mechanical and environmental factors we compared the areas under the cyclic curves up to 35% stretch for three environment factors that impart degradation to the polymer matrix as a function of time i.e heat (0%RH), water, and moisture (80%RH). However, it is to be kept in mind that during accelerated aging, water and humidity can not act in isolation. They synergize with temperature and impart higher damage as compared to temperature alone. As it can be clearly seen in all experimental results that eventually submerged state is the most severe aging condition. At higher 95°C, initially the humidity ingresses the polymer matrix before water but degradation due to water attack is very steep and continuous as compared to 80%RH which rather became severe after

initial aging. As more water continued to get absorbed, it imparted higher degradation to polymer matrix.

From another perspective, the relative stress softening, residual strain and hysteresis loss of PDMS-based adhesives eliminated the softening behaviors induced by hydrolytic aging. Moreover, the structural changes occurred during hydrolytic aging are capable of being decomposed by cyclic loading. Therefore, the constant values between unaged and aged adhesives (see Fig. 4.15 and Fig. 4.16), indicate the independent nature of deformation induced damage from environmental degradation.

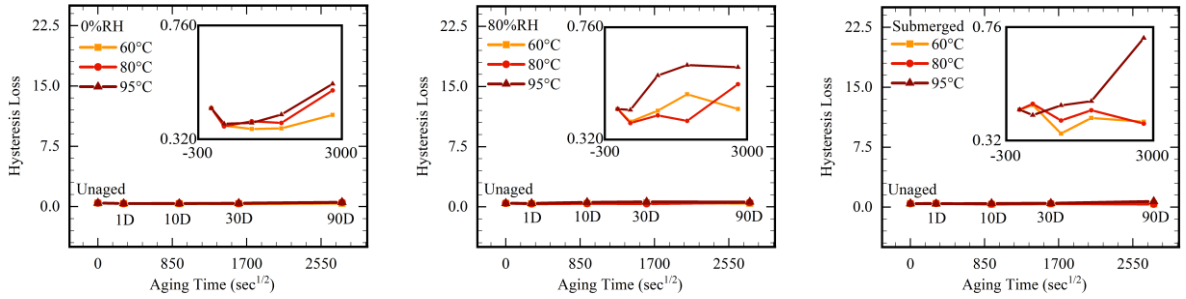

(a) Thermal-oxidation (0%RH)(b) Hygrothermal aging (80%RH) (c) Hydrolytic aging (submerged)
Figure 4.16: Hysteresis loss in each aging environment.

4.3.5 Toughness

While toughness remains a mechanical property; material properties are affected directly from environmental exposure. In case of cyclic loading, we superimpose mechanical damage on the specimens already degraded by weathering agents. Toughness is widely considered as a viable material property to gauge how much ability the polymer still retains to absorb energy after being exposed to damage from environmental degradation, we plotted the toughness parameter for all aging environments (see Fig. 4.17). Toughness reduced with increase in temperature (T) and aging time (t).

Fig.4.17 presents the temperature comparison of toughness in each aging environment; all of which show rapid loss in toughness during initial phase of aging (up to 10-days). In thermal oxidation (0%RH), the material toughness remained constant at 60°C after 10-days while further degradation could only be achieved with increase in the aging temperature (see Fig. 4.17a). Results show the cross-link formation being dominant in thermal oxidation (0%RH) as material shows hardening in constitutive behavior even though toughness parameter is going down (compare Fig. 4.5a, and Fig. 4.17a). Hardening trend in constitutive behavior occurs due to the increase in stress (ϵ_f) and loss of strain (ϵ_f). In hygrothermal and hydrolytic aging conditions, the constitutive behavior is opposite to that of thermo-oxidative aging, i.e., material softening is observed due to plasticization phenomenon

and higher chain scission because of water molecules attacking the polymer matrix (see Fig. 4.10, and Fig. 4.12). However, inspite of opposite constitutive behaviors, the trend for toughness remained same for all aging condition. The only difference noted was in terms of the severity of degradation. It is imperative to note that a comparison of material toughness in each environment generally followed a pattern that [0%RH] > [80%RH] > [submerged in distilled water]; at constant temperature (see Fig. 4.17). Temperature here is seen as a key factor, with higher temperature, degradation process is primarily dominated by higher loss of cross-links and chain scission processes.

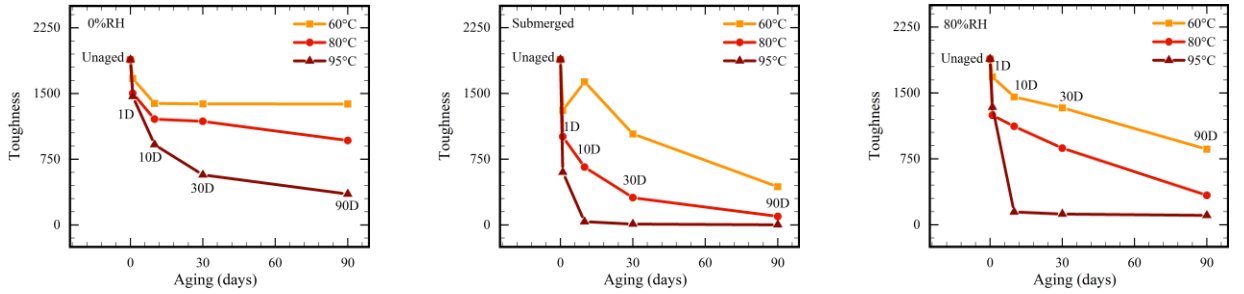

(a) Toughness during thermal-oxidation (0%RH)

(b) Toughness during hydrolytic aging

(c)Toughness in hygrothermal aging (80%RH)

Figure 4.17: Variation in material toughness during aging in each environmental condition.

4.4 Conclusion

This research investigated the accumulated damage due to heat, water, and moisture on the tensile properties of the polyurethane-based adhesive. We observed that the amount of water-uptake by the material is directly proportional to the degradation potential in that environment. By analyzing numerous mechanical and chemical tests, we observed that mechanical and environmental damage are independent in nature. While mechanical damage is mostly physical, DMA and cross-link density analysis showed the chemical nature of environmental damage. The characterization and deterioration mechanisms have been studied and analyzed. In terms of the damage induced by hydrolytic aging under desalinated water, water-uptake follows Fick's second law. Moist and submerged environments encouraged some initial plasticization in specimens, but further aging led to high chain scission and loss of material strength, which was also verified by the changes in Tg. Mass loss encountered in thermal oxidation and hygrothermal aging is attributed to chemical decomposition due to heat and oxygen. In contrast, the same is explained through leaching phenomena in the case of aging in a submerged state. Although hygrothermal aging showed a higher mass loss, still hydrolytic degradation in mechanical tests was higher than hygrothermal degradation. It can be concluded that humidity did not cause serious damage to the backbone chain of the polymer

matrix, unlike in submerged conditions. Water and humidity may not cause as much damage in isolation, but when coupled with heat, the nature of damage potential is multiplicative. The results show that the molar mass between cross-links decreases with exposure time; this decrease was magnified by increasing temperatures. This decrease in molar mass is a marker of the aging process driven mainly by cross-linking mechanism. This mechanism is predominant in the aging process, as confirmed by the decrease of mechanical properties such as ultimate stress and strain at break. Results are generally in good agreement with tests for specimens with different water profile gradients.

Chapter 5:

Effect of Sequential Aging in Dual Environment on PUB Adhesive

5.1 Introduction

Polyurethane-based elastomeric adhesives have been used in structural applications such as glass sealants for more than three decades [169]. While in most of these applications, the adhesives do not get direct surface exposure to weathering agents, still, one or more weathering factors can affect the adhesive performance. For instance, temperature exposure is unavoidable, as most materials heat up in service conditions. Moisture diffusion is also a potent concern for polymeric substrates, and this could affect the adhesive and cohesive properties of these materials. These factors together may cause the aging of the adhesive itself or the combination of the adhesive and the substrate. Typically, bonding strength gets affected by degradation visible in the mechanical behavior of materials. In terms of fatigue, impact, damping, and safety, they present critical application advantages in the automotive industry particularly. Assessment of the durability of structural adhesives with such applications has been of much interest among the research community lately. Dargazany et al. modeled the constitutive behavior of cross-linked polymers using a multi-physics modular approach [14]. Polymers undergo degradation when in contact with aggressive environmental agents like humidity, water, and temperature [13, 12, 166]. Bahrololoumi et al. modeled the constitutive behavior of cross-linked polymers with FE implementation on the combined degradation effects of thermal aging and mechanical fatigue [15]. Mechanics involved in isolated aging environmental effects are well understood but not much has been done to ascertain how multiple aging environments act in combination impact the materials, whether the effects are in collaboration or in competition with each other. We designed this experiment as a phased aging process involving combinations of different weathering environments to access the dual aging performance of the polyurethane adhesive. More detail about experiment setting is covered in follow-up sections. We have considered two-way combinations of thermo-oxidation, hydrolytic and hygrothermal aging (80%RH). Cross-linked polymers possess a broad spectrum of mechanical properties [29, 138, 78, 35, 199, 137], and these properties are well documented physical and chemical behaviors through many published academic research articles [84, 83, 165, 43, 100, 69, 68].

Polyurethane is utilized in the automotive industry for joining components since the obtained joints are resistant to oils, and water [185, 195]. These materials are currently finding increasing applications for both the automobile [122] industry, such as seals and fluid flow line coatings [104, 58, 177, 25].

Table 5.1: Summary of methods used to maintain desired environmental conditions.

Environment	Temperature	Method
	Thermal Oxidation	
0%RH	60°C, 80°C, 95°C	Moisture absorbent molecular sieves
	Hygrothermal	
80 ± 3%RH	60°C, 80°C, 95°C	Binary salt solution (KCl)
	Hydrolytic	
Submerged	60°C, 80°C, 95°C	Distilled water

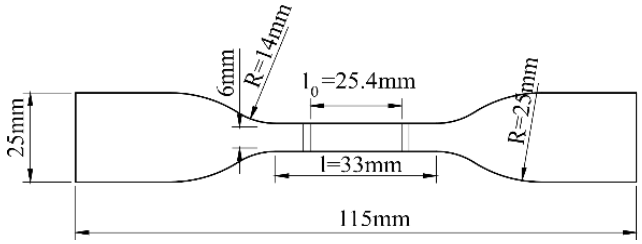

Figure 5.1: Dimensions of specimens aged and then tested under uniaxial tension.

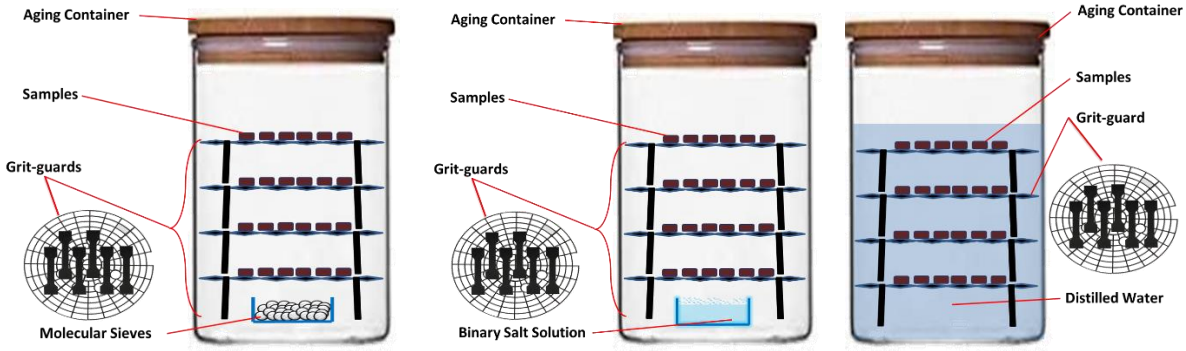

(a) (b) (c)

Figure 5.2: Set-ups used for specimens during aging in different environmental chambers. (a) 0%RH (thermo- oxidation), (b) 80%RH (hygrothermal aging), and (c) Submerged in distilled water (hydrolytic aging).

The mechanical properties of the cured adhesive were evaluated in line with the relevant methods mentioned in ASTM D412 [6]. In the current work, mechanical testing was the main technique employed. In addition to the changes in constitutive behavior of the material, we have also considered variations in material toughness to characterize as-received and aged samples. The paper is outlined as follows. After discussing the experimental method in section 5.2, the results and

discussion are presented in section 5.3. Finally, section 5.4 includes the summarized concluding remarks for this experimental effort.

Table 5.2: Summary of dual aging experiments along with the type of resulting environmental contributions in each aging regime.

Environment	Aging Process		Aging Interaction Type	
	Ph-1	Ph-2	60°C	80°C
Hygrothermal	Thermal-aging	80%RH aging	Collaborative	Competitive
Hydrolytic	Thermal-aging	Hydrolysis	Collaborative	Competitive
Thermo-hygro	80%RH aging	Thermal-aging	Competitive	Competitive
Thermo-hydro	Hydrolysis	Thermal-aging	Competitive	Competitive

5.2 Methodology

This study is planned considering following environment regimes:

a. Hygrothermal dual aging (0%RH to 80%RH).

b. Hydrolytic dual aging (0%RH to hydrolysis).

c. Thermo-hygro dual aging (80%RH to 0%RH).

d. Thermo-hydro dual aging (hydrolysis to 0%RH).

The schematic diagrams representing dual-aging experiment profiles are reflected in Fig. 5.3. During the dual- environment aging process, the temperature was kept constant while other weathering factors were altered in two phases. Also, the aging time durations are slightly different for each environment regime.

A dual effect aging experiment is designed in 60°C and 80°C. Samples were aged at the same temperature for the complete aging duration. During this study, the adhesive specimens were subjected to a two-phase aging. For hygrothermal and hydrolytic dual-aging, in phase-1, specimens were aged in thermoxidation (0%RH) condition, and after 10 days, all batches were shifted to ph-2, which were hygrothermal (80%RH) and hydrolytic (submerged) aging conditions for 3, 10, and 30 days (see Fig. 5.3a). Whereas, for thermo-hygro and thermo-hydro dual-aging (see Fig. 5.3b), samples were kept in hygrothermal/ hydrolytic (phase-1) conditions for 30 days and then were shifted to ph-2 in thermoxidation (0%RH) aging for 3, 10, and 30 days. Aging containers (see Fig. 5.2) with multiple layers of grit guards were used to age samples in desired conditions. A summary of techniques utilized for maintaining required weathering conditions is shown in Table. 5.1, whereas the aging sequence for all aging regimes is explained in Table. 5.2. Furthermore, for comparison and reference purposes, we

also aged and tested specimen batches after aging in phase-1, which was 10-days and 30-days for different cases.

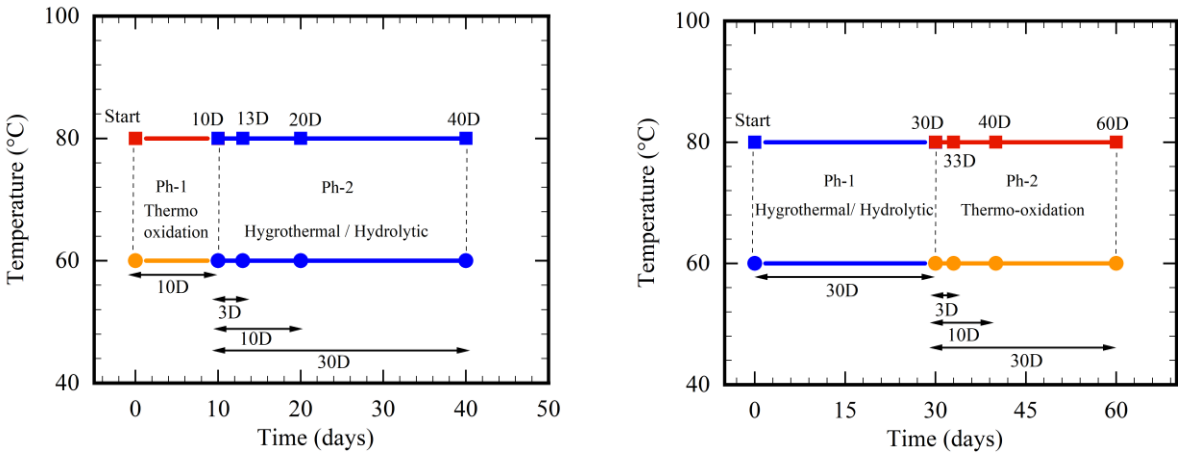

Figure 5.3: Schematic showing profile of dual effect aging conditions (a) Hygrothermal/ hydrolytic dual environment aging (0%RH to 80%RH/ submerged, and (b) Thermo-hygro (80%RH to 0%RH) and thermo-hydro dual environment aging (submerged to 0%RH).

5.2.1 Material For this study, we have used 3M™ 590 Polyurethane Glass adhesive sealant. It is a flexible polyurethane adhesive used in the automobile industry. The material, when fully cured has a nominal hardness of 60-65 Shore-A.

5.2.2 Sample Preparation The specimens were cast using a customized mold with a thickness of 3.175mm (see Fig.5.1). Once fully cured, the samples were aged in weathering chambers as explained at the beginning of section-5.2

5.2.3 Uni-axial Tensile Test A universal testing machine (Test Resources 311 Series Frame) with a 5kN force transducer was used for uni-axial tensile tests. All uniaxial tensile tests were conducted in accordance with methods given in ASTM D412 [6]. Tests were displacement controlled with a cross-head speed of 50 mm/min. The starting distance between the extensometer grips was set to 25.4mm. Temperature is known to affect the polymer chain configurations [119] both temporarily and permanently. Moreover, the mechanical behavior of PU sealants has been reported to be temperature-dependent [198]. For performing tensile tests, we had two options, (i) testing at aging temperatures or (ii) testing at normal room conditions. Since we had aged the specimens in diverse and contrasting environments for a range of durations; testing at elevated temperatures could affect certain thermally activated fillers, and undesirable deformation mechanisms could come into play. This would have further complicated the understanding of inter-environmental contributions. Therefore,

we opted to let the aged samples normalize for twenty-four hours and tested them in room conditions, i.e., 25±2°C, 30±3% RH. A minimum of four failure tests were performed for all specimen batches for reliability control.

5.3 Results and Discussion

5.3.1 Types of Contributions When we have multiple phenomena/ environmental factors acting on the material, and we want to see the combined effect on its properties; the question is how their contribution is co-related and added up towards the resulting effects. We have sub-divided these contributions into the following categories,

a. **Collaborative contribution** The final response is due to the linear superposition of two phenomena, A and B. In this case, the response is expected to be greater than or equal to either A or B responses.

b. Competitive contribution In this type of contribution, the final response is achieved by a competition between A and B. In this respect, if A is gaining, then B is at a loss; indicating the opposite direction of effect. In this case, the result could be expected between contributing phenomena.

c. Multiplicative contribution Here, the final response is a nonlinear superposition of two phenomena, A and B. Typically, this type will happen when either one or both A and B will act as a catalyst. For instance, we expect that in the absence of heat, the effect of moisture will be mild, and in the presence of heat, the same moisture's reaction rate is enhanced to degrade the material faster.

These collaborations are dictated by material responses to a single or a combination of multiple environmental sub-phenomena during aging. By expanding the characterization methods and aging period, future studies can further elaborate on this effect. For instance, considering if damage capacity is partially reached in phase-1 aging and the effect of phase-2 aging further adds to material degradation, we will consider it as a collaborative damage contribution. Whereas, if damage capacity achieved under phase-1 aging conditions is somewhat reversed during phase-2 and shows signs of healing, we can term it as a competitive contribution of environmental agents. It must be considered that material response in the case of dual-effect aging will be resulting from a much complex weathering interactions through a mutual relationship between environmental agents i.e., temperature, water, moisture, and oxygen.

5.3.2 Impact of Weathering Conditions This study encompasses thermo-oxidation, hydrolytic, and hygrothermal aging environments in different possible combinations. Thermo-oxidation consists of temperature and oxygen in an ambient environment. The oxidation reactions are known to cause cross-link formation, while the temperature is responsible for scission reactions. Usually, cross-linking dominates in most cases. In the case of submerged state aging, the material is exposed to water attacking the polymer matrix in combination with a thermal component. Hydrolytic aging has been reported to have dominant chain scission reactions. Hygrothermal aging was performed in relative humidity 80% using a potassium chloride binary salt solution. This environment is unique in the sense that it combines all the environmental agents that act separately during thermo-oxidation and hydrolytic aging, namely heat, oxygen, and moisture. We expect material behavior to be a complex outcome from a combination of competing and collaborating scenarios emerging with the following possible effects:

a. Cross-link development due to oxidation.

b. Cross-link reduction due to temperature.

c. Plasticization due to moisture.

d. Chain scission and cross-link reduction due to water molecules attack on polymer chain.

In thermo-oxidation, high temperature and oxidation reactions are the main contributors to damage; in hydrolytic aging damage is due to effects of water and temperature; and in hygrothermal aging, all of the above factors, namely oxidation, heat and moisture movement, compete with each other to impart damage. This section will include a discussion about synergized effect of these sub-aging environmental phenomena, resulting in changes in constitutive behavior and toughness of the aged material specimens.

Since the aging temperature was kept constant throughout dual-aging, we have grouped the results on the basis of temperature as it can be seen in Fig. 5.4, Fig. 5.5, Fig. 5.6, and Fig. 5.7, how dual-effect environment aging influences the material behavior.

5.3.3 Hygrothermal Dual-Environment Aging (0%RH to 80%RH)

To see the influence of dual-effect aging on the material for 0%RH to 80%RH; tensile testing was done to see the shifts in constitutive behavior of specimens, and then the material toughness is compared under each aging environment. During the aging process, desired humidity fixed points were achieved by using methods given in Table-5.1.

During hygrothermal dual-effect aging, polyurethane based adhesive continued to demonstrate dominant cross-link development over chain scission after phase-2 aging in hygrothermal (80%RH) conditions in 60°C (see Fig. 5.4a). We observe most degradation in the first three days of phase-2. Later on, while the constitutive behavior remained more-or-less the same, the material toughness shows a slight increase in toughness (see Fig. 5.4c) which can be attributed to plasticization causing slight increase in failure strain ϵf and simultaneous cross-link formation due to oxidation causing some increase in failure stress σf with an increase in time (t). Overall, in 60°C, we observed that phase-1 (0%RH) aging dominated phase-2 (80%RH) aging, implying that damage capacity was reached in the initial phase with a collaborative contribution of both environments.

In the case of dual-effect aging in 80°C, the higher temperature plays key role in degrading the material. Unlike aging in 60°C, here we see the opposite trend in constitutive behavior i.e., softening (see Fig. 5.5a).

In 80°C, during phase-1 (0%RH), we observe a hardening trend due to oxidation reactions. Aging in phase-1 caused higher loss of toughness as compared to the same phase in 60°C (see Fig. 5.4c and Fig. 5.5c). But after transition in phase-2 there is a sudden drop in material toughness within the initial 72 hrs (see Fig. 5.5c). This degradation caused a decrease in failure strain ϵ_f and simultaneous chain scission due to moisture, causing a decrease in failure stress σ_f as well. Overall, in 80°C we observed that phase-2 (80%RH) aging dominated phase-1 (0%RH) aging, implying that damage capacity was not reached in the initial phase, and it was a competitive environmental contribution in this case.

Polyurethane adhesive (3M-590 black); generally displayed a hardening trend in the constitutive behavior during dual-effect aging in 60°C (see Fig. 5.4a, c) and softening trend in 80°C (see Fig. 5.5a,c). In 60°C we observed a collaborative, and in 80°C we observed a competitive contribution between 0%RH (phase-1) with hygrothermal environment in (phase-2). In both temperatures, damage capacity associated with dual-environment effect is reached within the first three days of the dominant phase i.e., phase-1 for 60°C and phase-2 for 80°C. Later we do not observe any further significant degradation in toughness parameter till design aging culminated (see Fig. 5.4c and Fig. 5.5c).

It is also notable that phase-1 aging consists of a single environmental agent (heat), and in phase-2, the material is exposed to inseparable conditions (heat+moisture). Although the intensity of damage increases with an increase in temperature; Fig. 5.4c and Fig. 5.5c show that the combined

effect of phase-1 and phase-2 imparts much higher damage due to the collaborating effect of environments as compared with damage imparted during single aging environment.

5.3.4 Hydrolytic Dual-Environment Aging (0%RH to Submerged)

Phase-1 (0%RH) of hydrolytic dual-aging in 60°C shows a hardening trend (see Fig. 5.4b). The polyurethane adhesive behavior at 60°C resembles the constitutive behavior demonstrated earlier during hygrothermal dual aging (see Fig. 5.4a).

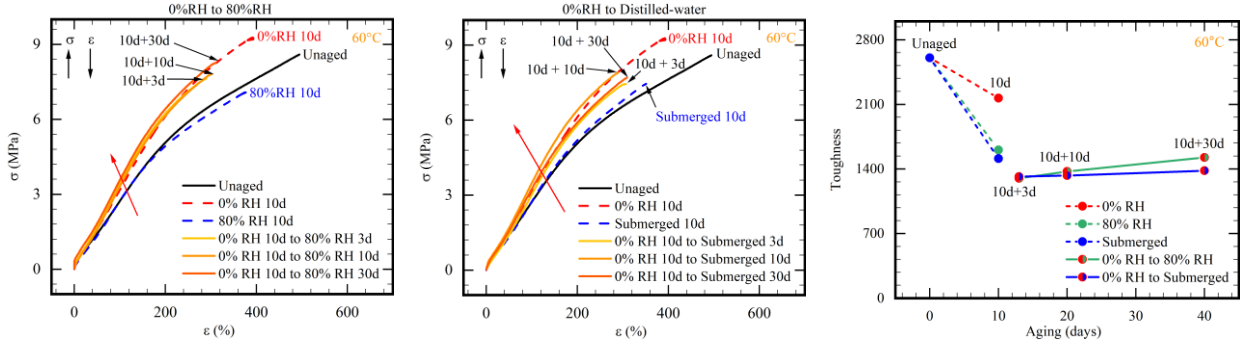

(a) (b) (c)

Figure 5.4: Polyurethane (3M-590 black) mechanical behavior after hygrothermal and hydrolytic dual-effect aging in 60°C (a) Constitutive behavior - 0%RH to 80%RH environment, (b) Constitutive behavior - 0%RH to submerged condition, and (c) Toughness comparison.

While constitutive behaviors look similar, the material appears to undergo a shock-effect when it transitions into a totally opposite environment (0%RH to submerged). That is why a high loss of toughness is seen in phase-2 within the first 72 hours. Overall, in 60°C, we observed that phase-1 (0%RH) aging dominated phase-2 (Submerged) aging, implying that damage capacity was reached in the initial phase.

In the case of aging in 80°C, after phase-1, material shows slight hardening trend due to oxidation reactions causing cross-link development but this phenomenon is dominated by chain scission under high temperature (see Fig. 5.5b) during phase-2 in submerged state. Hydrolytic dual aging is comparable with hygrothermal dual aging because here as well, phase-2 shows softening accompanied with higher degradation due to attacking water molecules. Phase-2 aging in hydrolytic environment caused increasing damage to mechanical strength as aging time increased. Overall, in 80°C, we observed that phase-2 (Submerged) aging dominated phase-1 (0%RH) aging.

In 60°C, we observed a collaborative contribution, and in 80°C, we observed a competitive contribution between 0%RH in (phase-1) and hydrolysis environment in (phase-2). In both temperatures, damage associated with dual-environment effect continues to variation with an increase in time (see Fig. 5.4b and Fig. 5.5b). The damage contribution is competitive in nature because phase-

1 is in totally dry environment while phase-2 is in wet state. Later we also observe further degradation in toughness parameter which is not too much but definitely more than what we observed in hygrothermal dual aging. It can be stated that degradation in hydrolytic dual-aging is higher than hygrothermal dual-aging damage (see Fig. 5.4c and Fig. 5.5c).

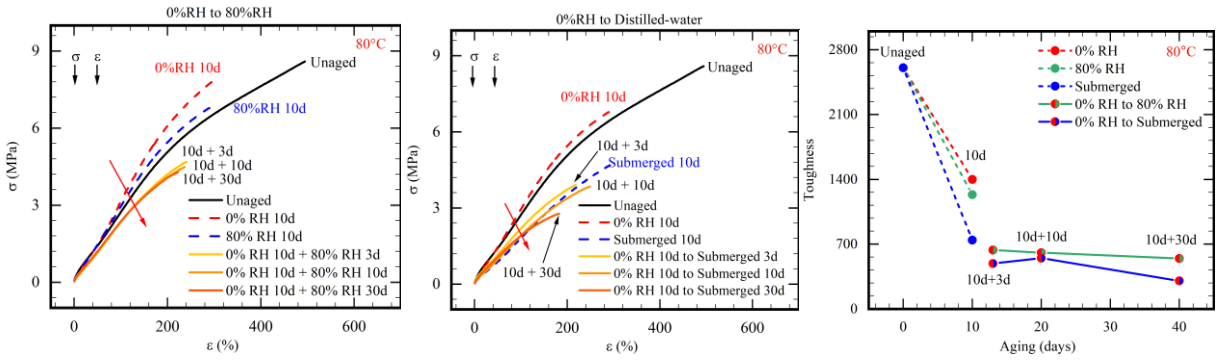

(a) (b) (c)

Figure 5.5: Polyurethane (3M-590 black) mechanical behavior after hygrothermal and hydrolytic dual-effect aging in 80°C (a) Constitutive behavior - 0%RH to 80%RH environment, (b) Constitutive behavior - 0%RH to submerged condition, and (c) Toughness comparison.

5.3.5 Thermo-Hygro Dual-Environment Aging (80%RH to 0%RH)

During thermo-hygro dual-effect aging, polyurethane based adhesive demonstrated dominant cross-link development at the end of the aging period. Phase-1 hygrothermal (80%RH) aging condition in 60°C show a slight softening trend. Phase-2, in this case is 0%RH, where we see dominant cross-link formation with an increase in time (see Fig. 5.6a). After completion of phase-2, the polyurethane adhesive behavior at 60°C has shown consistent hardening in constitutive behavior and recovery of material toughness (see Fig. 5.6a, and Fig. 5.6c). Tensile tests for all conditions show that with an increase in time (t), the σ increased and ϵ decreased. The interaction of environments in 60°C shows that phase-1 (0%RH) dominated the overall dual aging process and competitive collaboration of environments took place in this case.

In the case of aging in 80°C, material suffered degradation in phase-1 due to moisture attack resulting in dominant chain scission and no change in constitutive behavior (see Fig. 5.7a). In phase-2, the moist specimens with absorbed moisture show further degradation and loss of toughness after 3 days. But hereafter, the cross-link formation remained dominant and continued to show a hardening trend till the aging process finished. This hardening is attributed to oxidation reactions causing cross-link development during phase-2 in 0%RH (see Fig. 5.7a and 5.7c). Phase-2 (0%RH) was dominant phase and overall dual-aging resulted in competitive collaboration of environments in this case.

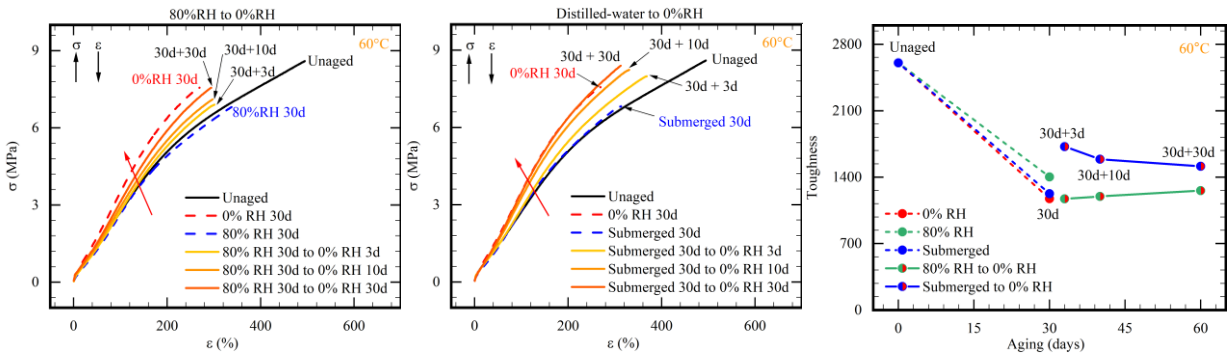

(a) (b) (c)

Figure 5.6: Polyurethane (3M-590 black) mechanical behavior after thermo-hygro and thermo-hydro dual-effect aging in 60°C (a) Constitutive behavior - 80%RH to 0%RH environment, (b) Constitutive behavior - submerged condition to 0%RH, and (c) Toughness comparison.

5.3.6 Thermo-Hydro Dual-Environment Aging (Submerged to 0%RH)

During thermo-hydro dual-effect aging, the adhesive specimens demonstrated dominant cross-link development at the end of the aging period. Phase-1 hydrolytic (submerged) aging condition in 60°Cshows damage without any prominent change in constitutive behavior (see Fig. 5.6b). In Phase-2, (0%RH), as expected, cross-link formation dominates due to thermal oxidation reactions. After completion of phase-2, the polyurethane adhesive behavior at 60°C has shown consistent hardening in constitutive behavior and recovery in material toughness (see Fig. 5.6b, and Fig. 5.6c). Tensile tests for all conditions show that with an increase in time (t), the σ increased and ϵ decreased. The interaction of environments in 60°C shows that phase-2 (0%RH) dominated the overall dual aging process and competitive collaboration of environments took place in this case.

In the case of aging in 80°C, material suffered maximum degradation in phase-1 due to water attack resulting in high damage due to dominant chain scission (see Fig. 5.7b). In phase-2, the specimens immediately started showing recovery with a hardening trend in constitutive behavior and an increase in toughness. Phase-1 dominated chain scission, and phase-2 shows dominant cross-link formation with a hardening trend till the aging process finished. This hardening is attributed to oxidation reactions causing cross-link development during phase-2 in 0%RH (see Fig. 5.7b and 5.7c). Phase-2 (0%RH) was the dominant phase, and overall dual-aging resulted in the competitive collaboration of environments in this case.

During thermo-hydro dual-effect aging, the most interesting phenomenon was the recovery/ healing observed in material toughness, especially in 60°C (see Fig. 5.6c). This is an intriguing phenomenon and requires further investigation to ascertain exactly why the material toughness in

thermo-hydro dual aging shows the opposite trend when compared with hydrolytic dual aging even though the aging environments are the same. Just the change in the sequence of aging results in different ways of environmental interaction.

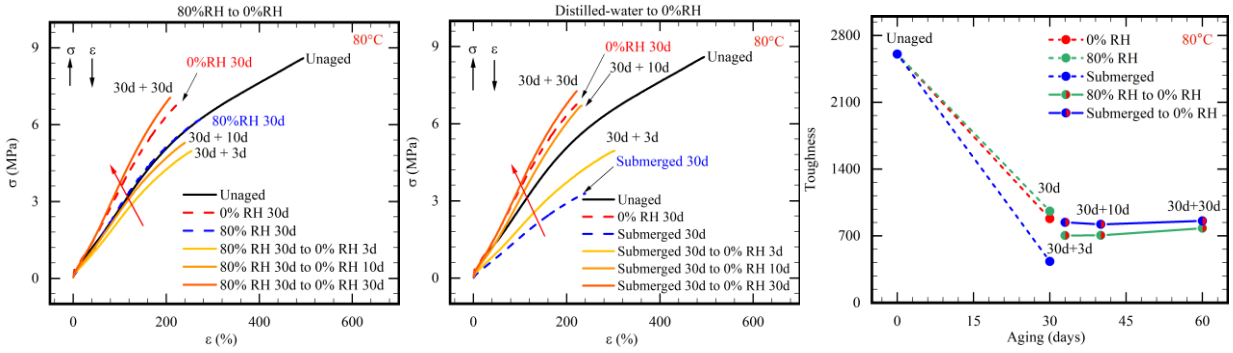

(a) (b) (c)

Figure 5.7: Polyurethane (3M-590 black) mechanical behavior after thermo-hygro and thermo-hydro dual-effect aging in 80°C (a) Constitutive behavior - 80%RH to 0%RH environment, (b) Constitutive behavior - submerged condition to 0%RH, and (c) Toughness comparison.

Both phase-1 hygrothermal (80%RH) and hydrolytic (submerged) aging conditions in 60°C showed a hardening trend (see Fig. 5.6a,b). Material shows energy degradation after phase-1 in (80%RH) and submerged aging through depletion in toughness as well. But during phase-2 in thermo-oxidation environment specimens show a noticeable increase in toughness; especially in the case of the thermo-hydro condition in phase-1. Tensile tests for all conditions show that with an increase in time (t), the σ increased and ϵ decreased.

5.4 Conclusion

In this experimental study, the analysis of dual-aging processes helped establish the damage-driven kinetics involved. Chain-scission and cross-link formation are two microstructural phenomena that occur during thermo-oxidative aging; while during hydrolytic aging, chains-scission and reduction of cross-links are generally observed. Hygrothermal aging environment combines all of the above i.e., chain scission, cross-link formation/ reduction. High temperature has contributed more towards damage accumulation. When above sub-aging conditions were combined, it was observed that oxidation reactions caused cross-linking, which helped reduce the effect of hydrolytic chain scission. The comparison of tensile test data in conjunction with variations in material toughness helped segregate the nature of environmental contributions as either collaborative or competitive.

In this dual aging study, the aged material endorses a damage capacity associated with specific environmental agents; may it be temperature, oxygen, or moisture. Material damage is essentially a

resultant outcome from the mutual contribution of all involved environmental agents. The nature of interactions observed by contributing environments was found to be either collaborative or competitive. Major takeaways from this aging experiment in terms of contribution trends are as follows:

a. Single aging environment We found that hygrothermal aging is a result of the competitive contribution of thermo-oxidation and hydrolytic aging.

b. Dual-environment aging The under study material followed collaborative contribution of involved aging environments when oxidation reactions took place in lower 60°C during the initial phase of hygrothermal and hydrolytic dual-aging. Remaining all six environmental regimes designed for dual aging resulted in competitive collaborations between the involved environmental agents See Table. 5.2.

Variation in material toughness remained relatively the same for hygrothermal and thermo-hygro dual aging. But opposite trends were observed in the case of hydrolytic and thermo-hydro dual aging, with prominent healing observed in the latter.

We hope to utilize these results and outcomes to develop an understanding of the kinetics involved in intra-environmental interactions. This work shall aid in developing service life prediction models for similar materials exposed to complex environmental aging scenarios.

Chapter 6:

Degradation of FEPM rubber in HPHT Downhole Conditions

6.1 Introduction

Fluoroelastomers are known for their exceptional sustainability in HPHT environments. These properties have been verified time and again in laboratory and field studies [124]. FEPM are fluorinated polymers composed of tetrafluoroethylene and propylene monomers being crosslinked using a wide range of curatives. Their sustainability due to excellent chemical stability and thermal resistance has earned vast applications in corrosive oilfield environments and in the general, automotive, and aerospace industries [102, 101]. Some coagents, such as triallyl cyanurate (TAC) and triallyl isocyanurate (TAIC), are necessary to obtain good mechanical properties during peroxide vulcanization. These coagents have the same characteristics as several double bonds in the molecule structure. Thus, stable crosslink bonds between the coagent and the macromolecule main chain can form through these double bonds [98, 66]. HPHT environments are implied when i) for temperature rating greater than 175.6°F; or ii) the maximum anticipated pressure is more than 15,000 psi.

Recently, many experimental investigations have been focusing on the degradation of fluoroelastomers. In 2014, Chuanbo Cong et al. conducted research on the curing of tetrafluoroethylene–propylene elastomer (FEPM) using highvinyl polybutadiene rubber (HVBR) as a concurring agent, as well as investigating the aging behaviors of FEPM and octa-vinyl-polyhedral oligomeric silsesquioxane (OVPOSS) composites exposed to hydrochloric acid (HCl) solution. The study found that HVBR significantly improved the properties of FEPM, increasing tensile strength, hardness, and thermal stability. As HVBR content increased, so did the blend's crosslinking density and glass-transition temperature (T_g). The study also found that crosslinks formed between HVBR and FEPM macromolecules. Meanwhile, the aging study showed that the tensile strength and crosslink density of FEPM-OVPOSS composites decline with the increase in aging time, while an upsurge in the mass and volume change rates occur simultaneously. These findings could expand the possibilities for curing FEPM and provide insights into the aging behavior of FEPM-OVPOSS composites. [44]. Ferrari et al., in 2019, studied the degradation of Ethylene Propylene Diene Monomer (EPDM) and Fluoroelastomer (FPM) elastomers under mixed neutron and gamma fields at high dose rates. The

research used a wide range of absorbed doses and dose rates, which is unique compared to previous studies, and found that crosslinking is the dominant radiation-induced degradation mechanism in both EPDM and FPM. The total absorbed dose was found to be the most influential parameter affecting material degradation, while radiation type and dose rate did not show significant effects. Fourier Transform Infrared (FTIR) spectroscopy was employed to analyze the composition of the EPDM and FPM O-rings. The study also investigated the effect of irradiation on the room-temperature tensile behavior of EPDM and FPM elastomers using uniaxial tensile tests on O-ring segments. The research contributes to the safe construction of new-generation accelerators and target systems. It provides valuable insights into the expected evolution of elastomeric O-rings used in such facilities [63]. In 2022, Wen-Yue Zhuoa and colleagues investigated the changes in the crosslinking network of FFKM elastomers cured by TAIC and DBPH under thermo-oxidative aging conditions. The study used FTIR and XPS to determine the crosslinking network's destruction at the molecular level, showing that network destruction primarily occurs at the crosslink points of the TAIC structure. At the same time, both the backbone and the pendent groups of FFKM remained stable. Additionally, TGA-FTIR-GC-MS tests were conducted to further elucidate the destruction mechanism. The research provides valuable insights into the aging behavior and decomposition mechanism of FFKM, which can be useful for applying FFKM materials [201]. Q Liu et al. investigated the thermal and thermo-oxidative aging behaviors of tetrafluoroethylene propylene elastomer (FEPM) in geothermal environments. They found that FEPM exhibited different aging behaviors under thermal and thermal oxidation conditions, with thermo-oxidative aging causing more damage to the elastomer's mechanical and thermal properties than thermal aging. They also observed that the triallyl isocyanurate (TAIC) crosslinked structure degraded during both aging processes, destroying the crosslinked network, which can lead to reduced mechanical strength and performance of the elastomer. These findings contribute to understanding the degradation mechanisms of FEPM in geothermal environments and offer insights for developing more robust fluoroelastomers [124].

Some studies have also examined the aging of fluoroelastomers in sour environments containing H_2S and other chemicals. For example, a study by Norris et al. [144] investigated the effect of H_2S exposure on the mechanical properties of fluoroelastomer (FKM). They found that exposure to H_2S caused a reduction in the stiffness and strength of the rubber and also observed changes in the morphology and chemical structure of the fluoroelastomer. Another study by Righetti et al. [153] investigated the effect of solvents on the performance of fluoroelastomers. They found that polymer–solvent interaction increases with decreasing temperature. This process was attributed to a T_g

regulation effect in which solvent crystallization occurs only when the crystallization temperature is higher than the T_g of the system. The studies indicate that exposing fluoroelastomers to sour environments containing H_2S, cyclohexane, heptane, or toluene under high-pressure and high-temperature conditions can greatly affect their properties and performance. James Williford et al. (2023) discussed the importance of material selection for completion products in high-pressure/high-temperature (HP/HT) sour-service applications of Indonesian oil and gas fields. The study presents a selection process based on reviewing well data to understand the corrosive environment and selecting materials based on their resistance to corrosion and compatibility with the well environment. The authors emphasize the significance of testing materials to ensure their compatibility and effectiveness in specific well environments. The paper includes case histories that demonstrate the selection process's effectiveness in selecting completion components for HP/HT applications, and the authors conclude that considering good data and selecting appropriate materials is crucial for ensuring product integrity and cost efficiency in such applications [184]. Jiaxiang Ren et al. developed and characterized modified fluoroelastomers for high-pressure/high-temperature (HPHT) downhole sealing applications in their study [152]. These materials have solid mechanical properties below their glass transition temperature (T_g) and stable elastomeric properties up to 400°C above T_g, surpassing the thermal rating of available commercial thermoplastics and elastomeric materials. The T_g of these materials can be adjusted between 97°C and 215°C. The modified polymeric materials also exhibited excellent resistance to crude oil and superior extrusion resistance compared to commercial elastomeric materials. The authors suggest that these materials have great potential for high-temperature sealing and other oil and gas applications. Another study by Shigeki investigated the conformational exchange behavior of an alternating copolymer of tetrafluoroethylene and propylene (TFE-P) using ^{19}F NMR spectroscopy and computational chemistry. The authors identified and assigned the two CF_2-CF_2 pairs of connection to meso or racemic configurations and discussed the population of the gtg and ttt conformers at different temperatures. The study provides a detailed structural analysis of TFE-P copolymer and sheds light on its behavior in solution [107].

The influence of aging often follows the measurement of tensile properties. This is one of the simplest tests to perform, yet it provides a deeper understanding of material behavior. In the current work, uniaxial tensile testing was the primary technique employed for mechanical characterization, and FTIR and NMR analysis methods further augmented it.

The paper is outlined in the following sequence. After discussing the design of the experiment and methodology in section 6.2, the discussion on results and our analysis are added in section 6.3. Finally, section 6.4 consists of the concluding remarks for this experimental effort.

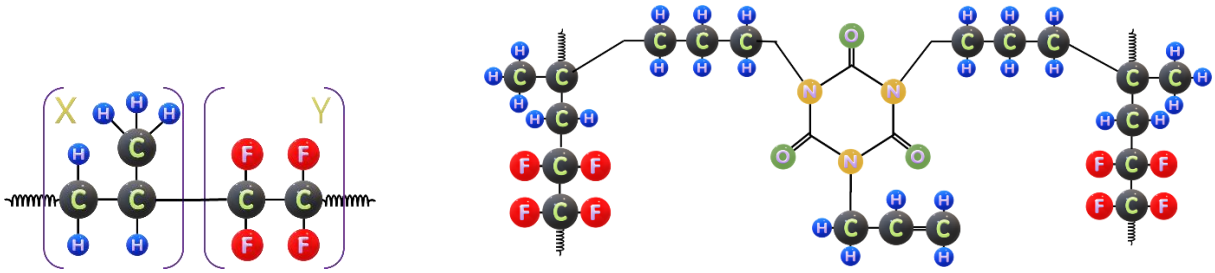

(a) Structure of pure FEPM (b) Crosslinked structure of FEPM vulcanizate

Figure 6.1: FEPM Structure.

6.2 Methodology

6.2.1 Aging

In this study, two types of FEPM rubber specimens were aged for 4 different durations in three different temperatures (200°C, 225°C, and 250°C) (see Table. 6.1). Specimens were suspended in Hastelloy C276 pressure vessels for exposure in the hydrocarbon liquid phase. The vessels were purged and pressure tested with nitrogen. Then the test gas was introduced through a dip tube. The vessels were heated with resistive heater bands under PID control. Temperature and pressure were continuously logged. At the completion of the aging duration, heat was discontinued and the vessels cooled overnight. Pressure was relieved through a caustic scrubber at a rate less than 15 psi per minute. Nitrogen was purged through a dip tube to remove residual sour gas. For comparing the test results of aged samples, we soaked each FEPM rubber type in solvent for 2 days at 232°C. The selection of 232°C as a controlled temperature for the baseline condition is a reasonable choice, as it falls approximately in the middle of the three aging temperatures (200°C, 225°C, and 250°C) used in the experiment. Using a mid-range temperature allows for a more representative comparison between the baseline and the aged samples, as the effects of temperature on the material can be observed across a range of values. Furthermore, this temperature is still within the typical operating range of FEPM elastomers, which generally have an upper limit of around 230−250°C. A soaked state for the baseline comparison is necessary to better simulate the actual service environment of the rubber, as the material is typically exposed to various chemicals and fluids during its operation. Soaking the samples in a solvent for 2 days at 232°C provides a more accurate representation of the material's behavior and

properties when subjected to real-world conditions. This soaked baseline, treated as an unaged condition, allows for a more meaningful assessment of the aging effects and the material's performance under different temperatures and durations by comparing the aged samples with a soaked yet unaged baseline.

Table 6.1: Aging conditions.

Days	Temperature		
	200°C	225°C	250°C
2	x	x	FEPM 1,3
7	FEPM 1,3	FEPM 1,3	FEPM 1,3
14	FEPM 1,3	FEPM 1,3	FEPM 1,3
28	FEPM 1,3	FEPM 1,3	FEPM 1,3
42	FEPM 1,3	FEPM 1,3	x

After the designed aging durations were finished, FEPM samples were removed from the ovens. At room temperature, aged specimens remained soaked in the aging medium/ solvents. The solvent consisted of sour fluids condition as per ISO-23936-2 with 60% Hydrocarbon (70% heptane, 20% cyclohexane, 10% toluene, 10% aqueous phase, i.e., DI water), and 30% gas phase (5% CO_2, 10% H_2S, 85% CH_4).

6.2.2 Characterization

Tensile testing

A Universal Testing Machine (Instron 68TM-5) with 5kN static load cell was used for tensile tests of material samples. ISO 37 type-II size specimens were die-cut from rubber slabs and then used for tensile failure with five samples per condition for reliability control. All tests were displacement controlled with a 500mm/min cross-head speed. During the course of deformation, the elongation of the central zone was measured by a contacting external extensometer (LTE-Class B-2). All the experiments were performed at room conditions (i.e., 26.11°C, 37 ± 3% RH) by stretching the samples until breakage.

FTIR

Various aging conditions inducing chemical alterations could be detected by FT-IR Spectroscopy on the specimen's surface. One sample per condition was tested using Jasco FT/IR - 4600 spectrometer; spectra were detected from 4000 to 600cm^{-1} at a resolution of 4cm^{-1} and an accumulation of 64. The angle of the incident was set at 45° with the monolithic diamond as the ATR prism.

NMR

Solid-state NMR investigations were carried out at room temperature utilizing a Varian InfinityPlus 400 MHz NMR spectrometer, employing 6mm zirconia rotors with Teflon inserts and caps. Kel-F rotor tips were used. Samples were rotated at 4kHz, maintaining the magic angle. FEPM samples (approximately 5 × 14 mm, 150-180 mg) were sectioned into tiny cubes (around 1-2 mm per edge). External referencing to adamantane (CH = 29.45 ppm) was performed for chemical shifts. Cross-polarization magic angle spinning (CP-MAS) experiments were conducted with contact times of 1.8 ms or 0.8 ms. Data analysis was completed using Mnova 14.3.0, with zero-filling to 8k data points. Exponential multiplication of 100 Hz was consistently applied, and Whitaker baseline correction was executed for all spectra.

Solution-state NMR analyses were conducted on a 600 MHz Bruker Avance NEO spectrometer outfitted with a 5mm TCI Prodigy cryoprobe. Solid-state NMR experiment samples were immersed in 0.6 ml of acetone-d6 for one hour, then relocated to 5mm NMR tubes for assessment. Proton (^{1}H) NMR was executed with 32 scans and a 20-second recycle delay, while fluorine (^{19}F) NMR employed 128 scans and a 1-second recycle delay. Data processing was performed using Mnova 14.3.0, implementing zero-filling to 128k, apodization of 0.3 Hz, and Whitaker baseline correction.

DMA

Rectangular specimens (35 × 12 × 3.175mm), unaged and aged, were subjected to DMA analysis. After carrying out the visual inspection, one representative sample from each condition was selected and tested. Single cantilever tests to record storage modulus, loss modulus, and Tan δ were performed on the TA Instrument DMA Q800 machine from −70°C to 10°C at a temperature rate of 3°C per min. The test has been performed in the linear viscoelastic region (LVR) using strain amplitudes of 15% and a frequency of 1.0 Hz.

6.3 Results and Discussion

6.3.1 Mechanical test

Tensile failure tests involve applying a tensile load to a material until it fails, allowing for the determination of its mechanical properties. In this case, the tests were conducted on ISO 37 type-II sized specimens, which are a standardized type of test specimen used in the evaluation of rubber and elastomer materials.

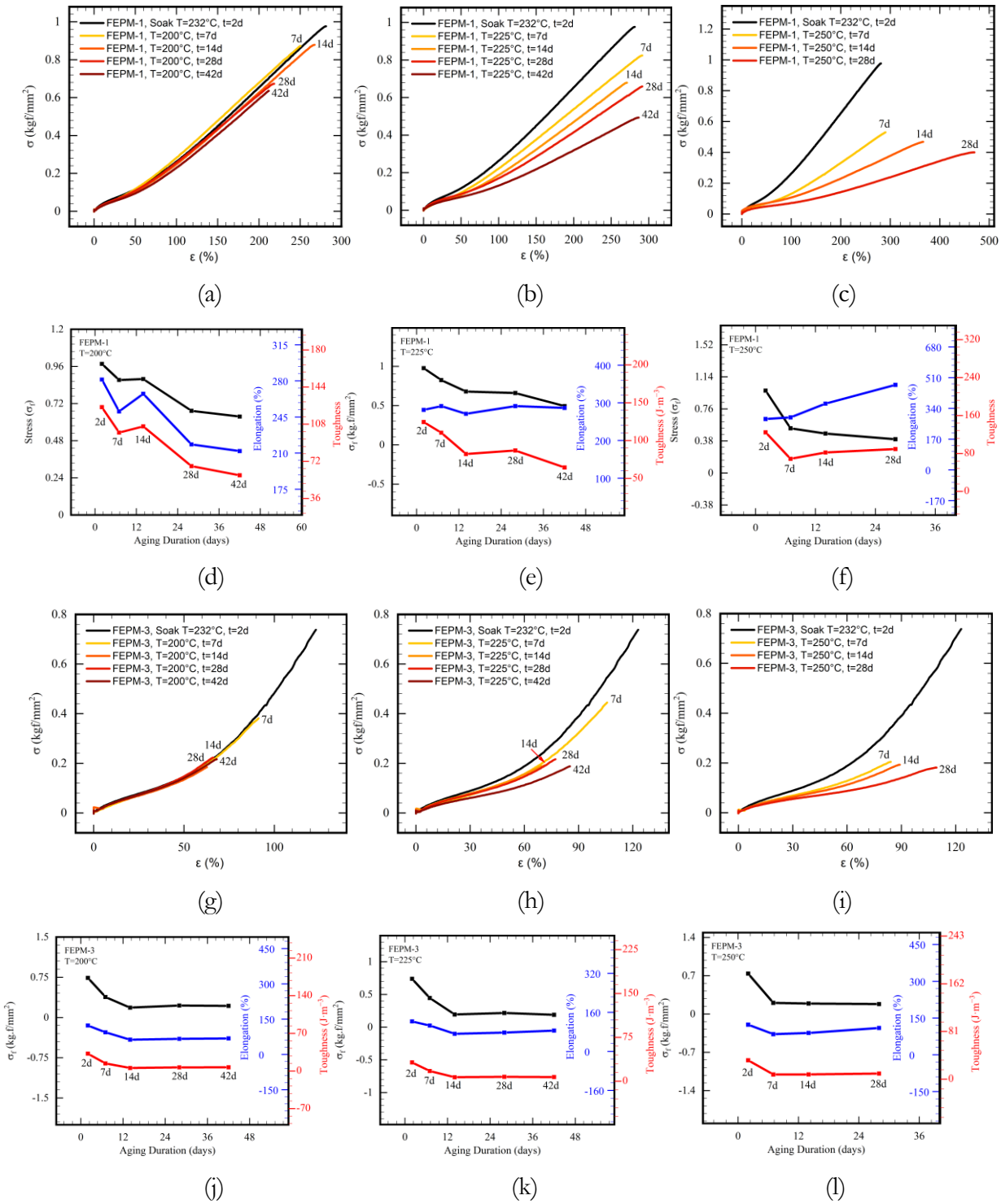

Figure 6.2: Mechanical behavior of FEPM specimens aged in 200°C, 225°C, and 250°C. a-c: Constitutive behavior of FEPM-1, d-f: Progression of Stress-Strain and toughness of FEPM-1 during aging; g-i: Constitutive behavior of FEPM-3, j-l: Progression of Stress-Strain and toughness of FEPM-3 during aging.

The observation made during the tests was that aged specimens showed a softening trend. This means that the specimens became less stiff and more flexible as a result of the aging process. This softening trend was attributed to plasticization, which in this case was due to the absorbed aging solvent within the polymer matrix. Thus, reducing the strength and stiffness of the material.

Overall, the observation of a softening trend in aged specimens during tensile failure tests is an important finding as it highlights the importance of considering the effects of plasticization on the mechanical properties of polymers (see Fig. 6.2).

6.3.2 Chemical test

We conducted FTIR analysis and DMA tests for the chemical investigation of the degradation. But before starting these tests, all sample surfaces were cleaned with acetone (see Fig. 6.3) and then dried in a vacuum oven at 60°C at 700 mmHg vacuum for 24h. This was done to record the amount of solvent absorbed by specimens during aging at each temperature.

During this process, sample weights were carefully recorded before and after vacuum drying. The weight of each specimen was measured and recorded using an electronic scale with a precision of 0.1 mg. The analysis of weight changes gave an insight into the mechanical response of the material affected by the amount of solvent absorbed during aging. It also reflected upon material response under the time-temperature superposition. In Fig.6.3b, we can observe the effect of temperature on solvent absorption for FEPM-1. The solvent absorption was found to be directly proportional to the increase in aging time and temperature. However, for FEPM-3, a similar trend can be seen in Fig.6.3b. In the comparison, FEPM-1 exhibited a higher absorption rate than FEPM-3. This higher absorption can be linked to the higher deterioration of the TAIC structure, as evidenced by the more pronounced degradation of the carbonyl peak in the FTIR spectra of FEPM-1 when compared to FEPM-3. These changes in TAIC effectively loosened the chains, and under the reduced crosslinking, we see the increased failure strain in tensile testing (see Fig. 6.2). Additionally, the reduced solvent absorption observed in FEPM-3 suggests that it possesses a higher cross-link density relative to FEPM-1. Therefore, the failure strain is comparatively much less than FEPM-1, which also affected the material toughness adversely in the designed aging conditions.

FTIR The observed peaks and their assignments have been reflected in Table-6.2 for reference. At 200°C, we did not observe any significant change in any of the functional groups, nor did any new peaks appear. FEPM-1 (see Fig. 6.6a) showed higher degradation in carbonyl (1689 cm^{-1}, 1564 cm^{-1}) and C-F (1326cm^{-1}) peaks while FEPM-3 (see Fig. 6.6c) did not reflect any prominent changes through FTIR spectra. In short, all FEPM specimens showed excellent thermal stability in these

temperatures. However, in the higher 250°C, degradation in oxygen-induced carbonyl group (1689 cm^{-1}), Carboxylate C=OO- asymmetric stretch (1564 cm^{-1}), C-F stretch (1326 cm^{-1}), and C-F2 stretch (1168 cm^{-1}, 1084 cm^{-1}, 1010 cm^{-1}, 955 cm^{-1}) were more prominent with the increase in aging time (see Fig. 6.4c and Fig. 6.6c). FEPM is reported to be susceptible to peroxide at high temperatures, and coagents, such as TAIC, are necessary to obtain good mechanical properties during peroxide vulcanization [106]. The structure of the peroxide-crosslinked FEPM in the presence of TAIC is shown in Fig. 6.1b. The changes observed in FTIR spectra at 1690 cm^{-1} correspond to the carbonyl group in TAIC [124]. Based on the above-mentioned analysis, the degradation process of TAIC (see Fig. 6.5). It can be explained as follows:

a. The C-N bonds in TAIC undergo two dissociations to produce a substance comprising an amide N radical [a] and an amide carbonyl radical [b], accompanied by the volatilization of the isocyanate derivative.
b. The radical [a] undergoes intramolecular rearrangement to produce a C=N-OH structure, and the free radical [b] couples with a macromolecular radical to produce a -(O=C)C-CF_2- or -(O=C)CH_2CF_2- structure. The specific degradation mechanism is shown in Fig. 6.5.

The degradation of the Carbonyl group was further investigated by integrating the FTIR peaks to calculate the area. The percent degradation was plotted to understand the effect of temperature and environmental exposure on the TAIC bonds.

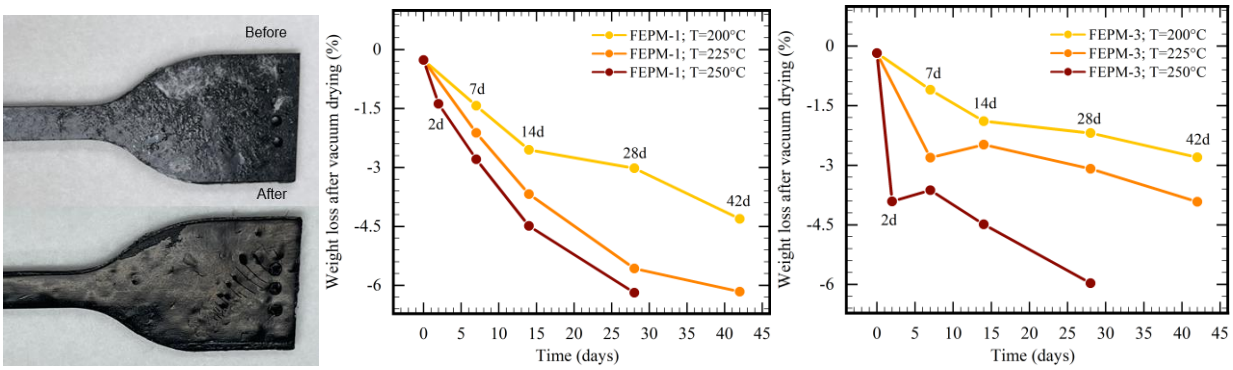

(a) (b) (c)

Figure 6.3: (a) Aged FEPM sample before and after cleaning with Acetone, (b) Solvent absorption FEPM-1, and (c) Solvent absorption FEPM-3.

Fig. 6.7a shows that the least degradation in the carbonyl group was in FEPM-3. Only 33% degradation was seen in the highest aging temperature (250°C) after 28 days, whereas, in the case of FEPM-1, the degradation reached almost 99%. Detailed statistics for degradation of the carbonyl peak

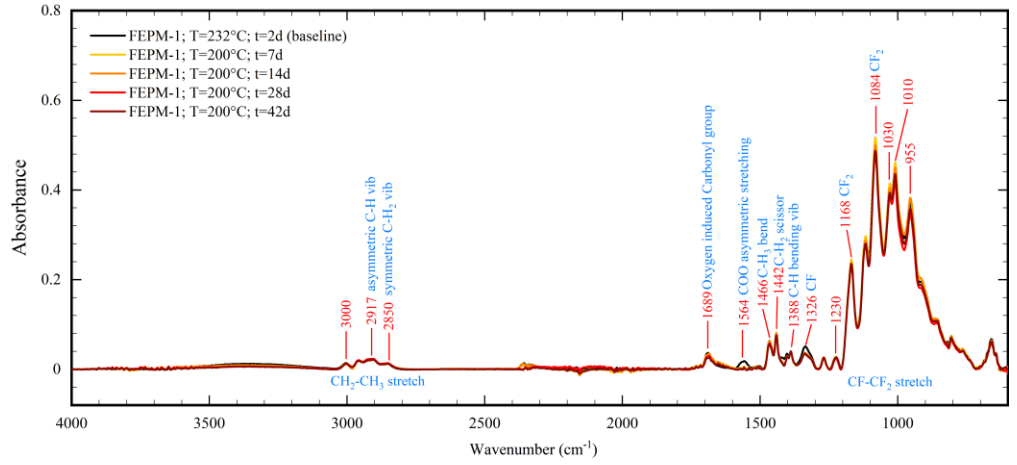

(a)

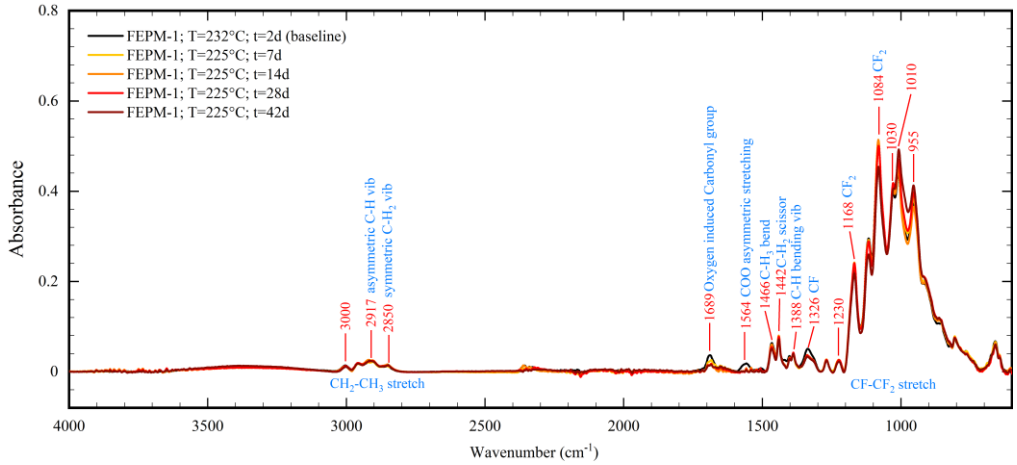

(b)

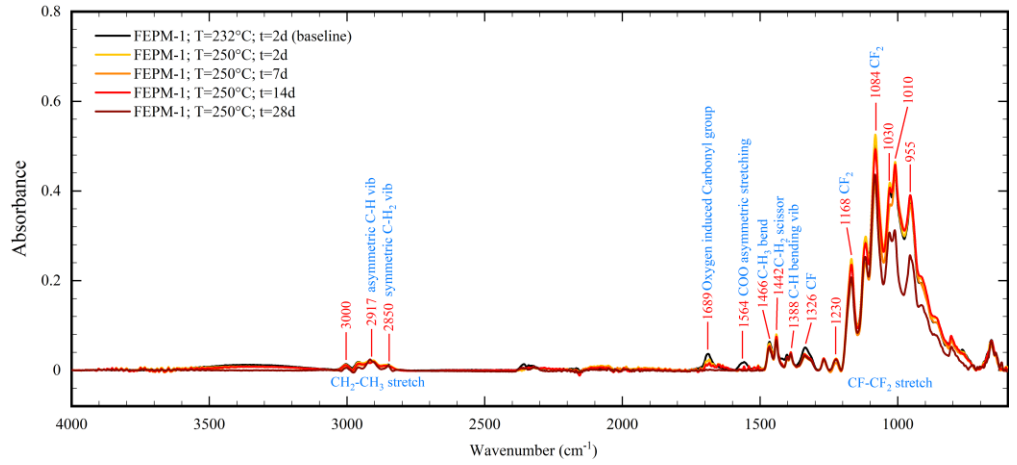

(c)

Figure 6.4: FTIR spectra of FEPM-1 aged at, (a) 200°C, (b) 225°C, and (c) 250°C.

in FEPM-1 and FEPM-3 are presented in Table-6.3. The table includes information on the extent of degradation at different temperatures and aging durations, allowing for a more comprehensive analysis of the degradation behavior of these materials.

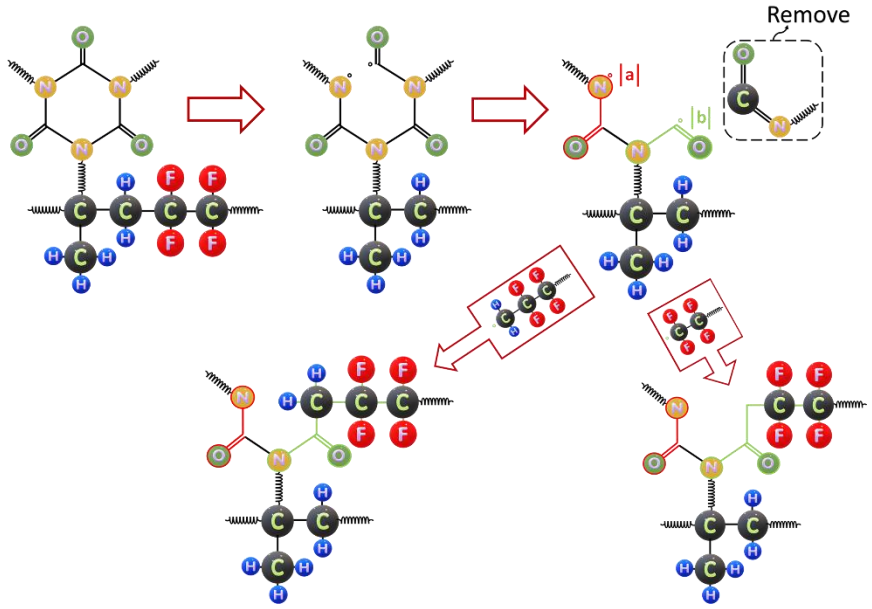

Figure 6.5: Thermal degradation mechanism of the TAIC structure.

Table 6.2: FTIR vibrations and their assignments.

Vibrations	Assignment
2917 cm^{-1}	C-H symmetric stretch
2850 cm^{-1}	C-H symmetric stretch
1689 cm^{-1}	Carbonyl C=O
1640 cm^{-1}	C=C
1564 cm^{-1}	Carboxylate C=OO- asymmetric stretch
1466 cm^{-1}	C-CH_3 bend
1442 cm^{-1}	C-CH_2 scissor
1326 cm^{-1}	C-F stretch
1168, 1084, 1010, 955 cm^{-1}	C-CF_2 stretch

NMR

Solid State NMR: Solid-state NMR experiments are an excellent tool to nondestructively probe the bulk atomic structure of materials and give valuable information about functional groups present, structural dynamics, and changes to the electronic environment of nuclei. 13C CP-MAS NMR, in particular, allows the investigation of the changes induced by heat or other degradative environments on the carbon backbone of carbon-based polymers.

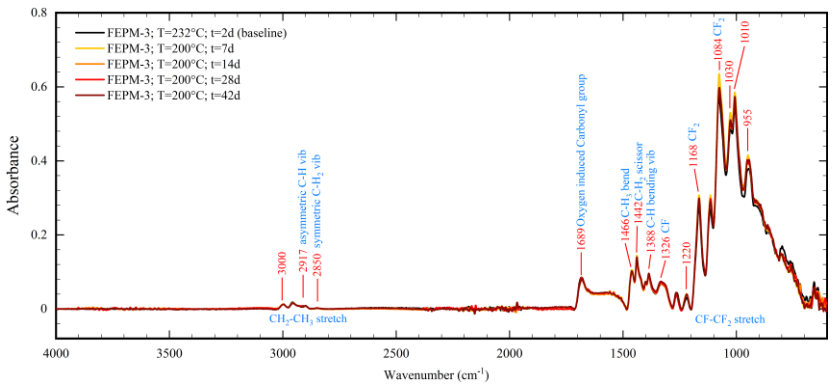

(a)

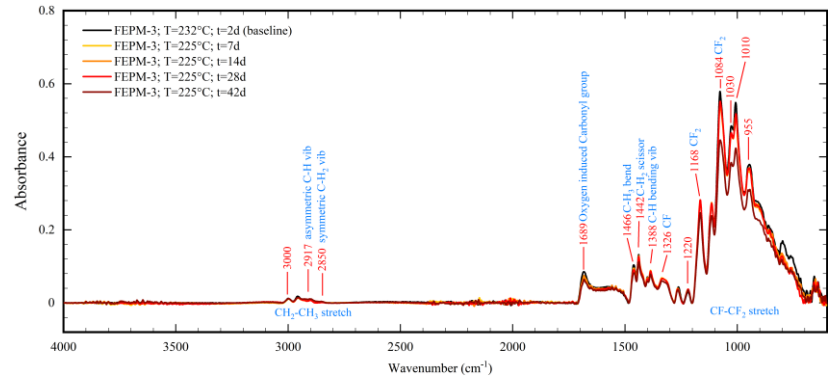

(b)

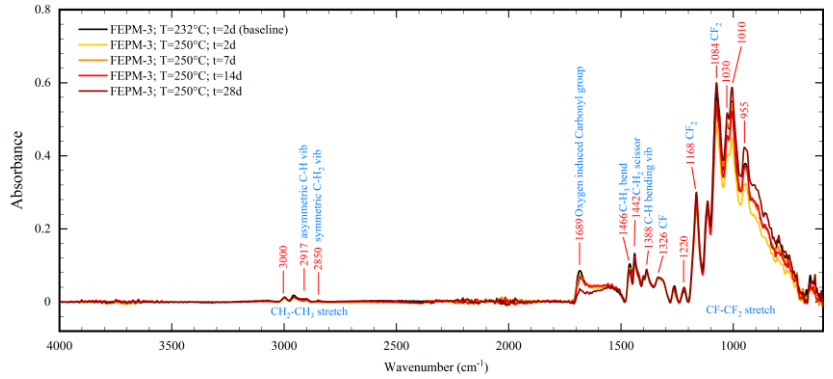

(c)

Figure 6.6: FTIR spectra of FEPM-3 aged at, (a) 200°C, (b) 225°C, and (c) 250°C.

a) **FEPM-1 at 200°C:** The spectral data of aged FEPM-1 sample at 200°C closely resemble those at 225°C. The carbonyl peak at approximately 174 ppm is no longer detectable after 7 days of aging at 200°C. The TAIC peak is not entirely depleted after 42 days, but it is notably diminished. In comparison to the CH3 peak, which remains constant during the aging process, the CH and CH2 peaks exhibit a pronounced increase in intensity. This augmentation in the CH and CH2 peaks

might be a result of more effective CP dynamics rather than any alteration in the polymer, necessitating additional experiments to identify the origin of this change.

Table 6.3: Percent degradation of Carbonyl group for FEPM-1 and FEPM-3.

Material	Area under Carbonyl Peak						
	Temperature	Days	0D	7D	14D	28D	42D
FEPM-1	200°C	Area	1.25422	1.24353	1.21751	0.99226	0.90177
		%	100	99.14768	97.07308	79.11371	71.89887
	225°C	Area	1.25422	0.81748	0.52885	0.52744	0.46808
		%	100	65.17836	42.16565	42.05323	37.32041
	250°C	Area	1.25422	0.56549	0.46471	0.03811	x
		%	100	45.08699	37.05171	3.03854	x
FEPM-3	200°C	Area	9.46542	9.64036	9.5995	9.44759	8.89074
		%	100	101.8482	101.4165	99.81163	93.92864
	225°C	Area	9.46542	9.24728	8.91782	8.19105	7.83602
		%	100	97.6954	94.21473	86.53657	82.78576
	250°C	Area	9.46542	8.95852	8.67264	6.40781	x
		%	100	94.64472	91.62446	67.69705	x

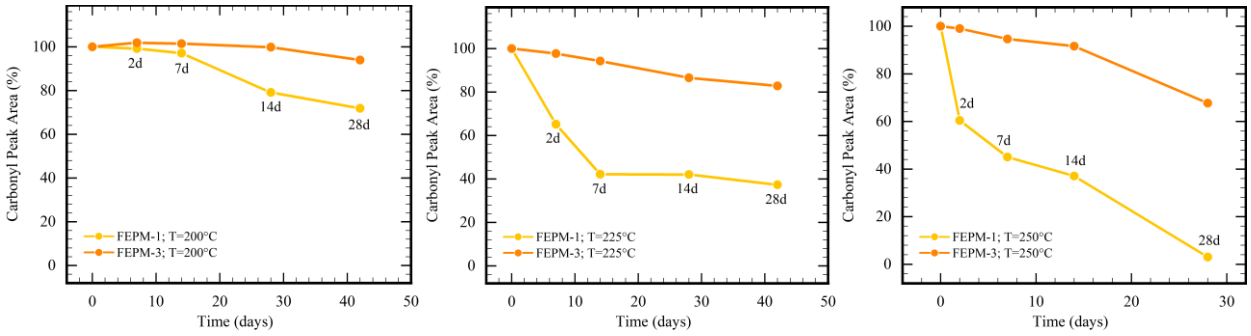

(a) (b) (c)

Figure 6.7: Carbonyl peak degradation trend of FEPM-1 and FEPM-3 at, (a) 200°C, (b) 225°C, and (c) 250°C.

b) FEPM-1 at 225°C: Similar to FEPM-1 at 250°C, the carbonyl peak at approximately 174 ppm is absent after 7 days of aging at 225°C. The TAIC peak, however, is not entirely depleted after 42 days, although it is significantly diminished. The CH and CH_2 peaks exhibit a pronounced increase in intensity compared to the CH_3 peak, which remains unchanged throughout the aging process, up to 14 days. The enhancement in the CH and CH_2 peaks could be attributed to more effective CP dynamics rather than any alteration in the polymer. This necessitates additional experiments to ascertain the source of this change.

c) FEPM-1 at 250°C: The ^{13}C CPMAS NMR data for FEPM samples relies on the polarization transfer from protons to carbons, making it more efficient for rigid structures and protonated carbons. FEPM-1 exhibited the most significant change in its CPMAS spectrum from the un-aged material to the 2-day aged sample at 250°C. The carbonyl peak at 173.6 (stabilizer) vanishes after

2 days, while the peak from TAIC at 149.4 ppm is barely above the noise threshold at 2 days, indicating their interaction with the aging medium (see Fig.6.8). The loss of the TAIC carbonyl is consistent with the degradation of TAIC reported by Liu et al. in their study of FEPM thermal degradation above 300°C[124] and by Zhou et al. in the thermo-oxidative aging of FFKM [201]. However, interestingly, unlike in NMR where degradation is observed for the first two days only, the degradation of the carbonyl peak in FTIR spectra continuously progresses with increasing aging duration and temperature. The spectral data for the aged samples of FEPM-1 at 200°C are nearly identical to those at 225°C. The carbonyl peak at ~174 ppm disappears after 7 days of aging at 200°C and 225°C. The peak from TAIC is not entirely consumed after 42 days but is significantly reduced. The CH and CH_2 peaks exhibit a marked increase in intensity relative to the CH_3 peak, which remains constant throughout aging. The increase in the CH and CH_2 peaks might be due to more efficient CP dynamics and may not be attributable to any change in the polymer, necessitating further experiments to determine the source of change.

A decrease in the intensity of the signals for the CH and CH_2 groups of the polypropylene chain is observed at 2 days, stabilizing at 7 days and declining again at 14 days. The methyl peak maintains its intensity throughout the 28-day aging process but exhibits a reduced width for the aged FEPM. These two alterations, along with the increased features in the CH_2/CH region (18 – 60 ppm), are consistent with heightened motion within the FEPM. The carbon signals from the polyfluorinated moieties demonstrate a decrease in intensity during the aging process, potentially indicating increased motional averaging.

The Direct Polarization (DP) ^{13}C NMR experiment depends on the direct excitation of carbon nuclei, resulting in sharper, stronger signals for regions with more motion. Signals from non-protonated carbons will be present but attenuated due to their slower relaxation.

FTIR results exhibited considerable differences between samples that were washed with solvent (acetone) and dried, and those that were not washed prior to analysis. Since FTIR is a surface technique, this result is not unexpected. Solid-state NMR, on the other hand, measures the bulk properties of a sample if RF can penetrate it. These samples are non-conductive and should allow for complete RF penetration. Nonetheless, washed samples were compared to unwashed. The spectral data showed little difference between the two samples.

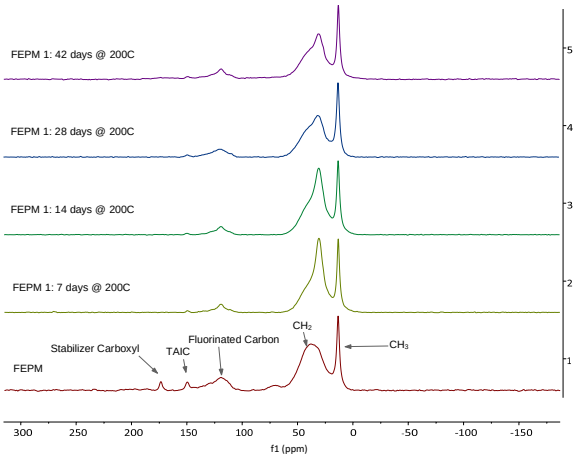

(a)

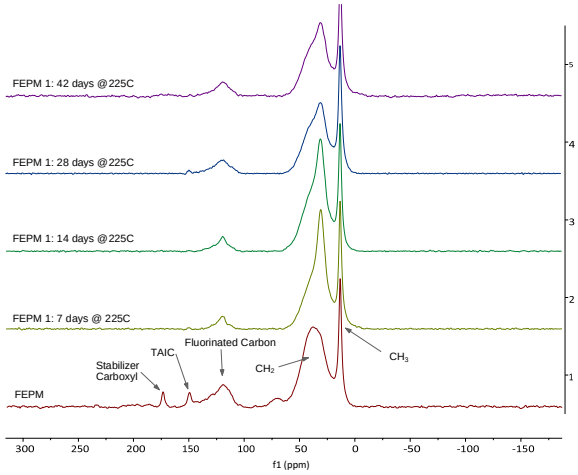

(b)

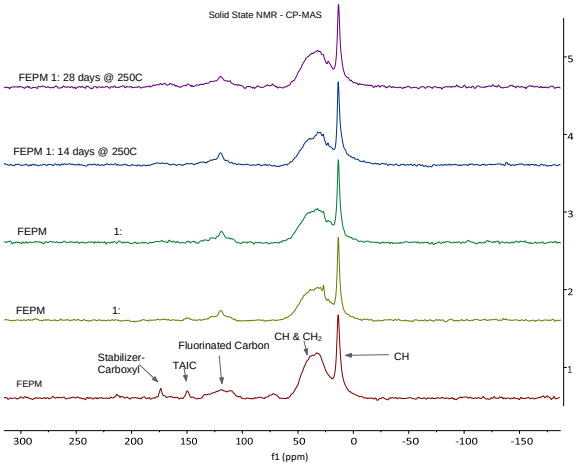

(c)

Figure 6.8: CP-MAS NMR Data of Aged FEPM-1 at, (a) 200°C, (b) 225°C, (c) 250°C.

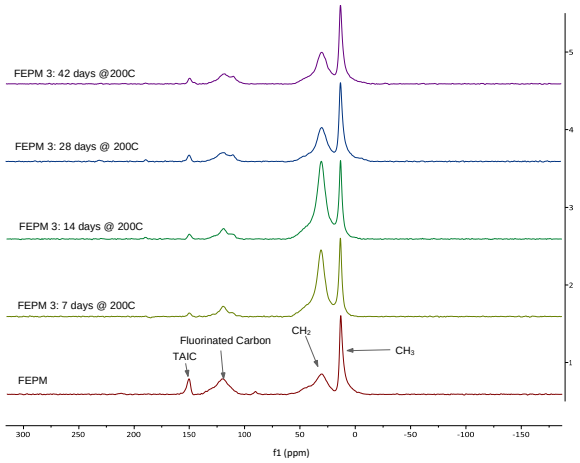

(a)

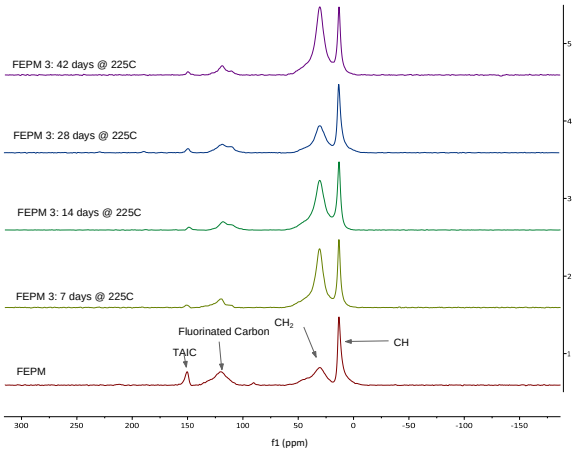

(b)

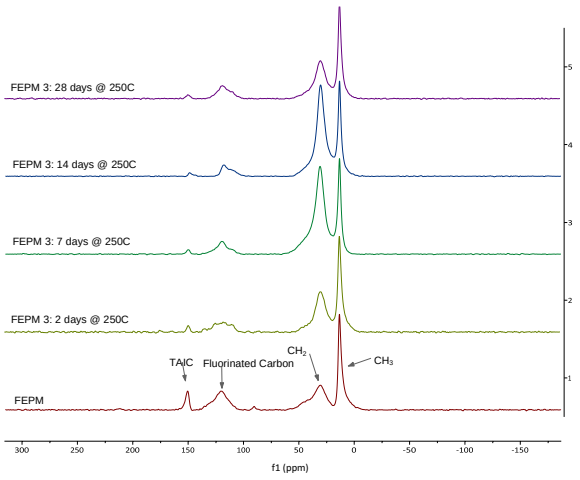

(c)

Figure 6.9: CP-MAS NMR Data of Aged FEPM-3 at, (a) 200°C, (b) 225°C, (c) 250°C.

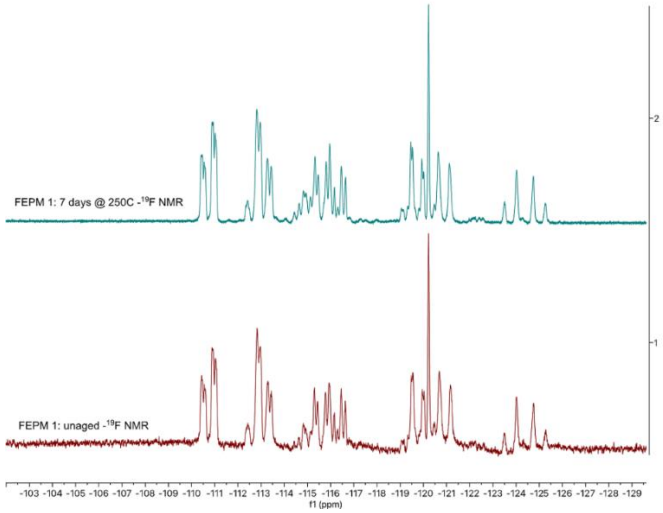

Figure 6.10: 19F NMR spectrum of acetone-d6 extract from 232°C 2-days (treated unaged) soaked FEPM-1 (bottom) and aged for 7 days at 250°C (top).

Table 6.4: Variation in (T_g).

Time (days)	FEPM-1											
	232°C (soaked)			200°C			225°C			250°C		
	T_gE'	T_gE''	$T_gTan\delta$	T_gE'	T_gE''	$T_gTan\delta$	T_gE'	T_gE''	$T_gTan\delta$	T_gE'	T_gE''	$T_gTan\delta$
2	2.53	-1.33	3.27							7.82	2.93	7.77
7				5.01	0.74	5.78	6.63	2.81	6.96	6.14	1.99	5.61
14				4.26	0.55	5.18	5.16	0.47	6.52	4.35	0.08	3.80
28				2.92	-1.62	9.28	3.67	-2.32	6.41	4.08	-0.06	4.37
46				0.49	-6.21	0.52	3.33	-4.24	8.95			
Time (days)	FEPM-3											
	232°C (soaked)			200°C			225°C			250°C		
	T_gE'	T_gE''	$T_gTan\delta$	T_gE'	T_gE''	$T_gTan\delta$	T_gE'	T_gE''	$T_gTan\delta$	T_gE'	T_gE''	$T_gTan\delta$
2	6.5	0.95	7.52							12.66	7.61	14.2
7				5.75	1.47	4.75	7.3	1.31	8.04	10.63	4.62	13.54
14				5.75	-3.21	12.98	10.56	3.21	13.23	10.04	3.11	12.96
28				7.33	1.11	8.44	6.41	1.41	7.36	9.42	4.46	11.02
46				6.44	1.51	7.09	6.17	1.41	6.62			

d) FEPM-3 at 200°Cand 225°C: The NMR data for aged FEPM-3 samples at 200°C and 225°C display remarkable similarity (as shown in Fig.6.9). Contrasting with FEPM-1, the aged FEPM-3 samples do not exhibit a significant decrease in the TAIC carbonyl peak, which is located around 150 ppm. This suggests that the carbonyl structure of FEPM-3 remains intact even after undergoing 42 days of aging.

In the aliphatic region, an increase in the CH and CH_2 peaks is observed, while the CH_3 peak experiences little to no change. It is important to note that the increase in the CH and CH_2 peaks may be attributed to more efficient Cross Polarization (CP) dynamics rather than actual alterations in the

polymer's structure. However, to ascertain the true source of this change, additional experiments are necessary.

This comparison between FEPM-1 and FEPM-3 samples highlights the differences in their aging behavior under similar conditions. Understanding the variations in the NMR data can provide valuable insights into the changes occurring within these materials over time. Furthermore, this knowledge can be utilized to develop better material models and enhance the performance of cross-linked elastomeric adhesives in various applications.

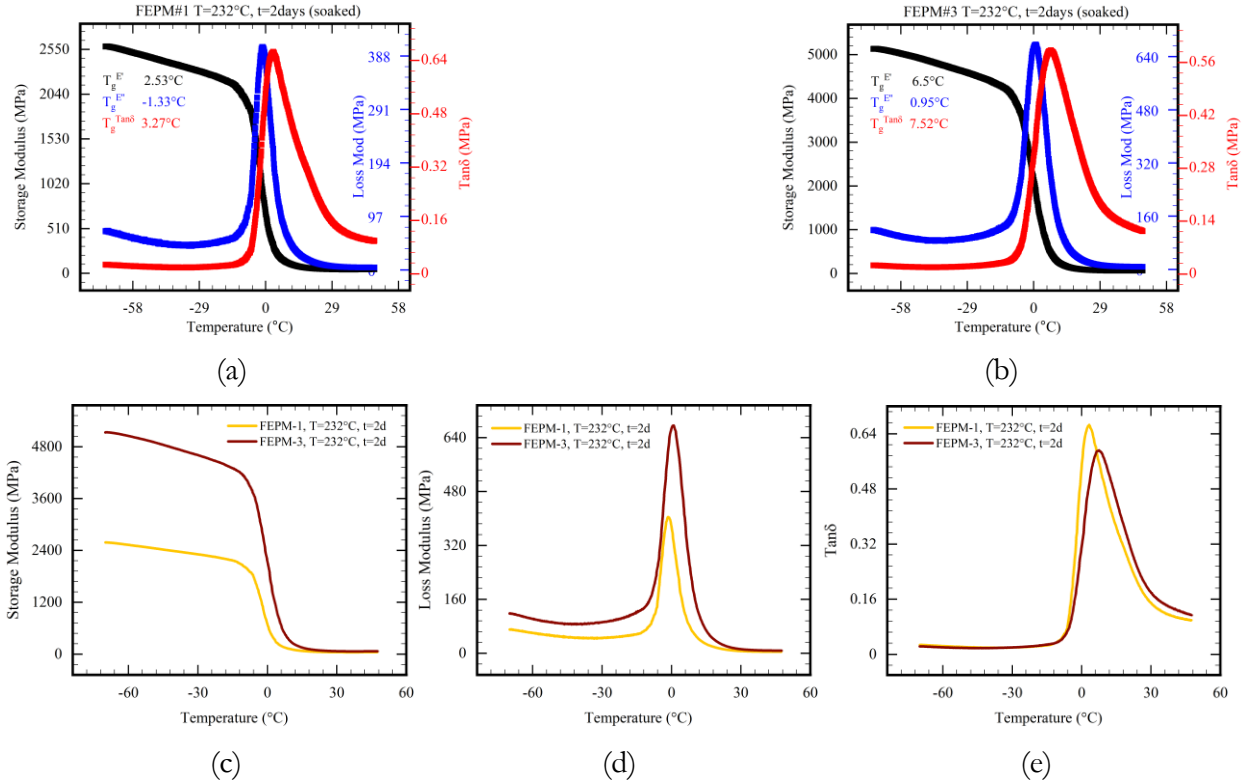

Figure 6.11: DMA (a) FEPM-1, (b) FEPM-3, (c) Comparison of Storage Modulus, (d) Comparison of Loss Modulus, and (e) Comparison of Tan δ.

e) FEPM-3 at 250°C: At 250°C, FEPM-3 did not exhibit a total loss of the TAIC carbonyl peak at approximately 150 ppm. While around 30% degradation was observed, the carbonyl peak still remained present after 28 days aging at 250°C. In the aliphatic region, there was an increase in the CH and CH_2 peaks with minimal change to the CH_3 peak. The rise in CH and CH_2 peaks could be attributed to more efficient CP dynamics rather than changes in the polymer itself. Further experiments are needed to determine the source of these changes (see Fig. 6.9).

f) Solution State NMR: ^{1}H NMR spectra are dominated by residual solvents (toluene, heptane, and cyclohexane) used in the aging process. For the samples aged at 250°C, there are no appreciable

changes from 2- to 7- to 14-day aging. ^{19}F NMR data, which does not suffer from the residual signals of the solvents, does not show any progression in either signal intensity or signal complexity (i.e., no new signals) because of the aging process (see Fig. 6.10). It is likely that any small molecules or oligomers resulting from aging were dissolved in the aging solvent leaving no trace in the FEPM samples.

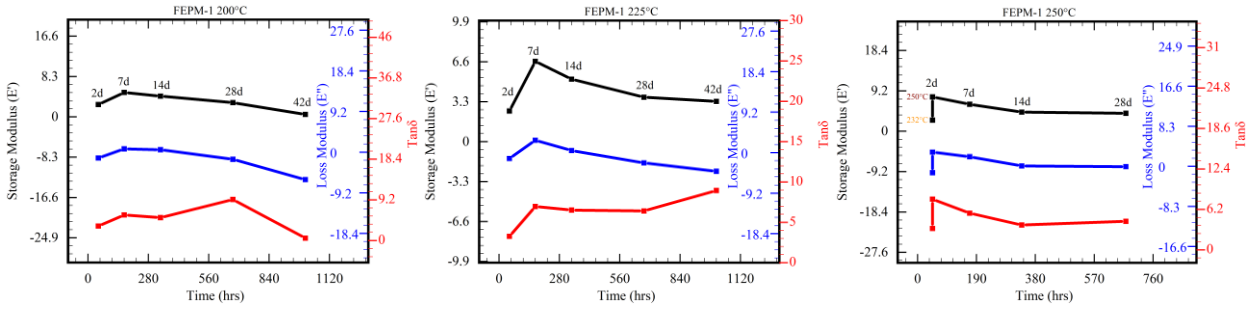

(a) (b) (c)

Figure 6.12: FEPM-1 variation of T_g in E', E", and Tan δ at different aging conditions.

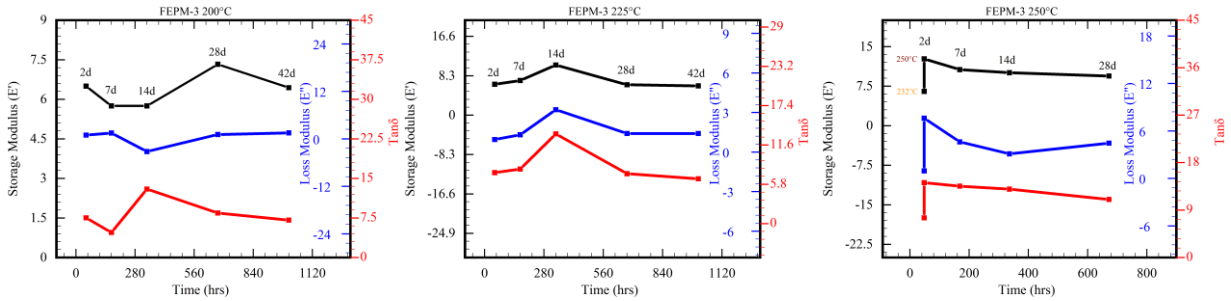

(a) (b) (c)

Figure 6.13: FEPM-3 variation of T_g in E', E", and Tan δ at different aging conditions.

DMA

For the baseline conditions, the T_g values for FEPM-1 and FEPM-3 came out as 2.53°C and 6.5°C respectively (see Fig. 6.11). It is generally observed that the Tan δ is reduced with an increase in aging time at each temperature. Decreasing Tan δ indicates that the material acts more elastic after aging, and applying a load has more potential to store the load rather than dissipate it (see Fig. 6.12 and Fig. 6.13). This effect is attributed to plasticization by the absorbed solvent in the polymer matrix. It can be better correlated by comparing Fig. 6.2 for constitutive behavior with Fig. 6.3 for the rate of solvent absorption during aging. It is evident from the softening behavior in stress-strain curves showing a decrease in stress and an increase in strain with the passing of time (see Fig. 6.2).

The glass transition temperature was calculated from the storage modulus by using the inflection offset method. At lower 200°C, there is an initial increase in T_g followed by a decrease

which depicts an initial cross-link formation followed by a reduction of cross-link. There is a linear decrease in T_g with an increase in aging time and temperature. It can be analyzed in conjunction with Fig. 6.3, showing solvent uptake and resultantly softening the constitutive behavior of the FEPM rubber.

6.4 Conclusion

In conclusion, this study has provided a comprehensive understanding of the aging behavior of two types of tetrafluoroethylene-propylene elastomers (FEPM-1 and FEPM-3) under specific aging conditions. The investigation revealed that the breakage of the PP molecular chain due to thermal aging led to the removal of partially saturated hydrocarbons, thereby reducing the carbon elemental content. In contrast, thermal aging in solvent presented a more complex phenomenon. The saturated hydrocarbon and CF2 structures exhibited a reduction after aging in the sour solvent at 250°C, with the degree of reduction being considerably greater than that observed for thermal aging at 200°C and 225°C. Furthermore, the TAIC structure experienced degradation during thermal aging at high temperatures, causing the destruction of the cross-linked network, especially in the case of FEPM-1.

The utilization of various characterization methods, including tensile tests, FTIR, NMR, and DMA, has offered valuable insights into the aging behavior of tetrafluoroethylene-propylene elastomers. These analyses emphasize the importance of considering the effects of plasticization on the mechanical properties of polymers. The results contribute to an enhanced understanding of the degradation mechanisms in FEPM materials, which is crucial for their effective application in high-temperature environments.

Solution State NMR data revealed the spectra being dominated by residual solvents used in the aging process, while and did not show, in most cases, any significant changes in signal intensity or complexity due to the aging process. It is likely that any small molecules or oligomers resulting from aging were dissolved in the aging solvent, leaving no trace in the FEPM samples.

This study provides essential theoretical guidance for the future development of fluoroelastomers. It underscores the significance of comprehending the material properties and degradation mechanisms of FEPM materials when exposed to varying thermal conditions. Further research could explore alternative methods for mitigating the impact of aging and identifying optimal coagents to improve the mechanical properties and durability of FEPM elastomers.

Chapter 7:

Summary and Future Works

This research aimed to experimentally investigate and characterize the damage trends of cross-linked elastomeric adhesives after environmental aging. The study focused on understanding the individual aging environments and their synergistic effects on the materials. The findings will be beneficial for developing new materials for specific serviceability conditions and creating constitutive models for similar cross-linked polymers under various aging scenarios. In this chapter, we provide a brief summary of each section of the dissertation, starting with an introduction to cross-linked polymers and their applications in chapter 1.

7.1 General Remarks

Throughout this research, the primary focus has been on examining the complex interplay of environmental factors and their impact on the degradation and performance of cross-linked elastomeric adhesives. By systematically analyzing individual aging environments and their synergistic effects, this study has contributed valuable insights into the underlying mechanisms of material aging. These findings hold significant implications for the development of new materials tailored to specific serviceability conditions and the establishment of constitutive models for similar cross-linked polymers under various aging scenarios. As a result, this research not only advances our fundamental understanding of elastomeric adhesive behavior but also provides practical guidance for enhancing the longevity and performance of materials in diverse applications. Before outlining the future research directions, let us briefly recapitulate the salient chapters of this dissertation, highlighting the key contributions and insights gained through the course of this study:

a. **Chapter 2** provides a comprehensive analysis of water-induced damage on the mechanical performance of silicon-based adhesives, particularly their constitutive and failure properties. The study correlates the loss of mechanical performance in aging with water-uptake and reveals that water-uptake is directly related to damage, which reduces strength and toughness.

b. **Chapter 3** presents the effects of accelerated thermo-oxidative, hydrolytic, and hygrothermal aging on the mechanical and chemical properties of a polyurethane-based (PUB) adhesive commonly used in the automobile industry. The study focused on comparing the effects of different aging environments on material behavior, finding

that hygrothermal aging results from competition between thermo-oxidation and hydrolytic aging environments. The total mechanical and environmental damage depends on various factors, including aging time, temperature, oxygen, water, and humidity.

c. **In chapter 4**, the research shows that environment-induced degradation is separable from mechanically induced damage. The study examined the effects of different relative humidity (RH) conditions on the PUB adhesive, confirming that environmental damage superposes mechanical damage and can be separated.

d. **In chapter 5**, a sequential dual aging experimental investigation was conducted to analyze the changes in constitutive behavior and toughness of aged materials under multiple environmental exposures. The study outlines how different environments affect the material individually and their interaction with other weathering conditions, aiming to better understand and model the damage mechanics involved in exposure to multiple environmental conditions.

e. **Chapter 6** investigates the degradation of tetrafluoroethylene propylene (FEPM) rubber exposed to sour high-pressure, high-temperature (HPHT) downhole conditions with simultaneous exposure to multi factor environmental agents. The study aimed optimize the performance and lifespan of equipment used in HPHT conditions by examining the degradation of the essential FEPM rubber component.

7.2 Future Research Direction

The complexity of natural aging in materials arises from the simultaneous interaction of multiple environmental factors. Accurately predicting material performance under such conditions requires a comprehensive understanding of coupled-aging phenomena. While this study has explored thermo-oxidation, hygrothermal, and hydrolytic aging environments in single and dual-aging experiments, there is still considerable potential for expanding this research to enhance our understanding of coupled-aging mechanisms in materials.

a. **Investigating Degradation Mechanisms in Sour HPHT Environments:** Future research should focus on fluoroelastomers and their degradation mechanisms in sour HPHT environments, considering various environmental parameters, including pressure, temperature, and humidity. This knowledge will guide the development of new materials, coatings, or surface treatments designed to withstand these challenging

conditions. Additionally, understanding the interaction between sour gas components and elastomers will provide valuable insights for designing more durable materials.

b. **Utilizing Computational Methods and Machine Learning:** Investigating the influence of material microstructure and molecular mechanisms on the aging process can offer valuable insights into material degradation. Advanced computational methods and simulations, combined with machine learning and artificial intelligence techniques, will enable researchers to identify patterns and trends in material aging and predict their behavior under diverse environmental conditions. These approaches can also help optimize material properties and processing techniques to enhance performance and durability.

c. **Implementing Trio-Aging Experiments:** Incorporating Trio-Aging experiments, which combine temperature, UV light exposure, and humidity, allows for a more realistic representation of real-world material degradation. By examining the synergistic effects of these factors, as well as the impact of varying the Trio-Aging cycles, researchers can obtain a comprehensive understanding of material aging dynamics. Furthermore, evaluating the role of mechanical stress alongside these environmental factors will enable more accurate predictions of material performance in service conditions.

d. **Analyzing Material Changes and Developing Predictive Models:** Conducting in-depth analyses of microstructural and molecular changes during Trio-Aging experiments can reveal the underlying mechanisms responsible for material degradation in complex environments. Developing predictive models for fluoroelastomer performance under Trio-Aging conditions will help optimize equipment used in demanding applications such as oil and gas extraction. These models can also serve as valuable tools for material selection and design, ensuring long-term reliability and cost-effectiveness.

e. **Exploring Innovative Material Solutions:** Investigating the potential of self-healing materials, smart materials with built-in monitoring capabilities, and advanced nano-materials or coatings will enable the development of more resilient, efficient, and sustainable systems. Such innovative materials can help reduce maintenance requirements, extend service life, and minimize environmental impact, all of which contribute to improved performance in various industries.

By addressing these research avenues, the materials science community can contribute to overcoming the challenges posed by harsh environmental conditions and improve the performance and lifespan of equipment in various industries. Pursuing these research directions will enable the development of a deeper understanding of the factors influencing material degradation and the creation of more resilient, efficient, and sustainable materials and systems that can better withstand complex environmental challenges.

BIBLIOGRAPHY

[1] MH Abd-El Salam, S El-Gamal,MMohsen, and DM Abd El-Maqsoud. Effect of conductive fillers on the cyclic stress-strain and nano-scale free volume properties of silicone rubber. *Chinese Journal of Polymer Science*, 32(5):558–567, 2014.

[2] Mahmoud R Abusrea and Kazuo Arakawa. Improvement of an adhesive joint constructed from carbon fiberreinforced plastic and dry carbon fiber laminates. *Composites Part B: Engineering*, 97:368–373, 2016.

[3] John O Akindoyo, MdDH Beg, Suriati Ghazali, MR Islam, Nitthiyah Jeyaratnam, and AR Yuvaraj. Polyurethane types, synthesis and applications–a review. *Rsc Advances*, 6(115):114453–114482, 2016.

[4] Sabina Alessi, Giuseppe Pitarresi, and Giuseppe Spadaro. Effect of hydrothermal ageing on the thermal and delamination fracture behaviour of cfrp composites. *Composites Part B: Engineering*, 67:145–153, 2014.

[5] Bruce Allen, Monika Bleszynski, Maciej Kumosa, and Erika Willis. Investigation into the effects of environmental stresses on rtv-1 silicone-based caulk materials. *IEEE Transactions on Dielectrics and Electrical Insulation*, 22(5):2978–2986, 2015.

[6] D ASTM. 412. *Standard Test Method for Vulcanized Rubber and Thermoplastic Rubbers and Thermoplastic Elastomer-Tension, ASTM, Philadelphia*, 6, 1992.

[7] D ASTM. Astm standard d-2240. ASTM Conshohocken, PA, 2010.

[8] Tariq Aziz, Mark Waters, and Robert G. Jagger. Analysis of the properties of silicone rubber maxillofacial prosthetic materials. *Journal of dentistry*, 31 1:67–74, 2003.

[9] Martin Badertscher, Philippe Bühlmann, and Ernö Pretsch. *Structure Determination of Organic Compounds: Tables of Spectral Data*. Springer, 2009.

[10] Khairiah Binti Haji Badri, Wong Chee Sien, MSBR Shahrom, Liow Chi Hao, Norhafiza Yuhana Baderuliksan, NR Norzali, et al. Ftir spectroscopy analysis of the prepolymerization of palm-based polyurethane. *Solid State Sci. Technol*, 18(2):1–8, 2010.

[11] Amir Bahrololoumi and Roozbeh Dargazany. Hydrolytic aging in rubber-like materials: A micro-mechanical approach to modeling. In *ASME International Mechanical Engineering Congress and Exposition*, volume 59469, page V009T11A029. American Society of Mechanical Engineers, 2019.

[12] Amir Bahrololoumi, Hamid Mohammadi, Vahid Moravati, and Roozbeh Dargazany. A physically-based model for thermo-oxidative and hydrolytic aging of elastomers. *International Journal of Mechanical Sciences*, 194:106193, 2021.

[13] Amir Bahrololoumi, Vahid Morovati, Emad A Poshtan, and Roozbeh Dargazany. A multi-physics constitutive model to predict quasi-static behaviour: Hydrolytic aging in thin cross-linked polymers. *International Journal of Plasticity*, page 102676, 2020.

[14] Amir Bahrololoumi, Vahid Morovati, Mamoon Shaafaey, and Roozbeh Dargazany. A multi-physics approach on modeling of hygrothermal aging and its effects on constitutive behavior of cross-linked polymers. *Journal of the Mechanics and Physics of Solids*, page 104614, 2021.

[15] Amir Bahrololoumi, Mamoon Shaafaey, Georges Ayoub, and Roozbeh Dargazany. Thermal aging coupled with cyclic fatigue in cross-linked polymers: Constitutive modeling & fe implementation. *International Journal of Solids and Structures*, page 111800, 2022.

[16] Mariana D Banea and Lucas FM da Silva. Static and fatigue behaviour of room temperature vulcanizing silicone adhesives for high temperature aerospace applications. *Materialwissenschaft und Werkstofftechnik*, 41(5):325–335, 2010.

[17] Antoine Bardin, Pierre-Yves Le Gac, Stéphane Cérantola, Gaëlle Simon, Hervé Bindi, and Bruno Fayolle. Hydrolytic kinetic model predicting embrittlement in thermoplastic elastomers. *Polymer Degradation and Stability*, 171:109002, 2020.

[18] G Baschek, G Hartwig, and F Zahradnik. Effect of water absorption in polymers at low and high temperatures. *Polymer*, 40(12):3433–3441, 1999.

[19] A Bele, G Stiubianu, S Vlad, C Tugui, CD Varganici, L Matricala, D Ionita, D Timpu, and M Cazacu. Aging behavior of the silicone dielectric elastomers in a simulated marine environment. *RSC advances*, 6(11):8941– 8955, 2016.

[20] Robert Bernstein, DoraKDerzon, andKenneth T Gillen. Nylon 6.6 accelerated aging studies: thermal–oxidative degradation and its interaction with hydrolysis. *Polymer Degradation and Stability*, 88(3):480–488, 2005.

[21] Lakshmana Rao Bhagavathi, Abhijit P Deshpande, GD Janaki Ram, and SK Panigrahi. Hygrothermal aging, fatigue and dynamic mechanical behavior of cellulosic particles reinforced one-component moisture curable polyurethane adhesive joints. *International Journal of Adhesion and Adhesives*, 105:102771, 2021.

[22] Monika Bleszynski and Maciej Kumosa. Silicone rubber rtv-1 aging in the presence of aqueous salt. *IEEE Transactions on Dielectrics and Electrical Insulation*, 23(5):2822–2829, 2016.

[23] CSP Borges, R Brandão, A Akhavan-Safar, EAS Marques, RJC Carbas, C Ueffing, P Weißgraeber, F Schmid, and LFM da Silva. Influence of water and surfactant contamination on the mechanical and chemical properties of a silicone adhesive before and after curing. *The Journal of Adhesion*, pages 1–28, 2022.

[24] MR Bowditch. The durability of adhesive joints in the presence of water. *International Journal of Adhesion and Adhesives*, 16(2):73–79, 1996.

[25] Mahshahr Branch and I Mahshahr. Use of polyurethane coating to prevent corrosion in oil and gas pipelines transfer. *International Journal of Innovation and Applied Studies*, 1(2):186–193, 2012.

[26] AB Brennan and F Feller III. Physical aging behavior of a poly (arylene etherimide). *Journal of Rheology*, 39(2):453–470, 1995.

[27] Adrian Brito. How polyurethane can be used in today's manufacturing industry. *Reinforced Plastics*, 64(5):268– 270, 2020.

[28] Michael A Brook, Hanns-Ulrich Saier, Julia Schnabel, Kaitlin Town, and Michael Maloney. Pretreatment of liquid silicone rubbers to remove volatile siloxanes. *Industrial & engineering chemistry research*, 46(25):8796– 8805, 2007.

[29] Michael R Buche and Meredith N Silberstein. Chain breaking in the statistical mechanical constitutive theory of polymer networks. *arXiv preprint arXiv:2104.08866*, 2021.

[30] J Burns, PS Dubbelday, and RY Ting. Dynamic bulk modulus of various elastomers. *Journal of Polymer Science Part B: Polymer Physics*, 28(7):1187–1205, 1990.

[31] S Cabral-Fonseca, JR Correia, MP Rodrigues, and FA Branco. Artificial accelerated ageing of gfrp pultruded profiles made of polyester and vinylester resins: characterisation of physical–chemical and mechanical damage. *Strain*, 48(2):162–173, 2012.

[32] Guillermina Capiel, Luis A Miccio, Pablo E Montemartini, and Gustavo A Schwartz. Water diffusion and hydrolysis effect on the structure and dynamics of epoxy-anhydride networks. *Polymer Degradation and Stability*, 143:57–63, 2017.

[33] Mat Celina, Kenneth T Gillen, and RA Assink. Accelerated aging and lifetime prediction: review of nonarrhenius behaviour due to two competing processes. *Polymer Degradation and Stability*, 90(3):395–404, 2005.

[34] Mathew C Celina. Review of polymer oxidation and its relationship with materials performance and lifetime prediction. *Polymer Degradation and Stability*, 98(12):2419–2429, 2013.

[35] Makram Chaabane, Ning Ding, and Fahmi Zaïri. An approach to assess the thermal aging effects on the coupling between inelasticity and network alteration in filled rubbers. *International Journal of Non-Linear Mechanics*, page 103783, 2021.

[36] Kimberly A Chaffin, Adam J Buckalew, James L Schley, Xiangji Chen, Matthew Jolly, Julie A Alkatout, Jennifer P Miller, Darrel F Untereker, Marc A Hillmyer, and Frank S Bates. Influence of water on the structure and properties of pdms-containing multiblock polyurethanes. *Macromolecules*, 45(22):9110–9120, 2012.

[37] Tianying Chang, Xiansheng Zhang, and Hong-Liang Cui. Evolution of terahertz dielectric permittivity of rubber during thermo-oxidative aging. *Microwave and Optical Technology Letters*, 60, 12 2017.

[38] ANChaudhry andNC Billingham. Characterisation and oxidative degradation of a room-temperature vulcanized poly (dimethylsiloxane) rubber. *Polymer degradation and Stability*, 73(3):505–510, 2001.

[39] Yang Chen, LingWang, ZefengWu, Junchen Luo, Bei Li, Xuewu Huang, Huaiguo Xue, and Jiefeng Gao. Superhydrophobic, durable and cost-effective carbon black/rubber composites for high performance strain sensors. *Composites Part B: Engineering*, 176:107358, 2019.

[40] Yi Chen, Julio F Davalos, Indrajit Ray, and Hyeong-Yeol Kim. Accelerated aging tests for evaluations of durability performance of frp reinforcing bars for concrete structures. *Composite Structures*, 78(1):101–111, 2007.

[41] Eun Yeob Choi, Jung-Chae Shin, Jae Young Lee, Mu Hyeon Kim, and Chang Keun Kim. Accelerated life testing of thermoplastic polyurethane encapsulants used in underwater acoustic sensor. *Macromolecular Research*, pages 1–7, 2019.

[42] Sung-Seen Choi and Sung-Ho Ha. Water swelling behaviors of silica-reinforced nbr composites in deionized water and salt solution. *Journal of Industrial and Engineering Chemistry*, 16(2):238–242, 2010.

[43] Ieuan Collinsa, Mokarram Hossaina, Wulf Dettmera, and Ian Mastersa. Flexible membrane structures for wave energy harvesting: A review of the developments, materials and computational modelling approaches. *Renewable and Sustainable Energy Reviews*, 2021.

[44] Chuanbo Cong, Cancan Cui, Xiaoyu Meng, and Qiong Zhou. Stability of poss crosslinks and aggregates in tetrafluoroethylene-propylene elastomers/ovposs composites exposed to hydrochloric acid solution. *Polymer degradation and stability*, 100:29–36, 2014.

[45] John Crank et al. *The mathematics of diffusion*. Oxford university press, 1979.

[46] ASTM D. 471. *Standard Test Method for Rubber Property - Effect of Liquids*, E01:13, 2006.

[47] ASTM D1141-98. Standard practice for the preparation of substitute ocean water, 2008.

[48] ASTM D412. Standard test methods for vulcanized rubber and thermoplastic elastomers–tension, 2006.

[49] Roozbeh Dargazany, Vu Ngoc Khiêm, and Mikhail Itskov. A generalized network decomposition model for the quasi-static inelastic behavior of filled elastomers. *International Journal of Plasticity*, 63:94, 2015.

[50] Peter Davies and Guy Evrard. Accelerated ageing of polyurethanes for marine applications. *Polymer Degradation and Stability*, 92(8):1455–1464, 2007.

[51] Francois De Buyl. Silicone sealants and structural adhesives. *International Journal of Adhesion and Adhesives*, 21(5):411–422, 2001.

[52] B De Neve and MER Shanahan. Physical and chemical effects in an epoxy resin exposed to water vapour. *The Journal of Adhesion*, 49(3-4):165–176, 1995.

[53] FelipeMde Souza, Pawan K Kahol, and Ram K Gupta. Introduction to polyurethane chemistry. In *Polyurethane Chemistry: Renewable Polyols and Isocyanates*, pages 1–24. ACS Publications, 2021.

[54] Morgan Deroiné, Antoine Le Duigou, Yves-Marie Corre, Pierre-Yves Le Gac, Peter Davies, Guy César, and Stéphane Bruzaud. Accelerated ageing and lifetime prediction of poly (3-hydroxybutyrate-co-3-hydroxyvalerate) in distilled water. *Polymer testing*, 39:70–78, 2014.

[55] Sonal Desai, IM Thakore, and Surekha Devi. Effect of crosslink density on transport of industrial solvents through polyether based polyurethanes. *Polymer international*, 47(2):172–178, 1998.

[56] Amina Dinari, Fahmi Zaïri, Makram Chaabane, Jewan Ismail, and Tarek Benameur. Thermo-oxidative stress relaxation in carbon-filled sbr. *Plastics, Rubber and Composites*, pages 1–16, 2021.

[57] JP Dismukes, L Ekstrom, and RJ Paff. Lattice parameter and density in germanium-silicon alloys1. *The Journal of Physical Chemistry*, 68(10):3021–3027, 1964.

[58] Mihail V Drapalyuk, Vladimir A Zelikov, Valerii I Posmetev, Vadim O Nikonov, and Eugene V Shatalov. Simulation results to assess effectiveness of seals made of polyurethane for hydraulic drives of machines. In *International Conference" Aviamechanical engineering and transport"(AVENT 2018)*. Atlantis Press, 2018.

[59] ASTM E. 1640. *Standard Test Method for Assignment of the Glass Transition Temperature By Dynamic Mechanical Analysis*, 14.01:05, 2004.

[60] Mostafa Eesaee and Akbar Shojaei. Effect of nanoclays on the mechanical properties and durability of novolac phenolic resin/woven glass fiber composite at various chemical environments. *Composites Part A: Applied Science and Manufacturing*, 63:149–158, 2014.

[61] Hans-Wilhelm Engels, Hans-Georg Pirkl, Reinhard Albers, Rolf W Albach, Jens Krause, Andreas Hoffmann, Holger Casselmann, and Jeff Dormish. Polyurethanes: versatile materials and sustainable problem solvers for today's challenges. *Angewandte Chemie International Edition*, 52(36):9422–9441, 2013.

[62] Robert M Evans. *Polyurethane Sealants: Technology & Applications*. CRC Press, 2014.

[63] Matteo Ferrari, Stefano Pandini, Aldo Zenoni, Giorgio Donzella, Davide Battini, Andrea Avanzini, Andrea Salvini, Fabio Zelaschi, Alberto Andrighetto, and Fabio Bignotti. Degradation of epdm and fpm elastomers irradiated at very high dose rates in mixed gamma and neutron fields. *Polymer Engineering & Science*, 59(12):2522–2532, 2019.

[64] Paul J Flory and John Rehner Jr. Statistical mechanics of cross-linked polymer networks i. rubberlike elasticity. *The journal of chemical physics*, 11(11):512–520, 1943.

[65] Xing Gao, Zhijun Shi, Changqing Liu, Guang Yang, Igor Sevostianov, and Vadim V Silberschmidt. Inelastic behaviour of bacterial cellulose hydrogel: in aqua cyclic tests. *Polymer Testing*, 44:82–92, 2015.

[66] Kojima Gen and Wachi Hiroshi. Vulcanization of a fluoroelastomer derived from tetrafluoroethylene and propylene. *Research report of Asahi Glass Co., Ltd.= Asahi Glass Research Report*, 28(2):p123–132, 1978.

[67] Aref Ghaderi,Vahid Morovati, Amir Bahrololoumi, andRoozbeh Dargazany. Aphysics-informed neural network constitutive model for cross-linked polymers. In *ASME International Mechanical Engineering Congress and Exposition*, volume 84607, page V012T12A007. American Society of Mechanical Engineers, 2020.

[68] Aref Ghaderi, Vahid Morovati, and Roozbeh Dargazany. A bayesian surrogate constitutive model to estimate failure probability of rubber-like materials. *arXiv preprint arXiv:2010.13241*, 2020.

[69] Aref Ghaderi, Vahid Morovati, and Roozbeh Dargazany. A physics-informed assembly of feed-forward neural network engines to predict inelasticity in cross-linked polymers. *Polymers*, 12(11):2628, 2020.

[70] Afshin Ghanbari-Siahkali, Susanta Mitra, Peter Kingshott, Kristoffer Almdal, Carsten Bloch, and Helle Kem Rehmeier. Investigation of the hydrothermal stability of cross-linked liquid silicone rubber (lsr). *Polymer degradation and stability*, 90(3):471–480, 2005.

[71] Kenneth T Gillen, Robert Bernstein, and Dora K Derzon. Evidence of non-arrhenius behaviour from laboratory aging and 24-year field aging of polychloroprene rubber materials. *Polymer Degradation and Stability*, 87(1):57– 67, 2005.

[72] Florian E Golling, Raul Pires, Andreas Hecking, JanWeikard, Frank Richter, Karsten Danielmeier, and Dirk Dijkstra. Polyurethanes for coatings and adhesives–chemistry and applications. *Polymer International*, 68(5):848– 855, 2019.

[73] Achim Göpferich. Mechanisms of polymer degradation and erosion. *Biomaterials*, 17(2):103–114, 1996.

[74] Sotirios A Grammatikos, Richard J Ball, Mark Evernden, and Ryan G Jones. Impedance spectroscopy as a tool for moisture uptake monitoring in construction composites during service. *Composites Part A: Applied Science and Manufacturing*, 105:108–117, 2018.

[75] N Grassie and IG Macfarlane. The thermal degradation of polysiloxanes—i. poly (dimethylsiloxane). *European polymer journal*, 14(11):875–884, 1978.

[76] Lewis Greenspan et al. Humidity fixed points of binary saturated aqueous solutions. *Journal of research of the national bureau of standards*, 81(1):89–96, 1977.

[77] JV Gulmine, PR Janissek, HM Heise, and L Akcelrud. Degradation profile of polyethylene after artificial accelerated weathering. *Polymer degradation and stability*, 79(3):385–397, 2003.

[78] Qiang Guo and Fahmi Zaïri. A micromechanics-based model for deformation-induced damage and failure in elastomeric media. *International Journal of Plasticity*, 140:102976, 2021.

[79] J Gutierrez, F Le Lay, and P Hoarau. A study of the aging of glass fibre–resin composites in a marine environment. *Nautical construction with composite materials*, pages 338–346, 1992.

[80] Soon Mok Ha, MichaelWissler, Ron Pelrine, Scott Stanford, GaborMKovacs, and Qibing Pei. Characterization of electroelastomers based on interpenetrating polymer networks. In *Electroactive Polymer Actuators and Devices (EAPAD) 2007*, volume 6524, pages 78–87. SPIE, 2007.

[81] Salah U Hamim and Raman P Singh. Effect of hygrothermal aging on the mechanical properties of fluorinated and nonfluorinated clay-epoxy nanocomposites. *International scholarly research notices*, 2014, 2014.

[82] James A Harvey. Chemical and physical aging of plastics. In *Handbook of environmental degradation of materials*, pages 153–163. Elsevier, 2005.

[83] Mumtahin Hasnat, Mahdi Ghazavi, Angela Farina, Aksel Seitllari, and M Emin Kutay. Laboratory evaluation and mechanistic-empirical performance analysis of polymer coated rubber (pcr) mixtures. Technical report, 2021.

[84] Claude Hepburn. *Polyurethane elastomers*. Springer Science & Business Media, 2012.

[85] Mohsen Heshmati, Reza Haghani, and Mohammad Al-Emrani. Durability of cfrp/steel joints under cyclic wet-dry and freeze-thaw conditions. *Composites Part B: Engineering*, 126:211–226, 2017.

[86] Paul C Hiemenz and Timothy P Lodge. *Polymer chemistry*. CRC press, 2007.

[87] Bin Hong, Guijun Xian, and Hui Li. Effects of water or alkali solution immersion on the water-uptake and physicomechanical properties of polyurethane. *Polymer Engineering & Science*, 58(12):2276–2287, 2018.

[88] John M Hutchinson. Physical aging of polymers. *Progress in polymer science*, 20(4):703–760, 1995.

[89] DIN ISO. Rubber, vulcanized–determination of the effect of liquids. *British Standard Institution, London*, 2005.

[90] ISO 1817:2015(en) Rubber vulcanized or thermoplastic Determination of the effect of liquids, 2015.

[91] Minoru Isshiki, Katsutoshi Mine, Yoshiko Otani, and Kimio Yamakawa. Semiconductor device comprising silicone adhesive sheet, October 16 2001. US Patent 6,304,000.

[92] Mangala Joshi, Bapan Adak, and BS Butola. Polyurethane nanocomposite based gas barrier films, membranes and coatings: A review on synthesis, characterization and potential applications. *Progress in Materials Science*, 97:230–282, 2018.

[93] MKasamori, YFunada, KAwaza, YWatanabe,MNakada, andYMiyano. Accelerated evaluation of mechanical degradation behavior of gfrp in hot water. *Progress in durability analysis of composite systems, Cardon, AH; Fukuda, H. & Reifsnider, K.(eds.), Taylor & Francis, London*, pages 273–277, 1996.

[94] Sima Kashi, Russell Varley, Mandy De Souza, Salwan Al-Assafi, Adriano Di Pietro, Christelle de Lavigne, and Bronwyn Fox. Mechanical, thermal, and morphological behavior of silicone rubber during accelerated aging. *Polymer-Plastics Technology and Engineering*, 2018.

[95] Ramesh Keshavaraj, Richard W Tock, and CVG Vallabhan. Effects of moisture on structural silicone rubber sealants used in window glazing applications. *Construction and building materials*, 8(4):227–232, 1994.

[96] Farideh Khabbaz, Ann-Christine Albertsson, and Sigbritt Karlsson. Chemical and morphological changes of environmentally degradable polyethylene films exposed to thermo-oxidation. *Polymer Degradation and Stability*, 63(1):127–138, 1999.

[97] Gayani Chandima Kodippili. *Structural characterization of polyurethane foam and implications of aging*. University of Nevada, Las Vegas, 2003.

[98] Gen Kojima and Hiroshi Wachi. Vulcanization of a fluoroelastomer derived from tetrafluoroethylene and propylene. *Rubber Chemistry and Technology*, 51(5):940–947, 1978.

[99] Ken Kojio, Shuhei Nozaki, Atsushi Takahara, and Satoshi Yamasaki. Influence of chemical structure of hard segments on physical properties of polyurethane elastomers: a review. *Journal of Polymer Research*, 27(6):1–13, 2020.

[100] Shabnam Konica and Trisha Sain. A reaction-driven evolving network theory coupled with phase-field fracture to model polymer oxidative aging. *Journal of the Mechanics and Physics of Solids*, 150:104347, 2021.

[101] George Kostov. Study of synthesis and properties of tetrafluoroethylene-propylene copolymers. *Journal of Fluorine Chemistry*, 29(1-2):109, 1985.

[102] GK Kostov and P Chr. Petrov. Study of synthesis and properties of tetrafluoroethylene–propylene copolymers. *Journal of Polymer Science Part A: Polymer Chemistry*, 30(6):1083–1088, 1992.

[103] Soilikki Kotanen, Minna Poikelispää, Alexander Efimov, Tapani Harjunalanen, Christopher Mills, Timo Laaksonen, and Essi Sarlin. Hydrolytic stability of polyurethane/polyhydroxyurethane hybrid adhesives. *International Journal of Adhesion and Adhesives*, 110:102950, 2021.

[104] Bindu Krishnan, Dwight Latham, Laura A Grier, Woo-Sung Bae, Hector Perez, Jorge Jimenez, and William A Koonce. Polyurethane based insulated glass sealant, January 17 2017. US Patent 9,546,307.

[105] Ján Kruželák, Ivan Hudec, and Rastislav Dosoudil. Influence of thermo-oxidative and ozone ageing on the properties of elastomeric magnetic composites. *Polymer degradation and stability*, 97(6):921–928, 2012.

[106] Ján Kruželák, Richard S`ykora, and Ivan Hudec. Vulcanization of rubber compounds with peroxide curing systems. *Rubber chemistry and technology*, 90(1):60–88, 2017.

[107] Shigeki Kuroki. A19f nmr signal assignment and a detailed structural study of alternating tetrafluoroethylenepropylene copolymer by high resolution 19f nmr spectroscopy and computational chemistry. *Polymer journal*, 41(5):449–454, 2009.

[108] Pierre-Yves Le Gac, Dominique Choqueuse, and D Melot. Description and modeling of polyurethane hydrolysis used as thermal insulation in oil offshore conditions. *Polymer testing*, 32(8):1588–1593, 2013.

[109] Pierre-Yves Le Gac, Vincent Le Saux,MParis, andYann Marco. Ageing mechanism and mechanical degradation behaviour of polychloroprene rubber in a marine environment: Comparison of accelerated ageing and long term exposure. *Polymer Degradation and Stability*, 97(3):288–296, 2012.

[110] Bong-Joo Lee, Ji-Hoon Lee, and Dong-Hun Kim. An alternative approach to conventional seepage meters: Buoy-type seepage meter. *Limnology and Oceanography: Methods*, 16(5):299–308, 2018.

[111] Jihoon Lee, Jungwoo Kim, Hyoungsub Kim, Young Min Bae, Kyeong-Hee Lee, and Hyoung J Cho. Effect of thermal treatment on the chemical resistance of polydimethylsiloxane for microfluidic devices. *Journal of Micromechanics and Microengineering*, 23(3):035007, 2013.

[112] Emily K Leitsch,William H Heath, and JohnMTorkelson. Polyurethane/polyhydroxyurethane hybrid polymers and their applications as adhesive bonding agents. *International Journal of Adhesion and Adhesives*, 64:1–8, 2016.

[113] H. Levine and L. Slade. Water as a plasticizer: physico-chemical aspects of low-moisture polymeric systems. In FelixEditor Franks, editor, *Water Science Reviews 3: Water Dynamics*, volume 3 of *Water Science Review*, page 79–185. Cambridge University Press, 1988.

[114] HARRY Levine and LOUISE Slade. Water as a plasticizer: physico-chemical aspects of low-moisture polymeric systems. *Water science reviews*, 3:79–185, 1988.

[115] James P Lewicki, John J Liggat, and Mogon Patel. The thermal degradation behaviour of polydimethylsiloxane/ montmorillonite nanocomposites. *Polymer Degradation and Stability*, 94(9):1548–1557, 2009.

[116] James P Lewicki, John J Liggat, Richard A Pethrick, Mogon Patel, and Ian Rhoney. Investigating the ageing behavior of polysiloxane nanocomposites by degradative thermal analysis. *Polymer degradation and stability*, 93(1):158–168, 2008.

[117] Xiaoming Li and Y Jack Weitsman. Sea-water effects on foam-cored composite sandwich lay-ups. *Composites Part B: Engineering*, 35(6-8):451–459, 2004.

[118] Xie Li, Wei Li, Zhiqing Liu, Xiaolin Wang, Heling Guo, Rongjie Wang, Xuhong Guo, Cuihua Li, and Xin Jia. Underwater polyurethane adhesive with enhanced cohesion by postcrosslinking of glycerol monomethacrylate. *Journal of Applied Polymer Science*, 135(32):46579, 2018.

[119] Yingjie Li, Tong Gao, Jian Liu, Kung Linliu, C Richard Desper, and Benjamin Chu. Multiphase structure of a segmented polyurethane: effects of temperature and annealing. *Macromolecules*, 25(26):7365–7372, 1992.

[120] Zisheng Liao, Mokarram Hossain, Xiaohu Yao, Rukshan Navaratne, and Grégory Chagnon. A comprehensive thermo-viscoelastic experimental investigation of ecoflex polymer. *Polymer Testing*, 86:106478, 2020.

[121] Zisheng Liao, Jie Yang, Mokarram Hossain, Gregory Chagnon, Lin Jing, and Xiaohu Yao. On the stress recovery behaviour of ecoflex silicone rubbers. *International Journal of Mechanical Sciences*, page 106624, 2021.

[122] Fang Liu and Shuming Chen. The preparation and characterization of polyurethane foam with coconut oil polyol and rapeseed oil polyol. *Journal of Polymers and the Environment*, pages 1–14, 2021.

[123] Hao Liu, Jianzhang Wang, Pengfei Jiang, and Fengyuan Yan. Accelerated degradation of polyetheretherketone and its composites in the deep sea. *Royal society open science*, 5(4):171775, 2018.

[124] Qingkun Liu, Jia Li, Chuanbo Cong, Haomeng Cui, Lixin Xu, Ying Zhang, Xiaoyu Meng, and Qiong Zhou. Thermal and thermo-oxidative degradation of tetrafluoroethylene–propylene elastomer above 300° c. *Polymer Degradation and Stability*, 177:109180, 2020.

[125] Gao Ma, Libo Yan, Wenkai Shen, Deju Zhu, Liang Huang, and Bohumil Kasal. Effects of water, alkali solution and temperature ageing on water absorption, morphology and mechanical properties of natural frp composites: Plant-based jute vs. mineral-based basalt. *Composites Part B: Engineering*, 153:398–412, 2018.

[126] Uttam Manna, Matthew CD Carter, and DavidMLynn. "shrink-to-fit" superhydrophobicity: Thermally-induced microscale wrinkling of thin hydrophobic multilayers fabricated on flexible shrink-wrap substrates. *Advanced Materials*, 25(22):3085–3089, 2013.

[127] Rod Martin. *Ageing of composites*. Elsevier, 2008.

[128] Aji P Mathew, S Packirisamy, and Sabu Thomas. Studies on the thermal stability of natural rubber/polystyrene interpenetrating polymer networks: thermogravimetric analysis. *Polymer Degradation and Stability*, 72(3):423– 439, 2001.

[129] Hendrik Meyer-Lueckel, Sebastian Paris, Jan Mueller, Helmut Cölfen, and AndrejMKielbassa. Influence of the application time on the penetration of different dental adhesives and a fissure sealant into artificial subsurface lesions in bovine enamel. *Dental materials*, 22(1):22–28, 2006.

[130] Hamid Mohammadi and Roozbeh Dargazany. A micro-mechanical approach to model thermal induced aging in elastomers. *International Journal of Plasticity*, 118:1–16, 2019.

[131] Hamid Mohammadi and Roozbeh Dargazany. A micro-mechanical approach to model thermal induced aging in elastomers. *International Journal of Plasticity*, 118:1–16, 2019.

[132] Hamid Mohammadi, Vahid Morovati, Abd-Elrahman Korayem, Emad Poshtan, and Roozbeh Dargazany. Constitutive modeling of elastomers during photo-and thermo-oxidative aging. *Polymer Degradation and Stability*, 191:109663, 2021.

[133] Hamid Mohammadi, Vahid Morovati, Emad Poshtan, and Roozbeh Dargazany. Understanding decay functions and their contribution in modeling of thermal-induced aging of cross-linked polymers. *Polymer Degradation and Stability*, 175:109108, 2020.

[134] Hamid Mohammadi, Vahid Morovati, Emad Poshtan, and Roozbeh Dargazany. Understanding decay functions and their contribution in modeling of thermal-induced aging of cross-linked polymers. *Polymer Degradation and Stability*, page 109108, 2020.

[135] J Castillo Montes, D Cadoux, J Creus, Sébastien Touzain, E Gaudichet-Maurin, and O Correc. Ageing of polyethylene at raised temperature in contact with chlorinated sanitary hot water. part i–chemical aspects. *Polymer degradation and stability*, 97(2):149–157, 2012.

[136] Junho Moon, Sung Bok Kwak, Jae Yong Lee, and Jeong Seok Oh. Recent development in polyurethanes for automotives. *Elastomers and composites*, 52(4):249–256, 2017.

[137] Vahid Morovati, Amir Bahrololoumi, and Roozbeh Dargazany. Fatigue-induced stress-softening in cross-linked multi-network elastomers: Effect of damage accumulation. *International Journal of Plasticity*, 142:102993, 2021.

[138] Jason Mulderrig, Bin Li, and Nikolaos Bouklas. Affine and non-affine microsphere models for chain scission in polydisperse elastomer networks. *Mechanics of Materials*, 160:103857, 2021.

[139] Shigeru Murata, Tetsuya Nakajima, Nobuko Tsuzaki, Masahiko Yasuda, and Tadaya Kato. Synthesis and hydrolysis resistance of polyurethane derived from 2, 4-diethyl-1, 5-pentanediol. *Polymer degradation and stability*, 61(3):527–534, 1998.

[140] Bruno Musil, Michael Johlitz, and Alexander Lion. On the ageing behaviour of nbr: chemomechanical experiments, modelling and simulation of tension set. *Continuum Mechanics and Thermodynamics*, pages 1–17, 2018.

[141] Jingxin Na, Yisa Fan,Wei Tan, Shouwu Guo, andWenlong Mu. Mechanical behavior of polyurethane adhesive bonded joints as a function of temperature and humidity. *Journal of adhesion science and Technology*, 32(5):457– 472, 2018.

[142] Valérie Nassiet, Celine Gros, Mathieu Charlas, and Jean-Pierre Habas. Chemical structure influence of silicone adhesives on curing process. In *Advanced Materials Research*, volume 112, pages 19–28. Trans Tech Publ, 2010.

[143] Pei Ni and RonaldWThring. Synthesis of polyurethanes from solvolysis lignin using a polymerization catalyst: mechanical and thermal properties. *International Journal of Polymeric Materials*, 52(8):685–707, 2003.

[144] CJ Norris, M Hale, and M Bennett. Composition and property changes of hnbr and fkm elastomers after sour gas aging. *Plastics, Rubber and Composites*, 45(6):239–246, 2016.

[145] GMOdegard and A Bandyopadhyay. Physical aging of epoxy polymers and their composites. *Journal of polymer science Part B: Polymer physics*, 49(24):1695–1716, 2011.

[146] Anny C Ospina, Víctor H Orozco, Luis F Giraldo, Mónica Fuensanta, José Miguel Martín-Martínez, and Noemi Mateo-Oliveras. Study of waterborne polyurethane materials under aging treatments. effect of the soft segment length. *Progress in Organic Coatings*, 138:105357, 2020.

[147] Mikael Ovegård, Andreas Sundelöf, and Daniel Valentinsson. Much ado about nothing: An example of how failed incentives thwarted the implementation of the eu landing obligation. *Marine Policy*, 123:104305, 2021.

[148] Ileana Panaitescu, Thomas Koch, and Vasiliki-Maria Archodoulaki. Accelerated aging of a glass fiber/polyurethane composite for automotive applications. *Polymer Testing*, 74:245–256, 2019.

[149] Wanfen Pu, Daijun Du, Rui Liu, Kewei Li, and Tengweicong Huang. Synthesis and evaluation of β-cyclodextrinfunctionalized hydrophobically associating polyacrylamide. *RSC advances*, 6(98):96006–96014, 2016.

[150] S Radice and M Bradley. Time-based ft-ir analysis of curing of polyurethanes, 2007.

[151] Mustafizur Rahman and Christopher S Brazel. The plasticizer market: an assessment of traditional plasticizers and research trends to meet new challenges. *Progress in polymer science*, 29(12):1223–1248, 2004.

[152] Jiaxiang Jason Ren, Dave Gerrard, Ping Duan, Chau Vu, and Hoi Yin Leung. Development and characterization of a modified polymeric material for hp/ht downhole sealing applications. In *SPE Deepwater Drilling and Completions Conference*. OnePetro, 2012.

[153] Maria Cristina Righetti, Giuseppe Ajroldi, Manuele Vitali, and Giovanni Pezzin. Influence of solvent and filler on some physical properties of a fluoroelastomer. *Journal of applied polymer science*, 73(3):377–384, 1999.

[154] J Rothka, R Studd, K Tate, and D Timpe. Outgassing of silicone elastomers. *ARLON–Silicone Technology Division, Bear DE*, 19701, 2002.

[155] Anna Rudawska. The effect of the salt water aging on the mechanical properties of epoxy adhesives compounds. *Polymers*, 12(4):843, 2020.

[156] Maria Rutkowska, Katarzyna Krasowska, Aleksandra Heimowska, Izabela Steinka, and Helena Janik. Degradation of polyurethanes in sea water. *Polymer degradation and Stability*, 76(2):233–239, 2002.

[157] Míriam Sáenz-Pérez, José Manuel Laza, Jorge García-Barrasa, José LuisVilas, and Luis Manuel León. Influence of the soft segment nature on the thermomechanical behavior of shape memory polyurethanes. *Polymer Engineering & Science*, 58(2):238–244, 2018.

[158] W Salgueiro, A Marzocca, A Somoza, Giovanni Consolati, S Cerveny, Fiorenza Quasso, and S Goyanes. Dependence of the network structure of cured styrene butadiene rubber on the sulphur content. *Polymer*, 45(17):6037–6044, 2004.

[159] G Samay, L Palotas, T Nagy, and ZS Seregely. Lifetime-affecting factors of rubber products. *Journal of Applied Polymer Science*, 50(0):359–367, 1992.

[160] Lin Sang, Chuo Wang, Yingying Wang, and Wenbin Hou. Effects of hydrothermal aging on moisture absorption and property prediction of short carbon fiber reinforced polyamide 6 composites. *Composites Part B: Engineering*, 153:306–314, 2018.

[161] Moyeenuddin Ahmad Sawpan, Peter G Holdsworth, and Peter Renshaw. Glass transitions of hygrothermal aged pultruded glass fibre reinforced polymer rebar by dynamic mechanical thermal analysis. *Materials & Design*, 42:272–278, 2012.

[162] Moritz Schwabe, Dennis Bedorf, and Konrad Samwer. Influence of stress and temperature on damping behavior of amorphous pd77. 5cu6. 0si16. 5 below tg. *The European Physical Journal E*, 34(9):1–5, 2011.

[163] Philip A Schweitzer et al. *Fundamentals of corrosion: mechanisms, causes, and preventative methods*. CRC press, 2009.

[164] Ivana Šeděnková, Miroslava Trchová, and Jaroslav Stejskal. Thermal degradation of polyaniline films prepared in solutions of strong and weak acids and in water–ftir and raman spectroscopic studies. *Polymer Degradation and Stability*, 93(12):2147–2157, 2008.

[165] A Seitllari, M Ghazavi, and ME Kutay. Effects of binder modification on rutting performance of asphalt binders. In *Proceedings of the 9th International Conference on Maintenance and Rehabilitation of Pavements— Mairepav9*, pages 607–615. Springer, 2020.

[166] Mamoon Shaafaey, Amir Bahrololoumi, Hamid Mohammadi, Sharif Alazhary, and Roozbeh Dargazany. Investigation of hygrothermal aging on the polyurethane-based (pub) adhesive: substantiating competition scenario between sub-aging thermo-oxidation and hydrolytic phenomena. *Journal of Polymer Research*, 28(12):1–25, 2021.

[167] Mamoon Shaafaey, Amir Bahrololoumi, Hamid Mohammadi, Sharif Alazhary, and Roozbeh Dargazany. Investigation of hygrothermal aging on the polyurethane-based (pub) adhesive: substantiating competition scenario between sub-aging thermo-oxidation and hydrolytic phenomena. *Journal of Polymer Research*, 28(12):1–25, 2021.

[168] Mohammad Javad Sharifi, Vahab Ghalehkhondabi, and Alireza Fazlali. Investigation of the underwater sound absorption and damping properties of polyurethane elastomer. *Journal of Thermal Analysis and Calorimetry*, pages 1–6, 2021.

[169] HMCC Somarathna, SN Raman, D Mohotti, AA Mutalib, and KH Badri. The use of polyurethane for structural and infrastructural engineering applications: A state-of-the-art review. *Construction and Building Materials*, 190:995–1014, 2018.

[170] Robson F Storey and Douglas C Hoffman. Polyurethane networks based on poly (ethylene ether carbonate) diols. *Polymer*, 33(13):2807–2816, 1992.

[171] Leendert Cornelis Elisa Struik. Physical aging in amorphous polymers and other materials. 1977.

[172] PR Sundararajan. Crystalline morphology of poly (dimethylsiloxane). *Polymer*, 43(5):1691–1693, 2002.

[173] Lik-ho Tam, Denvid Lau, and Chao Wu. Understanding interaction and dynamics of water molecules in the epoxy via molecular dynamics simulation. *Molecular Simulation*, 45(2):120–128, 2019.

[174] Wei Tan, Jingxin Na, Guangbin Wang, Qianhui Xu, Hao Shen, and Wenlong Mu. The effects of service temperature on the fatigue behavior of a polyurethane adhesive joint. *International Journal of Adhesion and Adhesives*, 107:102819, 2021.

[175] Andreia C Tavares, Joseane V Gulmine, Carlos M Lepienski, and Leni Akcelrud. The effect of accelerated aging on the surface mechanical properties of polyethylene. *Polymer Degradation and Stability*, 81(2):367–373, 2003.

[176] Adrián Tenorio-Alfonso, Mª Carmen Sánchez, and José Mª Franco. A review of the sustainable approaches in the production of bio-based polyurethanes and their applications in the adhesive field. *Journal of Polymers and the Environment*, 28(3):749–774, 2020.

[177] Alpesh U Vala, Ajay V Rane, Krishnan Kanny, Vayyaprontavida K Abitha, and Sabu Thomas. Aging behavior of composite-and nanocomposite-based polyurethane. In *Polyurethane Polymers*, pages 547–557. Elsevier, 2017.

[178] Jose Vega-Baudrit, Virtudes Navarro-Banon, Patricia Vazquez, and José Miguel Martín-Martínez. Addition of nanosilicas with different silanol content to thermoplastic polyurethane adhesives. *International journal of adhesion and adhesives*, 26(5):378–387, 2006.

[179] Alok Ranjan Verma and B Subba Reddy. Accelerated aging studies of silicon-rubber based polymeric insulators used for hv transmission lines. *Polymer Testing*, 62:124–131, 2017.

[180] P Vondráček, J Hrudka, J Sulc, and P Lopour. Hydrophilic and thermoformable silicone rubber composite. *Polymer Composites: Proceedings, 28th Microsymposium on Macromolecules, Prague, Czechoslovakia, July 8–11, 1985*, page 303, 2019.

[181] Man Wang, Xiaowei Xu, Jin Ji, Yang Yang, Jianfeng Shen, and Mingxin Ye. The hygrothermal aging process and mechanism of the novolac epoxy resin. *Composites Part B: Engineering*, 107:1–8, 2016.

[182] EL Warrick, OR Pierce, KE Polmanteer, and JC Saam. Silicone elastomer developments 1967–1977. *Rubber chemistry and technology*, 52(3):437–525, 1979.

[183] LiuWenji, TuWeiping,Wang Feng, and Chen Jun. Application and research progress of polyurethane materials for automobile. *Polyurethane Industry*, page 03, 2015.

[184] JamesWilliford, Pat Rice, and Thomas Ray. Selection of metallurgy and elastomers used in completion products to achieve predicted product integrity for the hp/ht oil and gas fields of indonesia. In *SPE Asia Pacific Oil and Gas Conference and Exhibition*. OnePetro, 1999.

[185] Zygmunt Wirpsza. *Polyurethanes: chemistry, technology, and applications*. Ellis Horwood, 1993.

[186] JWise, KT Gillen, and RL Clough. An ultrasensitive technique for testing the arrhenius extrapolation assumption for thermally aged elastomers. *Polymer Degradation and Stability*, 49(3):403–418, 1995.

[187] SN Wosu, David Hui, and L Daniel. Hygrothermal effects on the dynamic compressive properties of graphite/epoxy composite material. *Composites Part B: Engineering*, 43(3):841–855, 2012.

[188] Fan Wu, Ben Chen, Yizhi Yan, Yanan Chen, and Mu Pan. Degradation of silicone rubbers as sealing materials for proton exchange membrane fuel cells under temperature cycling. *Polymers*, 10(5):522, 2018.

[189] SouhengWu. Chain structure, phase morphology, and toughness relationships in polymers and blends. *Polymer Engineering & Science*, 30(13):753–761, 1990.

[190] Guijun Xian and Vistasp M Karbhari. Segmental relaxation of water-aged ambient cured epoxy. *Polymer Degradation and Stability*, 92(9):1650–1659, 2007.

[191] Kewei Xiang, Guangsu Huang, Jing Zheng, Xiaoan Wang, Guang xian Li, and Jingyun Huang. Accelerated thermal ageing studies of polydimethylsiloxane (pdms) rubber. *Journal of Polymer Research*, 19(5):9869, 2012.

[192] Yanling Xie, Adeel Ahmad Hassan, Pan Song, Zhen Zhang, and Shifeng Wang. High scission of butadiene rubber vulcanizate under thermo-oxidation. *Polymer Degradation and Stability*, 167:292–301, 2019.

[193] Norio Yanagibashi, Setsuo Iwasaki, Takafumi Mizobuchi, Ryoji Konishi, Tatsuya Konishi, and Takahiko Wato. Adhesive device for application to body tissue, February 13 1990. US Patent 4,900,554.

[194] Maha Zaghdoudi, Anja Kömmling, Matthias Jaunich, and Dietmar Wolff. Scission, cross-linking, and physical relaxation during thermal degradation of elastomers. *Polymers*, 11(8):1280, 2019.

[195] Maha Zaghdoudi, Anja Kömmling, Matthias Jaunich, and DietmarWolff. Erroneous or arrhenius: Adegradation rate-based model for epdm during homogeneous ageing. *Polymers*, 12(9):2152, 2020.

[196] Shamsul Zakaria, Frederikke Bahrt Madsen, and Anne Ladegaard Skov. Post curing as an effective means of ensuring the long-term reliability of pdms thin films for dielectric elastomer applications. *Polymer-Plastics Technology and Engineering*, 56(1):83–95, 2017.

[197] Nanami Zeniya, Eiichi Obataya, Kaoru Endo-Ujiie, and Miyuki Matsuo-Ueda. Application of time–temperature–humidity superposition to the mass loss of wood through hygrothermally accelerated ageing at 95–140 c and different relative humidity levels. *SN Applied Sciences*, 1(1):3, 2019.

[198] Jun Zhang, Hao zhong Shen, Xin Zhang, and Hai yu Li. Experimental and theoretical investigation of mechanical behavior related to temperature, humidity and strain rate on silane-modified polyurethane sealant. *Polymer Testing*, 103:107370, 2021.

[199] Zeang Zhao, Dong Wu, Ming Lei, Qiang Zhang, Panding Wang, and Hongshuai Lei. Mechanical behaviors and the equivalent network model of self-similar multinetwork elastomers. *International Journal of Solids and Structures*, 229:111135, 2021.

[200] Jiming Zhou and James P Lucas. Hygrothermal effects of epoxy resin. part ii: variations of glass transition temperature. *Polymer*, 40(20):5513–5522, 1999.

[201] Wen-Yue Zhuo, Qi-Long Wang, Gao Li, Guo Yang, Huan Zhang, Wen Xu, Yan-Hua Niu, and Guang-Xian Li. Detection of the destruction mechanism of perfluorinated elastomer (ffkm) network under thermo-oxidative aging conditions. *Chinese Journal of Polymer Science*, 40(5):504–514, 2022.